IRON MOBILIZATION IN MINERAL DUST AND THE POSSIBLE EFFECT OF ASIAN POLLUTION ON C-UPTAKE IN NORTH PACIFIC OCEAN

A Dissertation
Presented to
The Academic Faculty

By

Nicholas Meskhidze

In Partial Fulfillment
Of the Requirements for the Degree
Doctor of Philosophy in
Earth and Atmospheric Sciences

Georgia Institute of Technology
November, 2003

Iron Mobilization in Mineral Dust and the Possible Effect of Asian Pollution on C-uptake in North Pacific Ocean

Approved by:

Dr. William L. Chameides, Advisor

Dr. Athanasios Nenes

Dr. Rodney J. Weber

Dr. Gao Chen

Dr. Philip Froelich

Date Approved 18 November 2003

DEDICATION

This work is dedicated to the memory of my mother, Rusudan Nebieridze.

ACKNOWLEDGEMENTS

I would like to thank my thesis advisor, Bill Chameides, for his insight, thoughtful and valuable comments, advice and critical analysis during the years of my thesis work. I would also like to thank him for giving me the space to explore my own interests and develop independently my own approach to research.

I would also like to thank my thesis committee members, Thanos Nenes, Gao Chen, Rodney Weber, Flip Froelich, for their interest and time they have invested in my research.

Thanks go also to fallow graduate students, Alex Karabanov, Yan Huang, Ping Jing, Brent McDaniel, Kari Meier, Qian Tan, and Jing Zhang, for providing their friendship, advice, and encouragement throughout my Ph.D. research and making my stay at Georgia Tech enjoyable.

Finally, I would particularly like to thank my wife, Katy and my daughter, Helen, for their moral support, encouragement and love.

TABLE OF CONTENTS

LIST OF TABLES

LIST OF FIGURES

SUMMARY

Iron (Fe) is one of the nutrient elements needed for photosynthesis. Recent studies suggest that availability of Fe might limit phytoplankton productivity in large regions of the remote ocean. Therefore, the input of Fe to the ocean has a direct impact on marine ecosystem productivity and may even exert a global-scale influence on climate by affecting the rate at which atmospheric CO_2 is fixed by oceanic biota. Most Fe is delivered to the remote ocean via transport of iron-containing mineral aerosols (or dust) from the continent. While iron must be in dissolved form to be used by phytoplankton, continental iron is found primarily in insoluble minerals. An analysis of the global budget of oceanic Fe suggests that about 0.5 – 2% of the Fe delivered to the ocean in dust is in soluble form; however, the processes responsible for transforming the insoluble iron minerals into soluble forms in this amount remain poorly understood.

In this thesis, a combination of diagnostic data analysis and prognostic model simulations are used to assess the viability of a new mechanism for producing dissolved Fe in dust carried from the gobi deserts of East Asia to the remote North Pacific Ocean. The mechanism, referred here as "acid mobilization," involves the acidification of mineral dust by SO_2 from pollutant emissions and the subsequent dissolution of the Fe contained in the dust.

An initial confirmation for the viability of this "acid-mobilization" hypothesis is obtained from an analysis of data collected over the Yellow Sea during airborne atmospheric chemistry field campaign. Measured concentrations of selected trace gases and particle-phase components collected inside a dust-laden plume advecting from the Asian continent suggest that the mineral dust in the plume was accompanied by high

concentrations of acidifying air pollutants (particularly with SO_2). The range of pH implied from the measured concentration of gas-phase HNO_3 and particulate-phase NO_3^- is consistent with acid dissolution rate of Fe required to mobilize 0.5 - 2% of Fe in the dust within the nominal atmospheric lifetime of the dust particles.

To further test the hypothesis and explore the evolution of dissolved Fe in different cases of mineral dust advection from East Asia to the Pacific Ocean, a Lagrangian box model of the gas and aqueous-phase chemistry of reactive compounds within an air mass containing mineral dust was developed. The model encompasses forty five different chemical species distributed in the gas-phase and two aerosol modes (fine and coarse). Thermodynamic equilibrium of gas-, aqueous- and solid-phases of different species is accomplished using the numerical module ISORROPIA. The specific trajectories assumed for the plumes in the model and the associated conditions of pressure, temperature, and relative humidity are based on the actual trajectories estimated using the Hybrid Single-Particle Lagrangian Integrated Trajectory (HYSPLIT4) model. After the initial composition of mineral dust and air pollutants are specified, the concentrations of relevant gas-, aqueous- and solid-phase species in the advecting plume are determined by solving a system of coupled mass continuity equations.

The model simulations of dust transport episodes with different chemical compositions and advection paths were carried out to evaluate how varying plume conditions and trajectories affect the amount of mobilized Fe in these dust plumes. Model calculations indicate that the nominal springtime amounts of anthropogenic air pollutants (particularly SO_2) found in the urban and industrial centers of East China can acidify small dust-containing plumes and produce 0.5 - 2% of dissolved Fe during a typical

lifetime of dust particle. Therefore it is suggested that the major fraction of mobilized Fe could be delivered to the surface waters of North Pacific Ocean by small dust plumes. However, the role of the large dust episodes in the supply of biologically active Fe to the ocean should not be overlooked. Intensive pollution events occasionally observed in China can acidify significant dust plumes and reduce pH of deliquesced mineral dust particles to the values required to mobilize targeted amounts of Dissolved Iron Fraction (DIF). Simulations also revealed that the low air temperature, characteristic to the mid troposphere altitudes, can effectively impede hematite dissolution rates and reduce DIFs of advecting plumes well below 0.5 - 2% range. Subsidence of the dust plume to the marine boundary layer and photochemical reductive dissolution of hematite in acidic mineral aerosols were suggested as two possible mechanisms for mobilizing Fe during the high altitude dust passages.

Modeling results of two dust advection episodes suggest that some dust plumes, especially those mixed with unusually high concentrations of SO_2, can deposit enough bioavailable Fe to the surface waters of North Pacific Ocean to cause phytoplankton bloom. Calculations of the expected changes in marine ecosystem productivity caused by Fe enrichments to surface ocean waters based on the model simulations are generally consistent with the space-borne Moderate Resolution Imaging Spectrometer (MODIS) data used to diagnose the presence of local, transient phytoplankton blooms.

The model results suggest that future changes in SO_2-pollutant emissions from East Asia have the potential to affect the amounts of the dissolved Fe in mineral dust plumes emanating from the region. The full implications of such changes to ocean ecosystem productivity, the global C cycle, and climate have yet to be assessed.

CHAPTER 1

INTRODUCTION

1.1 Introduction

Microscopic single-celled marine organisms (phytoplankton) play a crucial role in the global carbon cycle. Making up less than one percent of plant biomass, phytoplankton carry out almost half of Earth's gross photosynthesis [Chisholm, 2000]. Using sunlight and dissolved inorganic nutrients, phytoplankton convert CO_2 to organic carbon, forming the base of the marine food chain. As this carbon passes through food chain in surface waters, most of it is converted back to CO_2, but some fraction sinks and thereby finds its way to the longer-lived carbon reservoirs of the deep ocean and ocean sediments. The net result of this process, also known as "biological pump", is the long-term removal or sequestration of C from the atmosphere [Chisholm, 2000].

Iron (Fe) is a micronutrient needed by phytoplankton in order to carry out photosynthesis [c.f., Sunda and Huntsman, 1995]. The transport and deposition of mineral dust from arid and semi-arid continental regions is believed to be a major, if not the dominant, source of Fe in the surface waters of the remote ocean [Duce et al., 1991; Duce and Tindale, 1991; Jickells and Spokes, 2001]. Recent studies suggest that Fe may limit phytoplankton productivity in roughly 50% of the world's ocean [de Baar et al., 2001; Moore et al., 2002]. Thus, alterations in the flux of Fe to the ocean may substantially affect ocean ecosystem productivity and, by changing the rate at which

atmospheric CO_2 is fixed by oceanic biota, may even exert a global-scale influence on climate [Zhuang et al., 1992a; Cooper et al., 1996; Turner et al., 1996]. For these reasons, it is important to understand the mechanisms that affect the delivery of Fe in mineral dust to the oceans, how this Fe is utilized by ocean biota, and to what extent, if any, human activities affect these processes.

In this research I present the first attempt to use a combination of diagnostic data analysis and prognostic model calculations to investigate Fe mobilization in dust plumes emanating from East Asia during the springtime outflow conditions. I developed a Lagrangian box model of the gas and aqueous-phase chemistry of reactive compounds within an air mass containing mineral dust. The model, in combination with data from airborne atmospheric chemistry field campaigns carried out over the western Pacific Ocean and the space-borne MODIS and SeaWiFS (Sea-viewing Wide Field-of-view Sensor), is used to assess the viability of acid mobilization triggered by air pollutants from China as a mechanism for producing soluble Fe in mineral dust plumes.

1.2 The Role of Fe in Ocean Productivity

Fe is the fourth most abundant chemical element in the Earth's crust, and an essential element required by all known living organisms. Plants, most microorganisms, and animals require well-defined amounts of iron for survival, replication, and differentiation. In phytoplankton metabolism, Fe is required for photosynthetic and respiratory electron transport, nitrate reduction, chlorophyll synthesis, and detoxification of reactive oxygen species [Sunda and Huntsman, 1995].

It has been proposed that phytoplankton productivity in major ocean regions is limited by the availability of Fe in the surface waters. The idea that Fe may be limiting marine primary productivity was first suggested by Gran [1931], but could not be investigated further at that time since it was not possible to obtain reproducible measurements of Fe concentrations in ocean water [Wells et al., 1995; Turner et al., 2001]. It was not until the 1980s with the development of clean sampling and handling techniques that ocean scientists were able to accurately quantify the concentrations of dissolved Fe in the surface waters of the world's oceans. Their measurements revealed the existence of so-called "high nitrate low chlorophyll" (HNLC) regions of the ocean that are characterized by high concentration of nitrate – which has historically been viewed as the nutrient limiting photosynthesis in the ocean [Minas et al., 1986; Chisholm, 2000] – but paradoxically low levels of biological productivity, as well as extremely low concentrations of dissolved Fe [Martin et al., 1991a]. This discovery lead John Martin and his colleagues to propose that the low availability of Fe (and not nitrate) was limiting phytoplankton productivity in the HNLC regions of the ocean [Martin and Fitzwater, 1988; Martin and Gordon, 1988; Martin et al., 1989, 1991b].

Qualitative confirmation of the hypothesis that Fe limits productivity in HNLC waters was obtained from a series of bottle enrichment studies [Martin and Fitzwater, 1988; Martin et al., 1990; Greene et al., 1994; Kolber et al., 1994] and mesoscale Fe enrichment experiments [Martin and Coale, 1994; Coale et al., 1996; Coale et al., 1998; Boyd et al., 2000; Dalton, 2002; Tsuda et al., 2003; Nishioka et al., 2003].

The role of Fe in limiting ocean productivity may prove to be quite extensive. The HNLC areas are large and potentially important regions of the ocean found in the

subarctic North Pacific, Equatorial Pacific and Southern Ocean [Minas et al., 1986; Martin et al., 1989; 1990]. As phytoplankton growth in these oceanic regions is limited by Fe availability, HNLC waters are distinguished by a continuous presence of nitrate, phosphate and silicic acid that makes them the largest repositories of unused macronutrients in the surface waters [McDonald et al., 1999; Boyd et al., 2000]. To that extent any process that could alter Fe supply to these regions can potentially play a critical role in the C-uptake of these waters and, as it will be shown below, can even affect global carbon budget. The estimated mean annual primary production in HNLC regions is about 140 g C m^{-2} yr^{-1} [McDonald et al., 1999; Wong et al., 2002] and the average surface area is approximately $35x10^{12}$ m^2 [Watson, 2001]. So with the current supply of Fe HNLC waters contribute roughly 10% of the global ocean photosynthesis [Fung et al., 2000; Moore et al., 2002]. However, mesoscale Fe enrichment experiments demonstrated that with the increased supply of Fe average primary productivity in HNLC waters could increase to at least 420 g C m^2 yr^{-1} [Boyd et al., 2000] sequestering ~ 16 Gt C yr^{-1} or more than 25% of the new potential global primary productivity of the ocean [Fung et al., 2000; Moore et al., 2002]. Although this estimate is somewhat speculative (since with the increased supply of Fe to HNLC regions fast growth of phytoplankton could deplete excess nutrients) it serves as an illustrative example highlighting the importance of Fe for the C-uptake of the oceans.

Moreover, recent modeling studies indicate that, in addition to the HNLC regions listed above, Fe limitation may extend to transitional zones located between the mid-ocean gyres and the HNLC regions. These transitional zones can shift from being primarily Fe limited to being nitrate limited and then back to Fe limitation as the supply

of Fe to the zone varies [Moore et al., 2002]. It has been estimated that, overall, Fe may limit biological productivity in about 50% of the surface waters of the world's oceans [de Baar et al., 2001; Moore et al., 2002]. It is believed that, in these regions, a relatively small increase in the input of Fe can result in floristic shifts in the algal community structure from predominantly pico- and nano-planktonic assemblages to ones dominated by fast growing macro-sized diatoms [Moore et al., 2002; Tsuda et al., 2003; Wells, 2003]. This is an important shift because the primary removal mechanism for pico-and nano-planktonic assemblages is pelagic recycling through the microbial food web within the surface ocean waters, while the major loss mechanism for macro-sized algal carbon is removal from the surface waters via sedimentation [Boyd and Harrison, 1999; Moore et al., 2002]. This enhanced sedimentation of the plankton has the potential to increase the rate at which C is transported from the surface waters to the longer-lived C-reservoirs of the deep ocean and sediments. Thus, variations in Fe inputs to the ocean may have an impact on C sequestration rates in the world's ocean, and by extension, the global C cycle and climate [Martin and Fitzwater, 1988; Zhuang et al., 1992a; Cooper et al., 1996; Turner et al., 1996; Coale et al., 1996; Boyd et al., 2000].

1.3 Dust as a Source of Fe to the Ocean

Atmospheric transport and deposition of mineral dust represents the dominant source of new (not acquired via nutrient recycling) Fe to the surface waters of the remote ocean [Duce et al., 1991; Duce and Tindale, 1991; Jickells and Spokes, 2001]. The fraction of Fe in soils and rocks varies from place to place ranging from 2.9 to 4.8% for large areas of the exposed continental crust [Taylor and McLennan, 1985; Warneck,

1988]. Since the enrichment of Fe in mineral dust plumes (i.e. from urban aerosols while dust plume advances over the industrial regions) relative to its crustal abundance is rather insignificant, it is commonly assumed that on average Fe accounts for 3.5 % of the total mineral dust mass [e.g. Taylor and McLennan, 1985; Duce and Tindale, 1991].

Dust entrainment into the atmosphere at the source regions is sensitive to a wide range of factors including soil composition and moisture content, surface condition, wind speed, and may be further modulated by human activities and land degradation [Luo et al., 2003]. Based on these parameters the highest dust production regions are found in arid and semiarid regions of northern Africa, the Arabian Peninsula, eastern Asia, Australia, Patagonia, and southern Africa [Tegen and Fung, 1994; Ginoux et al., 2001; Jickells and Spokes, 2001]. As the atmospheric lifetime of dust is relatively short (from several hours to less than two weeks [Tegen and Fung, 1994; Ginoux et al., 2001; Luo et al., 2003]), the largest inputs of the mineral Fe to the oceans occur downwind of continents, in the vicinity of the dust source regions [Fung et al., 2000; Moore et al., 2002]. Table 1.1 summarizes seasonal and annual deposition of mineral Fe to the major oceanic basins. From this table we can see that the present day atmospheric flux of Fe to the oceans is probably in a range of 14 - 35 $x10^{12}$ g yr^{-1}. However, it is should be noted that dust-Fe production from soils is a strong function of local meteorological conditions and hence the transport and deposition rates of dust are highly variable on daily, weekly, seasonal and annual time scales [Jickells and Spokes, 2001; Kurosaki and Mikami, 2003].

Table 1.1 Seasonal and annual deposition of mineral dust to the major oceanic basins[1]

Ocean Basin	Seasonal Dust Deposition [2]				Annual Fe Deposition [3]				
	Spring	Summer	Fall	Winter	Duce & Tindale [1991]	Prospero [1996]	Ginoux et al. [2001]	Gao et al. [2001]	Jickells & Spokes [2001]
North Pacific	0.28	0.17	0.34	0.20	16.8	3.36	3.22	3.0	7.3
South Pacific	0.02	0.02	0.04	0.02	1.37	0.28	0.98	0.31	0.67
North Atlantic	0.43	0.78	0.72	0.26	7.70	7.7	6.44	6.6	6.0
South Atlantic	0.05	0.06	0.05	0.04	0.84	0.18	0.70	0.59	0.46
Indian	0.21	0.15	0.26	0.18	5.04	1.02	5.40	2.4	2.2
Antarctic	0.01	0.01	0.01	0.01	NA	NA	NA	0.07	NA
Arctic	0.01	0.01	0.02	0.01	NA	NA	NA	0.13	NA
Global Total					**32**	**13**	**17**	**14**	**17**

(1) Units are in Tg yr^{-1} ($1Tg=10^{12}$ g);
(2) From Gao et al. [2001];
(3) Assumes crustal material contains 3.5% of Fe by weight [Taylor and McLennan, 1985; Duce and Tindale, 1991].

Although atmospheric deposition has generally been considered to be the dominant source of Fe to the remote oceans, the importance of upwelling and vertical mixing of micronutrient Fe from below the euphotic zone can not be discarded. This source of Fe can be particularly important for HNLC regions characterized by the low atmospheric dust deposition and the high upwelling rates [de Baar et al., 1995; Wells et al., 1995; Watson, 2001]. Table 1.2 summarizes the estimates of aeolian and upwelled Fe fluxes to subarctic North Pacific, Equatorial Pacific and Southern Ocean regions.

These numbers however may be somewhat misleading, as subsurface Fe is dependent on the atmospheric inputs. In fact, some modeling studies indicate that a reduction in atmospheric Fe deposition below a critical threshold value can cause a rapid depletion of subsurface Fe and a drastic decrease of total primary productivity [Archer and Johnson, 2000; Moore et al., 2002]. Nevertheless, Table 1.2 suggests that of the three

HNLC areas, the subarctic Pacific has the lowest rate of Fe upwelling and the highest rate of Fe input from dust. Thus phytoplankton productivity in this region is likely to be the most sensitive to Fe input from dust depositions and is therefore an appropriate region to examine the effects of episodic dust deposition on marine ecosystem productivity.

Table 1.2 Estimates of aeolian and upwelling Fe fluxes[(1)]

Ocean region	Area (10^{12} m^2)	Upwelling flux (10^6 $m^3 s^{-1}$)	Aeolian dust flux (mg $m^{-2} y^{-1}$)	Atmospheric input of micronutrient Fe (10^6 mol y^{-1}) [(2)]	Upwelling Fe flux (10^6 mol y^{-1}) [(3)]
Subarctic Pacific	6.2	4.5	100-1000	7.8-390	86
Equatorial Pacific	18	44	10-100	2-100	280
Southern Ocean	10.8	25	1-10	0.14-6.8	240

(1) From Watson [2001];
(2) Calculated as 3.5% be weight of the dust flux, with 2% and 10% of it being in a dissolved form (see more discussion below);
(3) Calculated as upwelling water flux times concentration in deep waters, where this concentration is assumed to be 0.6 nmol L^{-1} for subarctic Pacific and Southern Ocean, and 0.2 nmol L^{-1} for the equatorial Pacific.

1.4 The Critical Role of Fe Dissolution in Aeolian Dust

Although atmospheric transport and deposition of aeolian dust is considered to be a dominant mechanism by which Fe is delivered to the surface waters of the open ocean [Duce et al., 1991; Duce and Tindale, 1991; Jickells and Spokes, 2001; Moore et al., 2002] virtually all Fe found in dust at the arid and semi-arid source regions is in highly insoluble crystalline Fe-III form (i.e., hematite [Hseung and Jackson, 1952; Claquin et al.,

1999] or goethite [Spokes et al., 1994]) a form that is not readily available for uptake by marine biota. Before the Fe in mineral dust can be utilized by phytoplankton it must be dissolved or mobilized*. There are two possible pathways for this to occur: the Fe can be mobilized in the ocean after deposition or it can be mobilized in the atmosphere prior to dust deposition. Figure 1.1 shows the thermodynamic equilibrium solubilities of hematite (Fe_2O_3) and goethite (α-FeOOH) in seawater as a function of pH. We can see from this figure that the solubilities of Fe-III oxides are strongly pH dependent with the lowest dissolved Fe concentrations calculated to be near pH=8, which is close to the pH of ocean water [Stumm and Morgan, 1981]. In addition to having a low solubility in seawater, the dissolution rates of Fe-III minerals at pH=8 is extremely slow [Jickells and Spokes, 2001]. Simple calculations using a mineral dissolution rate law discussed in more detail in Chapter 3 of this thesis suggests that the dissolution of 2% of hematite in seawater would take longer than the residence time of dissolved Fe in the ocean (32-200 years [Johnson et al., 1997; de Baar et al., 2001]). So at present, the common understanding among scientists is that Fe in mineral dust can not become bioavailable through dissolution in the ocean and must therefore be mobilized while in the atmosphere during its transport from the continents to the remote oceanic areas [c.f., Fung et al., 2000; Jickells and Spokes, 2001; Moore et al., 2002; Gao et al., 2003].

* Note, that in marine science dissolved (<0.4 μm) form of Fe usually comprises soluble and colloidal (>1 kDa-0.4 μm) size fractions [Wells, 2003]. In the discussion of dissolution or mobilization of Fe in mineral aerosols we only imply soluble (<1kDa) fraction.

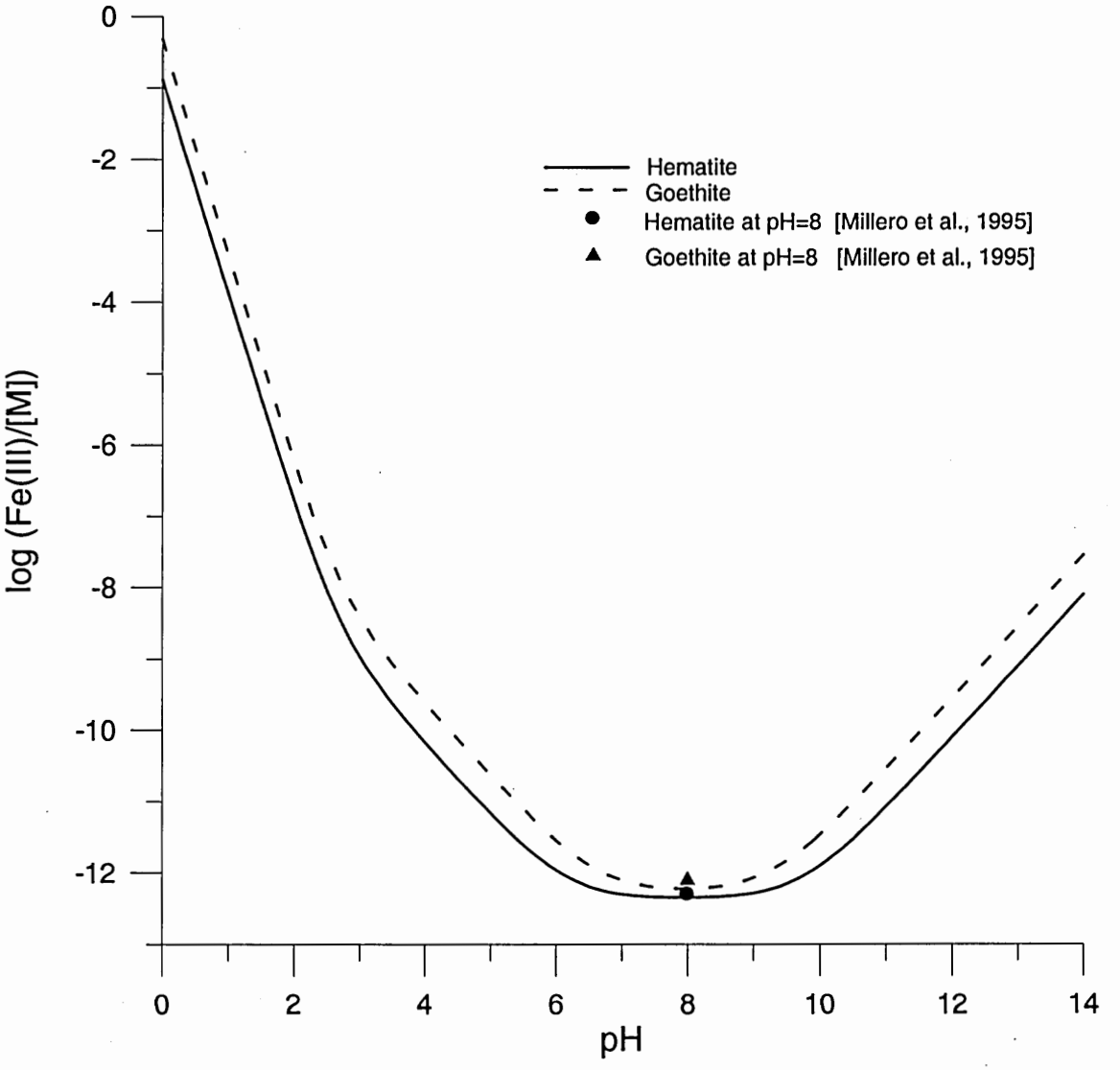

Figure 1.1 Thermodynamic solubilities of goethite and hematite in seawater as a function of pH. The effect of organic ligands on the Fe(III) speciation was determined assuming an average ligand concentration in seawater [L]= 4nM [Gledhill and van den Berg, 1994; Millero, 1998]. Equilibrium constants for hematite, goethite and all Fe(III) complexes were taken from Millero et al. [1995].

1.5 Key Uncertainties That Remain

For the reasons discussed above, some fraction of the Fe in mineral dust must be transformed into a soluble form (and thus available for uptake by biota) while the dust is being transported in the atmosphere and before it is deposited on the ocean surface. However, while the fraction of Fe in airborne mineral dust that is mobilized or dissolved (referred to here as the Dissolved Iron Fraction or DIF) is a key parameter in understanding the role of mineral dust in ocean productivity and global C cycle, the value of DIF in mineral dust, its natural variability, the mechanisms that control DIF and the role, if any, of anthropogenic pollutants in influencing DIF remain poorly defined. For example, Table 1.3 summarizes some of the DIFs reported in the literature from the collection and laboratory analysis of mineral dust samples. The smallest DIF-value (0.001%) given in the table would, if representative of all dust, render Fe deposition in mineral dust an insignificant source of Fe to the surface waters of HNLC areas [Jickells and Spokes, 2001]. The largest values (50%) would change HNLC waters from being strongly Fe limited to Fe saturated. A range in DIF-values that is perhaps more representative of mineral dust inputs to the remote ocean was provided in a recent review by Jickells and Spokes [2001]; they derived a range in DIF from 0.8 to 2.1 % on the basis of estimated fluxes of dust to the ocean, measurements of Fe in dust and data on the abundance and residence time of dissolved Fe in the ocean. In the work described here, I will use the range 0.5 – 2% as reasonable target for assessing the viability of a hypothesized mechanism for mobilizing Fe in mineral dust.

With regard the processes that mobilize Fe in dust as it is transported from the continents to the remote ocean, so little is known that most modeling studies attempting

to simulate the input of Fe in mineral dust to the ocean simply treat DIF as an empirical parameter to be specified on the basis of measurements like those summarized in Table 1.3. As described below, it is this later scientific uncertainty – the mechanism or mechanisms responsible for mobilizing (or dissolving Fe in aeolian dust) – that is the subject of this thesis.

1.6 This Work

Clearly, understanding the combination of processes that act to mobilize Fe in mineral dust along its atmospheric trajectory from soils to the ocean is key to assessing the role of Fe in controlling ocean productivity and to assessing the extent to which human-induced and/or natural perturbations to the biogeochemical cycling of dust and the Fe contained therein can affect ocean productivity. To that end, I explore in this thesis the viability of one such mechanism for mobilizing Fe in aeolian dust: acid mobilization. It has been well-established that the Fe in crustal minerals can be mobilized in highly acidic solutions [Colin et al., 1990; Duce and Tindale, 1991; Zhu et al., 1992; 1993; Zhuang et al., 1992a; Spokes et al., 1994; Spokes and Jickells, 1996; Desboeufs et al., 2001]. Indeed referring back to Figure 1.1, note that the Fe-III solubility increases dramatically as pH falls. However, sands from arid and semi-arid regions are typically alkaline in nature (mainly due to the presence of $CaCO_3$) and before Fe mobilization takes place dust needs to be acidified. It is not unreasonable to expect that mineral dust particles can be acidified in the atmosphere; the atmosphere typically contains an abundance of acidifying species, especially near urban and industrial centers. One of the most powerful atmospheric acidifying species is SO_2, whose oxidation in the atmosphere

Table 1.3 Typical DIF-values for atmospheric aerosols suggested in the literature

Reference	pH	conditions	DIF (%)
Desboeufs et al. [2001]	0.5 2.7	Saharan aerosols, pH cycling	28 5.6 - 6.1
Spokes and Jickells [1996]	2	Saharan aerosol, pH cycling	4.7±0.2
Spokes et al. [1994]	2	Saharan aerosol	4.5-5.5
Guieu and Thomas [1996]	6-8	Fine fraction desert soil	0.001-0.02
Zhu et al. [1993]	1	Polluted crustal aerosols from Barbados	6.9-9.2
Zhuang et al. [1992b]	NA	Marine mineral aerosols from: Central North Pacific Barbados	 56 ±32 49 ±15
Model estimates			
Gao et al. [2003]	Based on the estimate of global deposition of dissolved Fe to the ocean.		4-30
Jickells and Spokes [2001]	Based on estimated fluxes of dust to the ocean, measurements of Fe in mineral dust and data on the abundance and residence time of dissolved Fe in the ocean.		0.8 - 2.1
Fung et al. [2000]	Based on the comparison of demand and supply of Fe in the global ocean.		1-10

via both gas- and aqueous-phase as well heterogeneous reactions lead to the production of the strong acid H_2SO_4 [Judeikis, et al., 1978; Dentener et al., 1996; Herring et al., 1996; Phadnis and Carmichael, 2000; Goodman et al., 2001; Ullerstam et al., 2002]. Hence, the "acid-mobilization hypothesis" to be investigated here:

> *Fe in mineral dust is mobilized during transport in the atmosphere in a two-step process consisting of: (1) acidification of the mineral dust by the incorporation of acids arising from air pollutants (and in particular SO_2) that are mixed into the plumes containing dust as these plumes advect over the urban and industrial centers; and (2) dissolution of the Fe in the resultant acidic solutions.*

To assess the viability of this hypothesis, I examine if 0.5 - 2% of DIF can be attained via acid mobilization in plumes containing wind blown dust from the gobi deserts in the springtime outflow emanating from East Asia and advecting over the western North Pacific Ocean. The Asian outflow was chosen, because i) it represents one of the largest sources of mineral dust to the remote ocean [Duce and Tindale, 1991; Tegen and Fung, 1994; Prospero, 1996; Ginoux et al., 2001; Luo et al., 2003]; ii) analyses of dust-storm tracks indicates that these storms often pass through the highly populated and industrialized regions of Beijing, Qingdao, and Shanghai before leaving the coast and therefore have ample opportunity to entrain significant amount of pollutants from urban and industrial activities [e.g., Hoell et al., 1996; Hoell et al., 1997; Sun et al., 2001]; iii) during the springtime, prevailing westerly winds can transport this dust far into the HNLC regions of subarctic North Pacific Ocean [Husar et al., 2001]; and iv) it is

expected that the continued economic development of East Asia will lead to changes in the rates at which pollutants are emitted from the region [Elliott et al., 1997; Nakicenovic et al., 2001; Streets et al, 2001; Klimont et al., 2001; Carmichael et al., 2002] and, if our hypothesis is correct, such changes could alter the flux of dissolved Fe to the North Pacific Ocean.

I begin in Chapter 2 with a diagnostic analysis of a specific dust plume that had originated from the gobi deserts and advected over the Yellow Sea to obtain an initial assessment of the viability of the acid mobilization hypothesis. In Chapter 3, a Lagrangian box model is described that simulates the evolution of DIF of a mineral dust plume as it advects from the east coast of China to the western Pacific Ocean. In Chapter 4 the results of simulations using the model are discussed for three different dust plumes with diverse compositions and advection paths. The range of DIF-values produced in these plumes as a function of the trajectory and various input parameters such as the input of dust and SO_2-pollution are explored.

In Chapter 5 I examine in more detail two dust plumes that originated from the gobi deserts and advected to the North Pacific Ocean. Using model calculated DIF-values estimates are made of the likely inputs of bioavailable Fe to the receptor regions of the North Pacific Ocean and these results are correlated with satellite measured ocean chlorophyll *a* concentrations. Chapter 6 presents a summary of the present study, conclusions, and recommendations for the further investigation of the interactions between airborne dust and air pollutants.

CHAPTER 2

TESTING THE VIABILITY OF ACID MOBILIZATION HYPOTHESIS

2.1 Introduction

The central argument of my thesis is that Fe in mineral dust from East Asia is made bioavailable as it is transported in the atmosphere from the continent to the North Pacific Ocean via acid mobilization, with the acidification arising from the incorporation of sulfur oxides from pollution. In this chapter, I present the results of an initial test of the viability this hypothesis using a diagnostic analysis of data collected during the TRACE-P airborne field study that documented the chemical composition of a dust laden plume that originated from the gobi deserts and advected over the Yellow Sea.

2.2 General Considerations – Acid Dissolution of Fe containing minerals

Analyses of mineral dust particles downwind from the gobi deserts show that acidic substances often deposit and/or form on the aerosol surface as they advect and, in so doing, change the aerosols from hydrophobic to hydrophilic (e.g., Song and Carmichael [2001]). When such aerosols are advected to the warm and moist marine boundary layer, they will likely deliquesce [Phadnis and Carmichael, 2000].

Deliquescence of mineral dust particles is a necessary but not sufficient condition for solubilization of Fe. As discussed in Chapter 1, Fe(III) oxides are highly insoluble under alkaline conditions, so the pH of a solution in contact with Fe-containing minerals

must decrease before the Fe in these minerals can begin to dissolve. Since most of the Fe in surface soils of the gobi deserts is found in the form of hematite (α-Fe_2O_3) [Hseung and Jackson, 1952; Claquin et al., 1999], we focus here on acid dissolution of hematite. Figure 2.1 illustrates measured and calculated acid dissolution rates, R_d, for hematite as a function of pH. The rates are expressed in units of moles of mineral dissolved per m^2 of mineral surface area per hour. Values for R_d are shown for two temperatures: 298 K in order to compare calculated rates with experimental data; and 288 K for simulating conditions encountered in the marine boundary layer over the Yellow Sea.

2.3 What rate of iron dissolution is needed? How acidic does the dust need to be?

If all Fe in mineral dust is originally in insoluble form and DIF when it deposits on the ocean surface is 0.5 – 2%, then R_{Fe}, the average fractional rate of iron mobilization in mineral dust as it is transported through the atmosphere, must be given by

$$R_{Fe}=DIF/\tau = (0.005–0.02)/\tau \qquad (2.1)$$

where R_{Fe} has units grams of dissolved Fe per grams of Fe in the mineral per unit time and τ is the average residence time of mineral dust in the atmosphere. Assuming a nominal atmospheric lifetime of 3 to 5 days for dust particles [Ginoux et al., 2001], then

$$R_{Fe}\sim(4\times10^{-5}–30\times10^{-5}) \text{ g Fe dissolved/(g total Fe)/hr} \qquad (2.2)$$

If soluble iron is arising from hematite dissolution and R_d is the rate of hematite dissolution, then

$$R_{Fe} = R_d\ A\ n\ M/w \qquad (2.3)$$

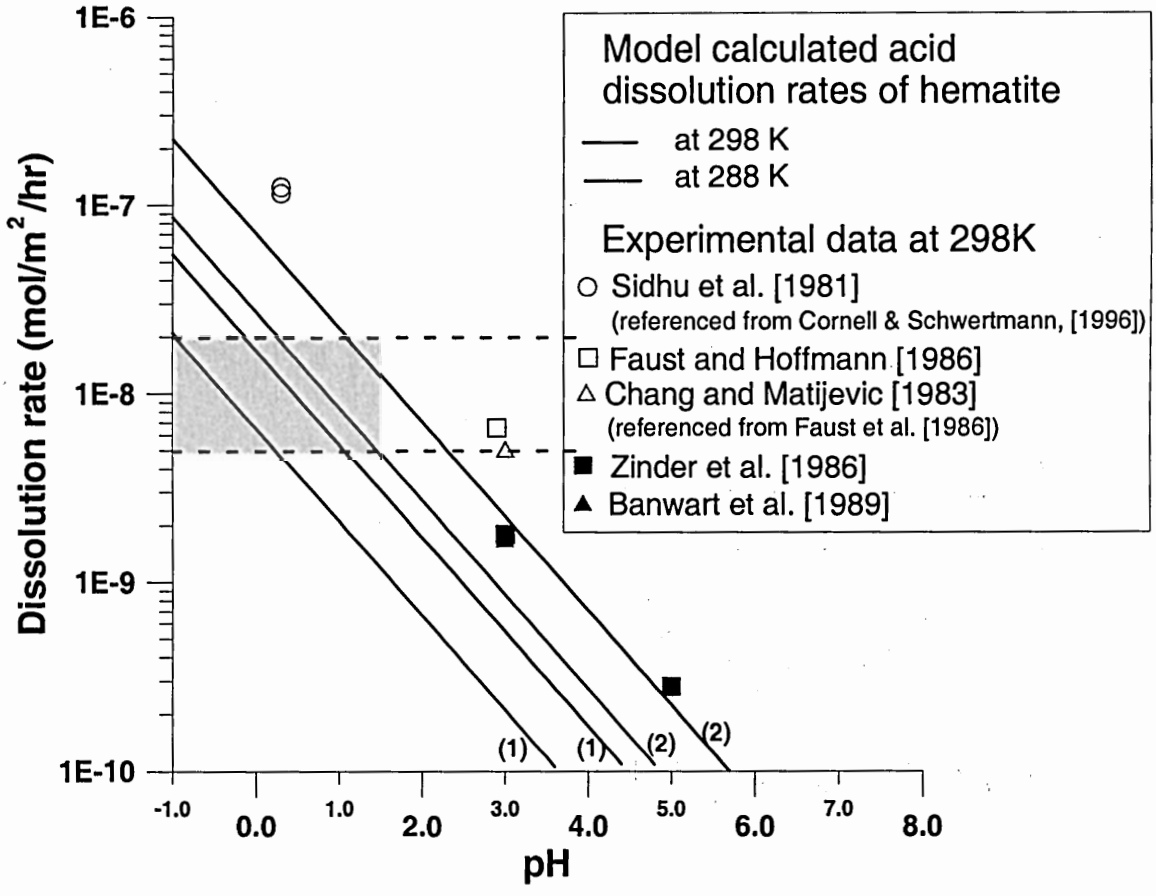

Figure 2.1 Experimental and model calculated rates, R_d, of hematite dissolution. The calculated rates are based on the hematite dissolution experiments of Azuma and Kametani [1964]. Lines (1) and (2) correspond to different regimes in the dissolution kinetics; i.e. when the mass of dissolved hematite is < 0.8% and is between 0.8–40%, respectively [Azuma and Kametani, 1964; Cornell and Schwertmann, 1996]. The shaded area shows the pH-range needed to mobilize 0.5 – 2% of the Fe in 3–5 days.

where A is the specific surface area of hematite ($m^2 g^{-1}$), n is the number of moles of Fe mobilized for each mole of hematite dissolved (i.e., 2), M is the gram-molecular weight of Fe, and w is the mass fraction of Fe in hematite(i.e., 0.7). Adopting an average value for A of 50 to 100 $m^2 g^{-1}$ [Cornell and Schwertmann, 1996; Skopp, 2000; Ullerstam et al., 2002] and combining Equations (2) and (3)

$$R_d = R_{Fe}\, w/(A\, n\, M) \sim (3\text{–}40)\times10^{-9} \text{ moles } m^2 \text{ hr}^{-1} \qquad (2.4)$$

Inspection of Figure 1 indicates that this range of hematite dissolution rates (at 288K) is attained for pH values less than 2. So, for acid mobilization to be a viable mechanism, the mineral dust over the ocean must have a pH of ~ 0 - 2.

2.4 Is there any evidence that mineral dust pH falls below 2?

To assess the acidity of mineral dust as it is advected in the Asian outflow over the western Pacific Ocean we examine the data collected during the TRACE-P (TRAnsport and Chemical Evolution over the Pacific) and ACE-Asia (Aerosol Characterization Experiment) field campaigns [Jacob et al., 2003; Huebert et al., 2003]. Among their various scientific objectives, these missions set out to document the concentration and chemical composition of aerosols and gaseous tracers in the Asian outflow during the springtime, when dust outbreaks on the Asian continent are most frequent [see e.g., Sun et al., 2001]. Both projects used airborne platforms to intercept and sample plumes over the western Pacific Ocean during the spring of 2001.

We begin by considering the data collected by the NASA DC-8 on March 21, (TRACE-P Flight 13). Analyses of the data collected during the course of this flight (discussed below) suggests that the aircraft intercepted a plume containing both mineral

dust and air pollutants over the Yellow Sea (30°N) around 4:40 UTC, thus making the plume well-suited for testing our hypothesis. Back trajectory analyses indicate that the dust originated from the gobi deserts, was then transported to the Shanghai metropolitan area where air pollutants could have mixed with the dust and then moved out over the Yellow Sea and the Pacific Ocean [Fuelberg et al., 2003]. The large mixing ratios of highly reactive species along with the back trajectory analysis suggest that the plume had left the East Asian continent less than one day before it was sampled [Talbot et al., 2003].

Measured concentrations of selected trace gases and particle-phase components during Flight 13 are plotted as a function of time in Figure 2. Of particular interest are the data collected between 4:30 and 5:00 UTC; unless otherwise stated, when we discuss TRACE-P data below we will be referring to the data from this segment of Flight 13. During this period the aircraft descended into the boundary layer and elevated concentrations of particulate-Ca^{2+}, SO_2 and gas-phase HNO_3 (HNO_3(g)) were observed.

2.4.1 *Evidence of the presence of mineral dust:* The measured Ca ranged from 10–15 ppbv; this is significantly larger than 30-45 pptv typically observed in the marine boundary layer [Dibb et al., 1999]. There are three possible Ca sources: sea salt, anthropogenic emissions, and mineral dust. An upper limit estimate of the sea salt contribution to the observed Ca can be obtained by assuming that all of the particulate Na observed during the flight segment came from sea salt. With this assumption, the measured Na concentration of ~ 6 ppbv and a Ca:Na ratio in seawater of 0.038 g/g [Stumm and Morgan, 1981], we find that < 1% of the Ca was from sea salt. Similarly given a typical S:Ca ratio for anthropogenic emissions of ~ 25g/g [Lee and Pacyna, 1999] and the SO_2 and SO_4^{2-} observations, we find that < 10% of the Ca was anthropogenic.

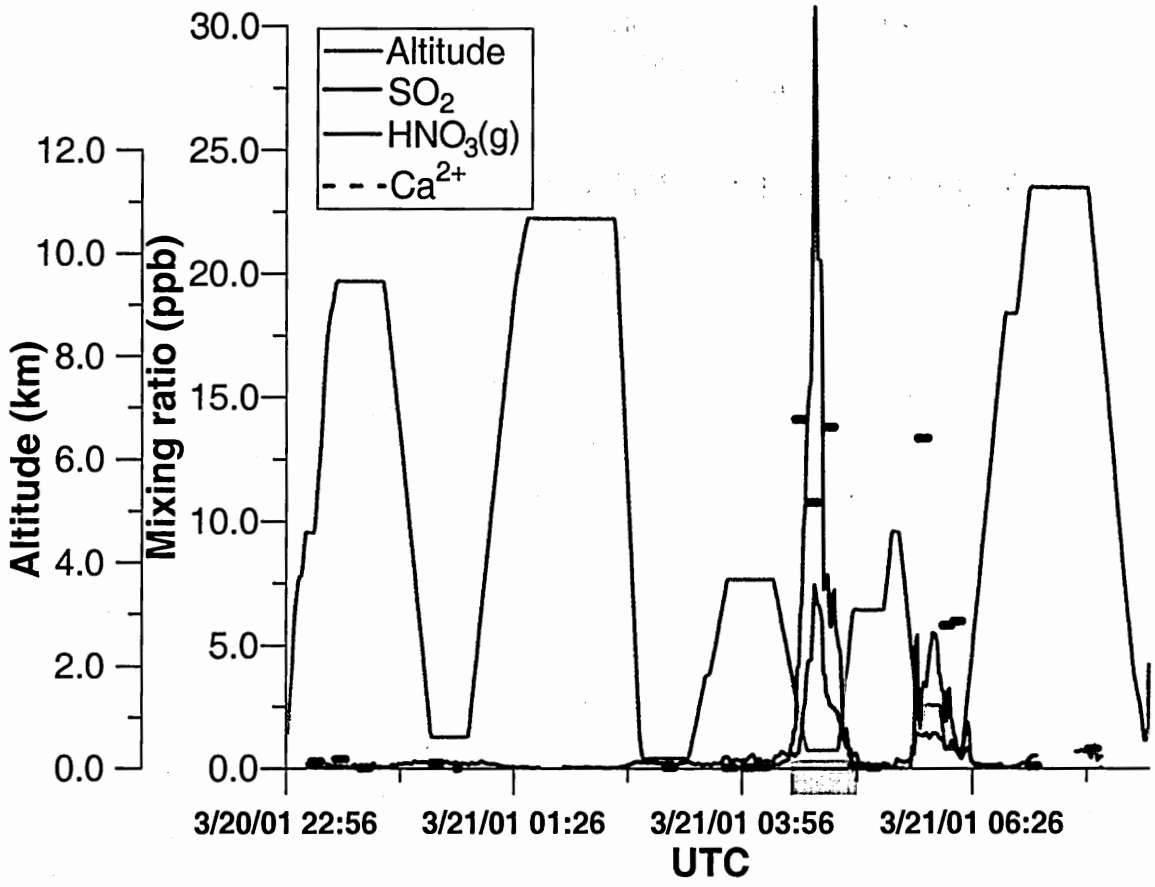

Figure 2.2 Flight altitude and observed concentrations of $SO_2(g)$, $HNO_3(g)$, and particulate Ca as a function of time for TRACE-P DC-8 Flight 13. The shaded area along the x-axis highlights a period when the aircraft intercepted a plume of dust and air pollutants.

Assuming that all of the Ca arose from mineral dust and a Ca-to-mineral dust ratio of 6.2:100 (see Table 3.3, as well as Song and Carmichael [2001] and Zhang et al. [2003]), we obtain a mineral dust concentration of ~ 300 $\mu g/m^3$, suggesting the presence of a large dust plume.

2.4.2 *Evidence of the presence of urban/industrial air pollutants:* Under typical springtime conditions in the marine boundary layer of the Yellow Sea, SO_2 generally ranges from ~ 0.03–1 ppbv [Thornton et al., 1997]. Thus, the measured SO_2 of 20–30 ppbv is a clear indication of the presence of air pollution. Consistent with this inference are the high concentrations measured for SO_4^{2-} ~11 ppbv, NO_3^- ~13 ppbv, NH_4^+ ~14 ppbv, C_2H_2~ 10 ppbv [Talbot et al., 2003].

2.4.3 *Evidence of acidification:* $HNO_3(g)$ over the Yellow Sea typically ranges from 0.2–0.6 ppbv [Kondo et al., 1997]. However, the measured $HNO_3(g)$ exceeded 2 ppbv and, at approximately the same time that SO_2 reached its peak, $HNO_3(g)$ approached 10 ppbv. The enhanced $HNO_3(g)$ could perhaps be viewed, like the enhanced SO_2, as simply reflecting the fact that the plume being sampled had been impacted by air pollutants. However, the $HNO_3(g)$ lifetime in the plume against dust uptake is <10 min (see Appendix A), while the DC-8 sampling time of the plume was ~30 min. Thus, the extremely large $HNO_3(g)$ can not be explained solely by the presence of air pollutants.

HNO_3 is a strong acid with a high solubility [Clegg et al., 1998]. According to several laboratory studies [Underwood et al., 1999; Goodman et al., 2000; Hanisch and Crowley, 2001b] and model simulations [Dentener et al., 1996; Metzger et al., 2002], $HNO_3(g)$ rapidly partitions to the particulate phase when non-acidic aerosols are present. Moreover, modeling studies of the Asian outflow predict that under normal conditions,

with dust concentrations of 150 $\mu g\ m^{-3}$ or less, NO_3^- will almost exclusively reside in the particulate phase [Dentener et al., 1996; Phadnis and Carmichael, 2000]. In our case, we have $HNO_3(g)$ concentrations orders of magnitude higher than normal despite the presence of 100's $\mu g\ m^{-3}$ of mineral dust.

Further evidence of the anomalous nature of the $HNO_3(g)$ observations can be obtained by considering the nitrate volatilization ratio, $[NO_3^-]_{vol}$, defined as

$$[NO_3^-]_{vol} = 1 - \frac{[NO_3^-]}{[NO_3^-] + [HNO_3(g)]} \tag{2.5}$$

where $[NO_3^-]$ and $[HNO_3(g)]$ are the measured mixing ratios of NO_3^- and $HNO_3(g)$, respectively. In Figure 2.3 $[NO_3^-]_{vol}$-values calculated from the observations of $HNO_3(g)$ and the particulate NO_3^- reported by Talbot et al. [2003] are illustrated. $[NO_3^-]_{vol}$-within the plume ranged from 25–45%. For this much of the nitrate to have resided in the gas-phase as $HNO_3(g)$ in the presence of large amounts of mineral dust requires that the mineral dust, along with the rest of the particulate phase, was strongly acidified.

The aerosol acidity can be estimated by considering the conditions needed to have supported the observed values of $[NO_3^-]_{vol}$. Assuming thermodynamic equilibrium between $HNO_3(g)$ and particulate nitrate and neglecting (for the moment) solution non-idealities, it is easily shown that:

$$[NO_3^-]_{vol} = \frac{[H^+]}{[H^+] + K} \tag{2.6}$$

where $K = (H^*_{HNO_3} \cdot R \cdot T \cdot LWC)/(1000 \cdot P_0)$ in units of mole/kg; $H^*_{HNO_3}$ is the Henry's law equilibrium constant ($mole^2/kg^2/atm$) for the dissolution and dissociation of $HNO_3(g)$, R

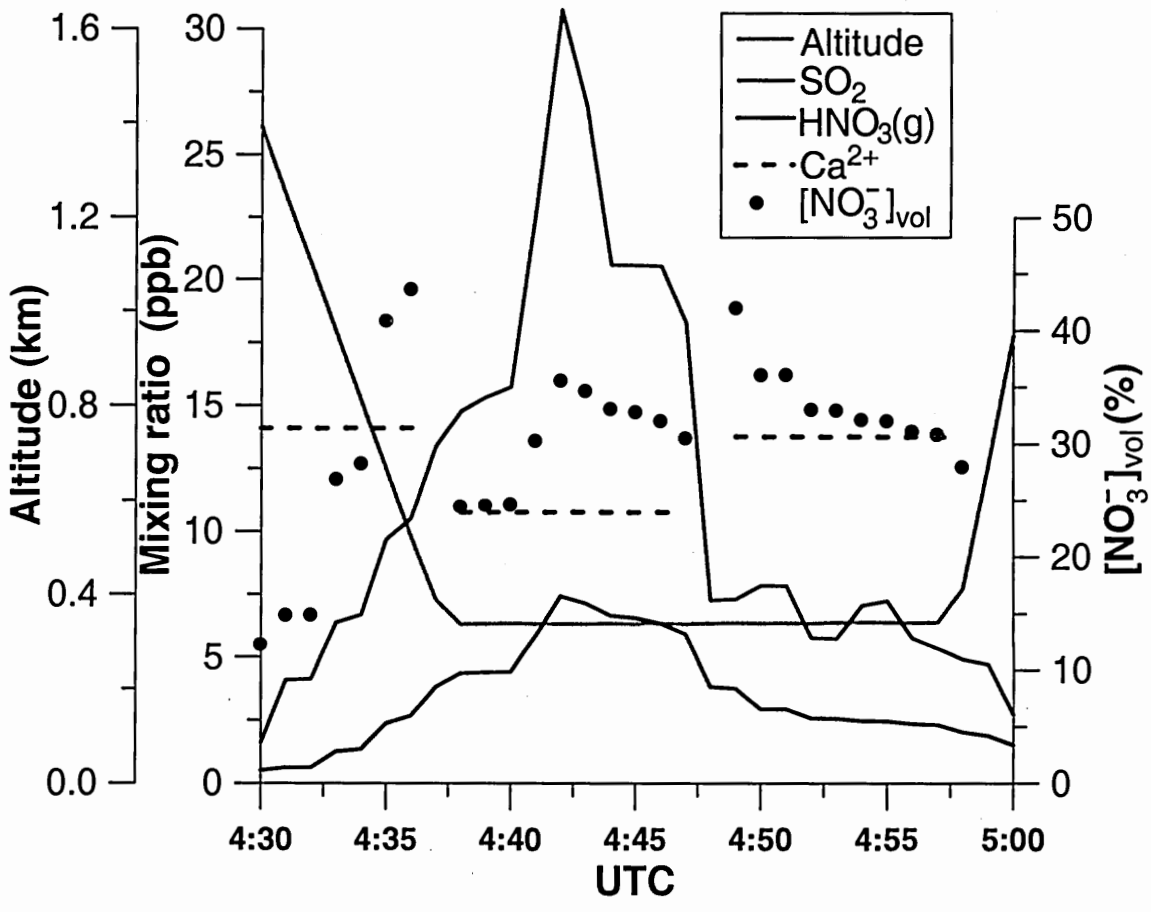

Figure 2.3 Flight altitude and observed concentrations of $SO_2(g)$, $HNO_3(g)$, and particulate Ca, as well as $[NO_3^-]_{vol}$ for highlighted portion of Flight 13.

is the universal gas constant (J/mole/K), T is ambient temperature (K), LWC is liquid water content of mineral dust particles (g/m^3air) and P_0 is the standard pressure (in Pa). The LWC was ~$9x10^{-4}$ g/m^3 air [Talbot et al., 2003] and T averaged 288 K. Adopting these values, along with the appropriate temperature dependence for $H^*_{HNO_3}$ [Clegg et al. 1998], we get K~0.15 mole/kg.

In Figure 2.4 $[NO_3^-]_{vol}$ calculated from Equation (2.6) is plotted as a function of pH. Also shown are the results of a more complete calculation using the thermodynamic model ISORROPIA [Nenes et al., 1998] which accounts for solution non-idealities. While the two calculations differ somewhat (most likely because of the influence of ionic strength effects), both calculations indicate that a pH of ~1 is needed to support the observed $[NO_3^-]_{vol}$-values. This value is within the previously estimated pH-range to make acid mobilization a viable mechanism for producing dissolved Fe in mineral dust.

Finally, we note that we found several other TRACE-P flight segments (DC-8 flights 9 and 16) that appear to have high dust and SO_2 content. During each of these segments, high values of $[NO_3^-]_{vol}$ were also inferred, suggesting that the dust was highly acidified in these cases as well.

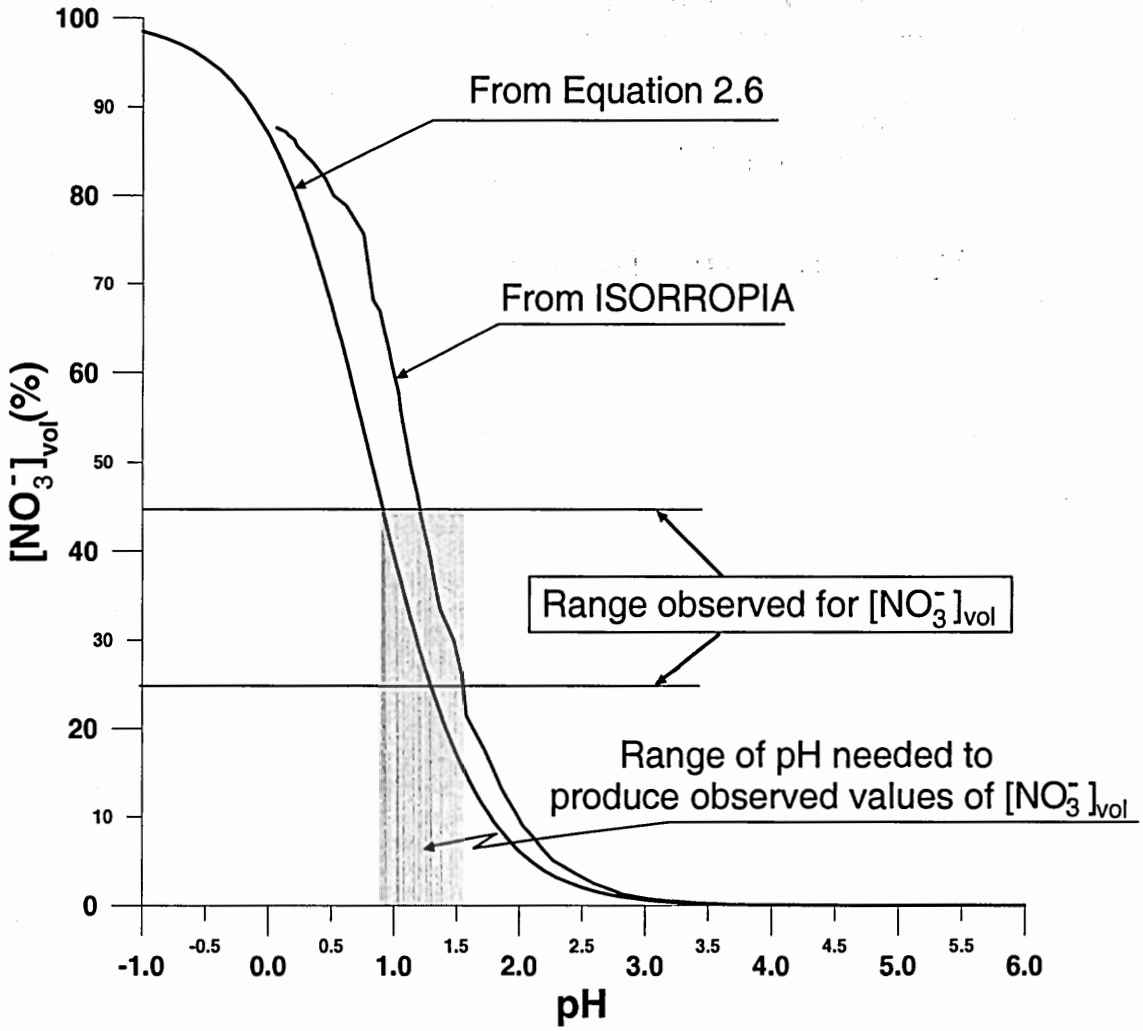

Figure 2.4 $[NO_3^-]_{vol}$ -value calculated as a function of pH.

2.5 Conclusion

Analysis of data collected on board of NASA DC-8 aircraft indicates that mineral dust plumes can be highly acidified when mixed with anthropogenic air pollutants advecting from the Asian continent. The range of pH obtained by considering nitrate volatilization indicates that acid dissolution of hematite could be a viable mechanism for mobilizing Fe in mineral dust plumes. There are only a few acids, commonly found in the atmosphere, that are capable of volatilizing HNO_3 and driving aerosol pH's below 2. One such acid is sulfuric acid. The high concentrations of SO_2 (see Figure 2.3) and nss-SO_4^{2-} [Jordan et al., 2003a] observed during the highlighted segment of Flight 13 suggest that there was in fact a considerable amount of sulfur oxide present in the plume. What is not clear is if the amounts of sulfur oxides that are typically found in polluted regions of East China and might be injected into a dust-containing plume are sufficient to produce a DIF of about 0.5 - 2%. Nor is it clear how variations in the amount of mineral dust and/or sulfur oxides contained in an advecting plume might affect the DIF. In the next Chapter of this thesis, we describe a Lagrangian box model that is then used to explore these issues.

CHAPTER 3

MODEL DESCRIPTION

3.1 Introduction

To further investigate the viability of acid mobilization as a mechanism to produce dissolved iron in mineral dust plumes, a Lagrangian box model of the gas and aqueous-phase chemistry of reactive compounds within an air mass containing mineral dust has been developed and used to simulate the evolution of DIF in three different cases of mineral dust advection from East Asia to the Pacific Ocean. In this chapter, the basic features of the model are described, and in Chapters 4 and 5 the results of the simulations are discussed.

In order to assess the relative importance of different parameters on dust Fe mobilization, the plumes were chosen to have varying chemical composition and physical properties (i.e. atmospheric pressure, temperature and relative humidity). Additionally, three separate plume trajectories over the North Pacific Ocean were simulated. These are referred here as: the *Boundary Layer* simulation; the *Mid-Troposphere* simulation; and the *Mid-Troposphere with Decent* simulation.

It is relevant to note at this point that iron solubilization in ambient aerosols can be a very complex process [see, e.g., Jickells and Spokes, 2001]. The solubility of iron oxides in acidic solutions can be strongly influenced by the presence organic (i.e., oxalate, acetate, formate and humic-like organic species, most as yet uncharacterized

[Jickells and Spokes, 2001]) and inorganic (i.e. SO_4^{2-}, Cl^-) complexing agents, as well as sunlight [Simnad and Smoluchowski, 1955; Faust and Hoffman, 1986; Behra and Sigg, 1990; Zhuang et al., 1992a; Zhu et al., 1992; Millero et al., 1995]. Concentrations of dissolved iron can be further controlled by complex redox cycling between highly insoluble ferric (Fe-III) and relatively more soluble ferrous (Fe-II) ions. However, the objective of developing the model discussed here is not to provide a comprehensive treatment of all the possible processes that can influence iron dissolution, but rather to: (1) assess if, given the basic kinetics and thermodynamics of Fe dissolution in acidic solution, acid mobilization represents a viable mechanism for producing bioavailable Fe in mineral aerosols; and (2) if so, how might the amounts of DIF in mineral aerosols be affected by changing levels of atmospheric pollutants.

3.2 Plume Trajectories and Conditions Adopted For Simulations

The gobi deserts of northern China and Mongolia (see Figure 3.1) are the primary source of the mineral aerosols that emanate from East Asia [Tegen and Fung, 1994; Parungo et al., 1994; Chang et al., 1996; Sun et al., 2001; Sugimoto, 2003] and, on the basis of an analysis of 40-years of dust-storm reports from China, Sun et al. [2001] estimated that a significant fraction of the mineral dust raised from this region passes near the Beijing (39°55′N, 116°25′E) metropolitan area before advecting over the Pacific Ocean. Beijing was therefore chosen as the nominal starting point for the plumes in the model simulations. At time t=0, the initial concentrations of Dust and pollutants in the plume to be simulated by the model are specified (based on observations of dust plume composition over the Beijing metropolitan area). The plume is then assumed to advect

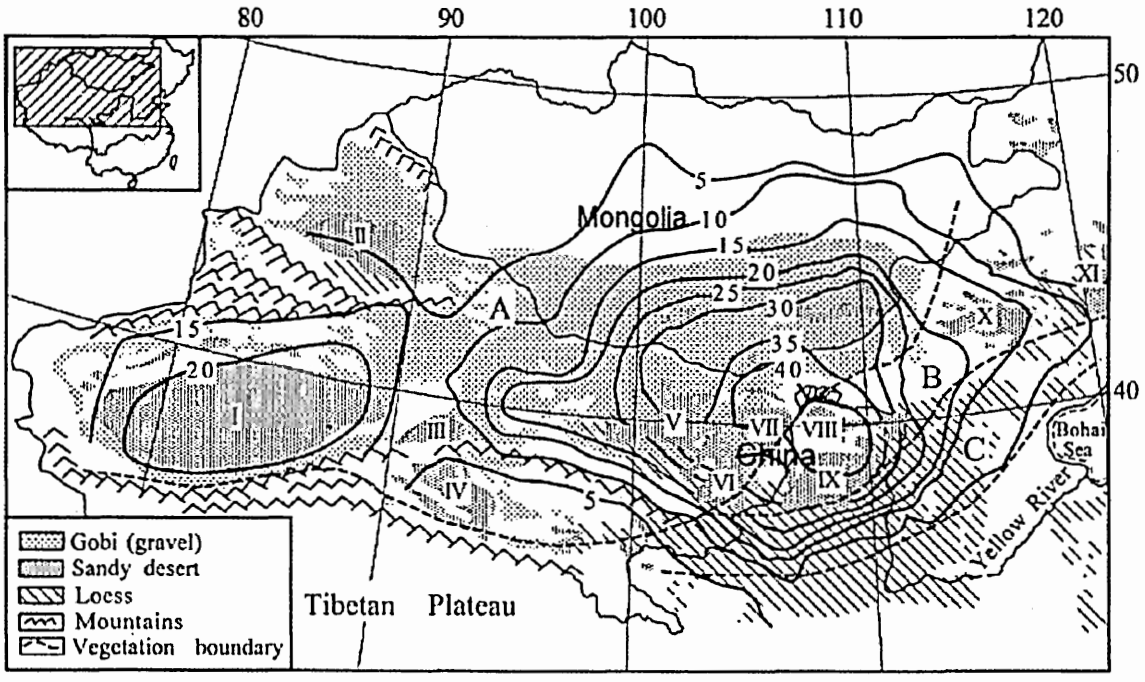

I. Taklimakan Desert II. Gurbantunggut Desert III. Kumtag Desert IV. Qaidam Desert
V. Badain Jaran Desert VI. Tengger Desert VII. Ulan Bhu Desert VIII. Hobq Desert
IX. Mu Us Desert X. Hunshandake Desert XI. Horqin Desert

Figure 3.1 Map of the major dust source regions in northern China and Mongolia. Contour lines are the isolines of the dust storms that occurred during the past 40 years (from Sun et al. [2001]).

from the Beijing area to the Pacific Ocean for a multiple-day period as the model simulates its gas-phase and particulate-phase chemical evolution. During this period of advection over the Pacific Ocean, Dust and pollutants are removed from the plume by depositional and mixing processes, but additional sources of pollutants (e.g., SO_2 from DMS oxidation) are neglected.

The specific trajectories assumed for the plumes in our model and their associated conditions of pressure, temperature, and relative humidity are based on the trajectories estimated for plumes that originated in the gobi deserts during actual, recorded dust storms using the Hybrid Single-Particle Lagrangian Integrated Trajectory (Hysplit4) model [Draxler and Rolph, 2003; Rolph, 2003]. In the sections below, the three trajectories considered in our simulations and their associated conditions are described.

3.2.1 *Boundary Layer* Simulations

Sun et al. [2001] suggest that the major fraction of dust raised from the gobi deserts gets entrained at low elevations and moves south eastward before departing the continent and advecting over the Yellow Sea and the Pacific Ocean. The advection altitude for these types of plumes is usually limited to the lower (<3000m) elevations [Sun et al., 2001; Chin et al., 2003; Lee et al., 2003; Jordan et al., 2003a]. The *Boundary Layer* simulations are intended to capture the essential features of these types of plumes.

For the *Boundary Layer* simulations, conditions were chosen to approximate those that likely applied to mineral-dust laden air masses that formed over the gobi deserts on April 9, 2001 during one of the most severe dust storms recorded over the region in recent time. The likely trajectory for the illustrative plume from this storm is

shown in Figure 3.2. The plume was assumed to originate over the gobi deserts of southern Mongolia (44°N, 106°E) at ~ 12 UTC on April 9, 2001 at an altitude of 2 km above ground. The location was chosen to roughly correspond to that indicated from Total Ozone Mapping Spectrometer Aerosol Index (TOMS AI) data to be the source of dust on April 9 and the altitude was chosen to ensure that the plume intersected the path of the NCAR C-130 aircraft as discussed below. In fact, during most storms the dust raised from the gobi deserts is entrained in the lowest 3000m of the atmosphere [Sun et al., 2001], so this altitude is reasonable. As illustrated in Figure 3.2, calculations using HYSPLIT4 suggest that the plume then moved eastward and southward across China and then out over the Pacific Ocean. After about 14-hours of transport, the plume moves off of the gobi-desert plateau and begins to descend in altitude. By the 18th hour of transport, HYSPLIT4 places the plume in the vicinity of Beijing metropolitan area. The model-predicted location of the plume in Beijing is consistent with both filter-based and lidar measurements in Beijing that indicated average boundary layer Dust concentrations of about 700 $\mu g/m^3$ on April 10, 2001 [Chen et al., 2001; Wild et al., 2003]. By the 30th hour, the plume-trajectory from HYSPLIT4 has traversed the Qingdao air shed and is about to advect over the Pacific Ocean. At the beginning of the third day, HYSPLIT4 predicts that the plume was located over the Yellow Sea. Confirmation of the accuracy of the HYSPLIT4 predictions at this point is provided by the fact that the trajectory of the plume between 2:00 and 3:00 UTC on April 11, 2001 overlaps with the time and location where mineral-dust laden air masses were intercepted and sampled by the NCAR C-130 aircraft operating in the region as part of the National Science Foundation sponsored ACE-Asia Project [Huebert et al., 2003]. The plume then moves in southerly direction,

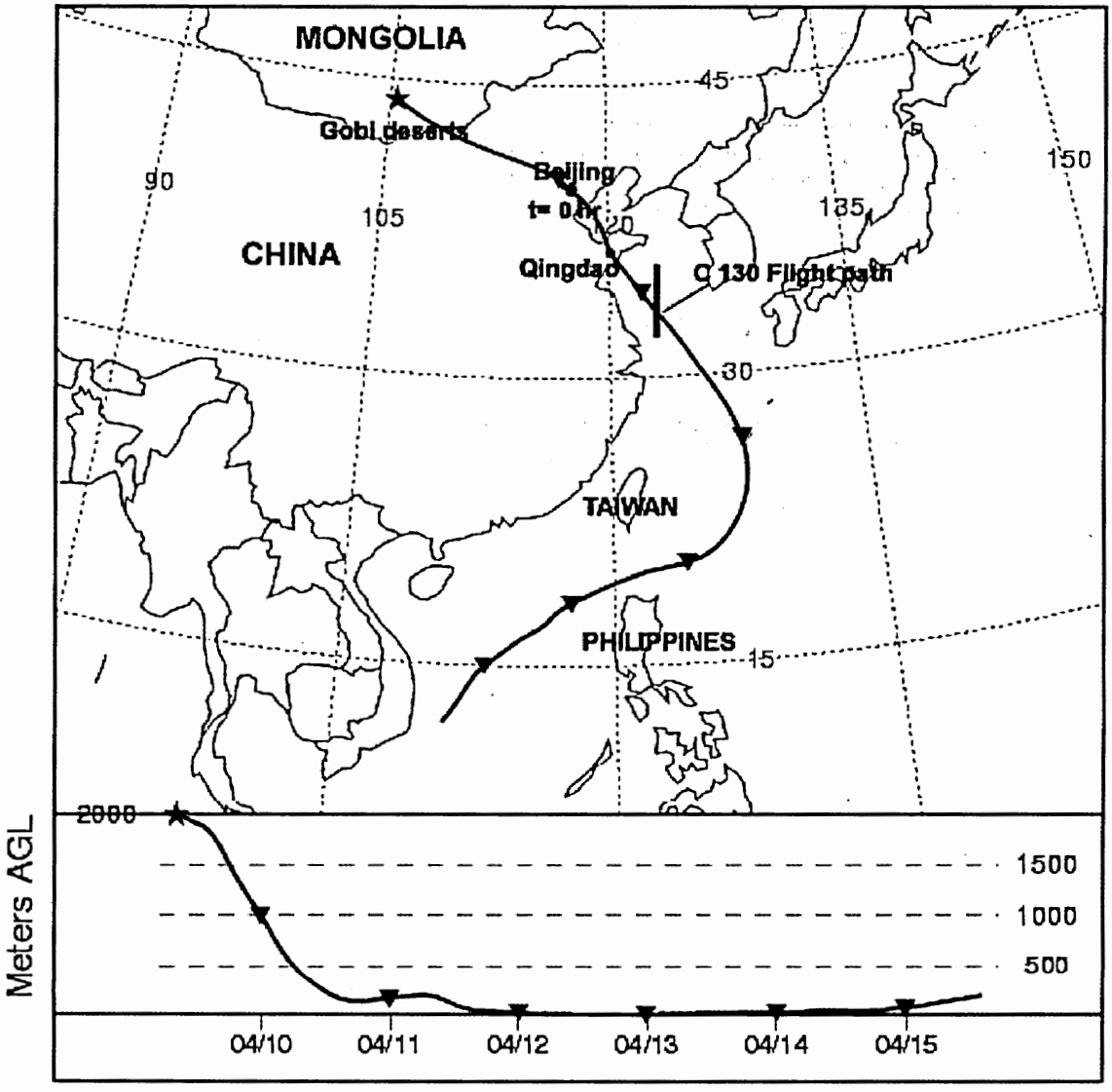

Figure 3.2 Possible trajectory for April 9, 2001 dust plume suggested by HYSPLIT4. Plume altitude is given in meters above ground level (AGL). The symbols are inserted at 24 hr intervals.

and by the fifth day after leaving the continent passes southward of 15°N, arriving in a region of the Pacific Ocean that is characterized as being under moderate iron-limitation stress [Fung et al., 2000].

The April 9th plume was chosen for the *Boundary Layer* simulations because it: (1) followed a low-altitude trajectory over the metropolitan areas of Beijing and Qingdao that provided ample opportunity to entrain air pollutants; (2) was sampled by the NCAR C-130 aircraft, thus providing some chemical constraints on the mode calculations; (3) remained in marine boundary layer during entire transport time over the Pacific Ocean; and (4) ultimately reached a region of the Pacific Ocean that is considered as being moderately iron-stressed, making its chemical evolution relevant to the issue of the production of dissolved Fe and its role in ocean productivity.

Figure 3.3 illustrates the resulting variations in pressure, temperature, and relative humidity as a function of model-simulated time prescribed for the calculations. (Recall that t=0 in model-simulated time corresponds to the actual time when the plume has passed near Beijing and is about to advect to the marine atmosphere overlying the Yellow Sea.) For completeness, I also illustrate the corresponding average temperature, humidity, and pressure observed by the NCAR C-130 for the dust-laden air masses sampled over the Yellow Sea on April 11, 2001. It can be seen that the physical parameters predicted by HYSPLIT4 for the approximate time and location when the NCAR C-130 measurements were made are quite consistent with the observations.

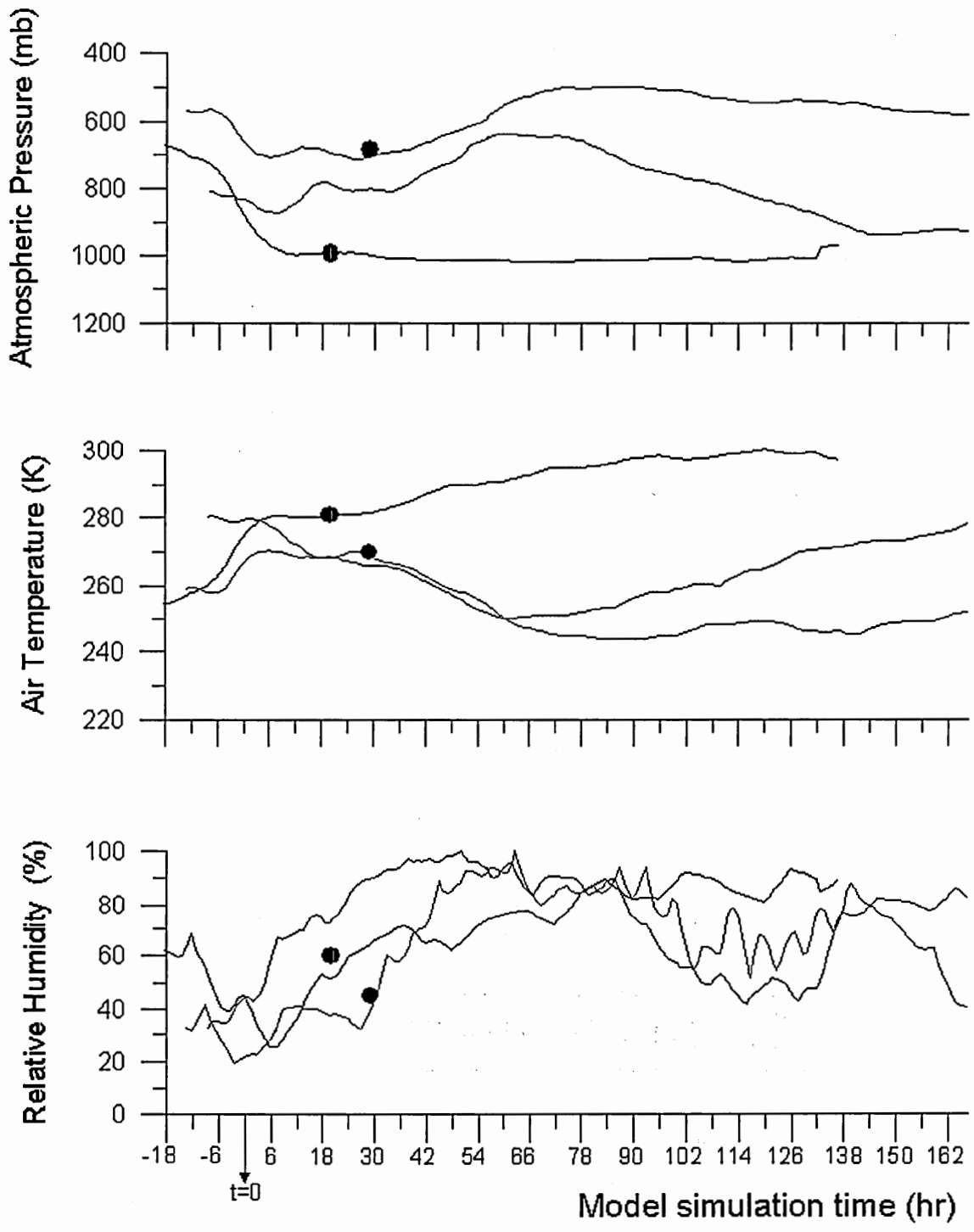

Figure 3.3 Variations in atmospheric pressure, temperature and relative humidity prescribed to *Boundary Layer* (black), *Mid-Troposphere* (blue) and *Mid-Troposphere with Descent* (red) Simulations. Solid circles show one hour averaged value measured on board of the NCAR C-130 aircraft and are correspondingly color coded.

3.2.2 *Mid-Troposphere* Simulations

While low altitude trajectories are common for plumes emanating from the gobi deserts, they are not conducive to the long-range transport of mineral dust. A more favorable trajectory for gobi-dust plumes to be engaged in trans-Pacific transport and reach Fe limited regions of the North Pacific Ocean would likely involve lifting of the dust into the mid-troposphere where it can be entrained into the westerly jet and rapidly transported to the east [Yienger et al., 2000; Husar et al., 2001; Murayama et al., 2001; Uno et al., 2001]. Sun et al [2001] estimated that about 10% of the dust storms that originate in gobi deserts follow such a mid-tropospheric path. (A good example is the gobi-dust storm event of April 19-20, 1998. During this episode, dust raised from the gobi deserts of Mongolia and China got entrained to the middle part of the troposphere, traversed the Beijing air shed and then was transported by the westerly jet stream across the North Pacific Ocean and reached West Coast of North America about 6 days later [Husar et al., 2001; Uno et al., 2001; Murayama et al., 2001; Sun et al., 2001].)

Such a high-altitude trajectory is adopted in the *Mid-Troposphere* simulation. The conditions for these simulations are based on the trajectory of a plume that formed over the gobi deserts on April 6, 2001; i.e., a few days earlier than that chosen for the *Boundary Layer* simulations. The dust produced on this day was actually part of an exceptionally strong multi-day dust storm [Liu et al., 2003].

Figure 3.4 shows TOMS AI image for April 6, 2001. This figure suggests that there were three dust source regions (with aerosol index ≥ 3) in the north Asia on this day: the Taklimakan desert and the gobi deserts of Mongolia and northern China. Out of these

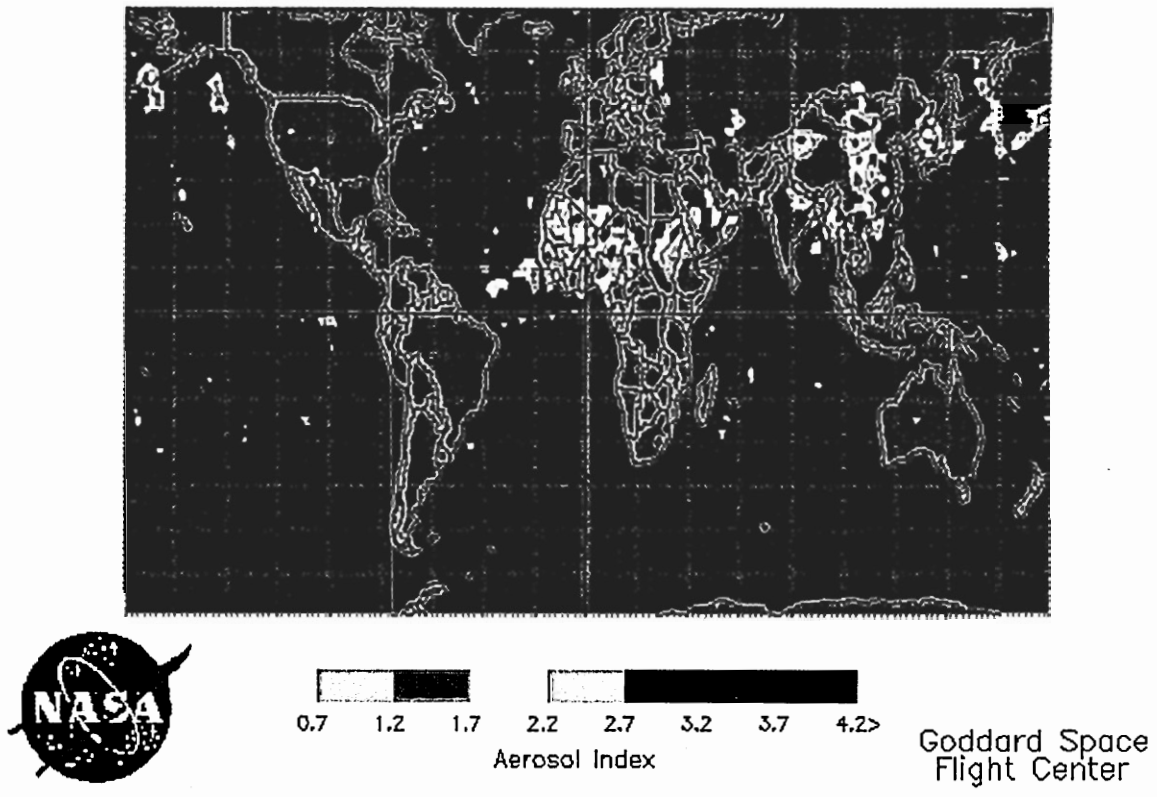

Figure 3.4 The earth probe TOMS aerosol index on April 6, 2001.

three source regions, our *Mid-Troposphere* simulations are based on dust originating from the gobi deserts of northern China, since the trajectory of plumes from this region on April 6, 2001 tended to traverse over the Beijing area and also overlapped with the time and location where mineral-dust laden air masses were intercepted and sampled by the NCAR C-130 aircraft (ACE-Asia Flight 5) over the Sea of Japan on April 8, 2001. The likely trajectory for the plume obtained from HYSPLIT4 is shown on Figure 3.5. The location of the plume (40.5°N, 103°E) was chosen to roughly correspond to that indicated by TOMS AI image and the initial altitude (3.3 km) was selected to ensure that April 6th plume intersected the path of the C-130 aircraft.

Figure 3.5 shows that the initial altitude for the April 6, 2001 dust plume predicted by HYSPLIT4 is somewhat higher than that chosen for the *Boundary Layer* simulations; a superposition of TOMS and Sea-viewing Wide Field-of-view Sensor (SeaWiFS) satellite observations for April 6 suggest that the dust plume in this case was initially lifted to about 3km [Herman et al., 1997; Alpert and Ganor, 2001; Husar et al., 2001]. (Note that the times for the HYSPLIT4-predicted plume trajectories are shown in UTC, while the TOMS AI data are collected at local solar noon.)

Figure 3.5 shows that April 6th plume, unlike the plume in the *Boundary Layer* simulation, followed more northerly path over the North Korea and the Sea of Japan. The predicted location of the Plume over the Sea of Japan between 8:00 - 9:00 UTC on April 8, 2001 is consistent with the NCAR C-130 observations of sharply increased concentrations of crustal elements at that location and time [Huebert et al., 2003; Lee et al., 2003].

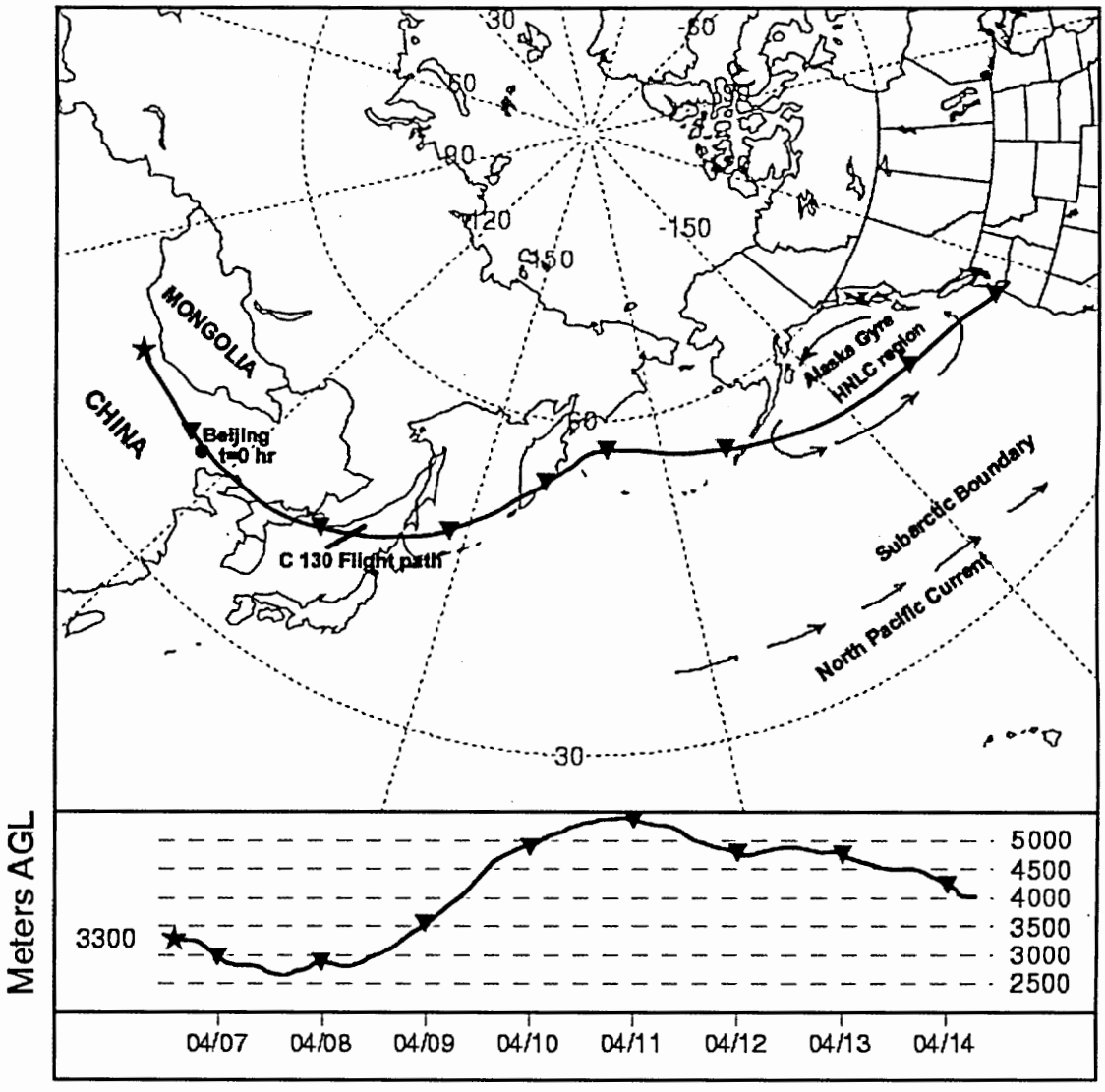

Figure 3.5 Possible trajectory for April 6, 2001 dust plume suggested by HYSPLIT4. Plume altitude is given in meters above ground level (AGL). The symbols are inserted at 24 hr intervals.

After leaving the continent, the plume rose to about 5km and moved in an easterly direction (see Figure 3.5), that brought it to the HNLC waters of subarctic North Pacific in about 5 days of transport time. Figure 3.5 also shows that the plume remained at mid-tropospheric altitudes (4 to 5 km) during its entire passage over North Pacific Ocean. Comparison of Figures 3.5 and 3.6 shows that plume trajectory predicted by HYSPLIT4 is consistent with TOMS AI data.

The resulting variations in pressure, temperature and relative humidity prescribed to *Mid-Troposphere* simulations are show on Figure 3.3. This figure shows that physical parameters predicted by HYSPLIT4 are consistent with the NCAR C-130 measurements.

The April 6, 2001 dust episode was chosen for the *Mid-Troposphere* simulations because it: (1) deposited large amounts of mineral dust to HNLC waters of subarctic North Pacific [Bishop et al., 2002] making its chemical evolution relevant to the issue of dust Fe deposition and marine ecosystem productivity in Fe stressed regions; and (2) was sampled by the NCAR C-130 aircraft, thereby providing detailed information on the chemical and physical properties of the plume for model tuning and evaluation.

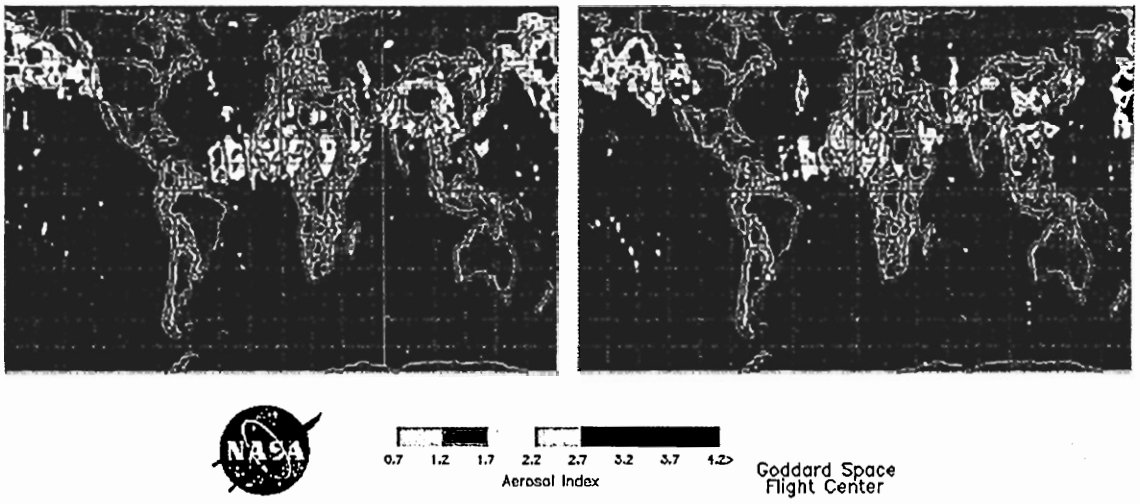

(a) (b)

Figure 3.6 The earth probe TOMS aerosol index on (a) April 12 and (b) April 13, 2001.

3.2.3 *Mid-Troposphere with Descent* Simulations

Because the plumes that follow high altitude, mid tropospheric path tend to be cold; and, as will be shown later, temperature has a significant impact on our results, an additional case is explored: the *Mid-Troposphere with Descent* simulation in which the plume eventually subsides into the marine boundary layer. For this case, a plume originating from the gobi deserts on March 12, 2001 was chosen, as discussed below.

TOMS AI data for March 13, 2001 (see Figures 3.7) indicate the presence of an average size dust storm advecting north of the Shenyang area in north-east China. Trajectory analysis using HYSPLIT4 suggests that this dust had originated at a relatively low altitude (~500 m) at ~17 UTC on March 12, 2001 in the Inner Mongolian part of the gobi deserts (40°N, 112°E) crossed the Beijing metropolitan area between 12 and 13th of March, reached the Shenyang region in the early morning hours of March 13, 2001. The location for the dust's origin predicted by HYSLPT4 can not be independently tested using TOMS AI data because the method is not able to detect low altitude dust [Herman et al., 1997; Husar, 2001]. However, theHYSPLIT4-predicted presence of a low-altitude dust plume over Beijing on the 12th and 13th of March, 2001 is consistent with lidar and ground-level filter-based measurements in Beijing that documented average boundary layer Dust concentrations of about 750 $\mu g/m^3$ during this interval [Chen et al., 2001; Wild et al., 2003].

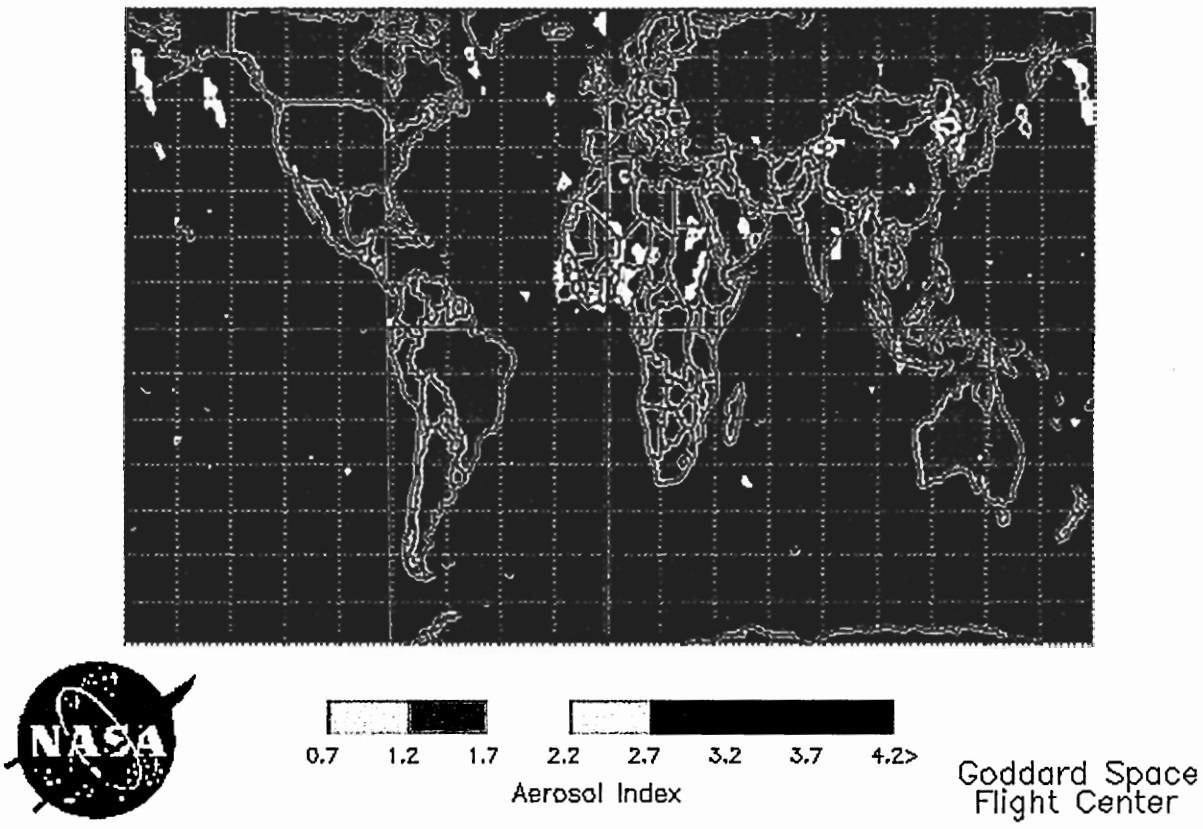

Figure 3.7 The earth probe TOMS aerosol index on March 13, 2001.

The likely trajectory for the dust plume predicted by HYSPLIT4 after leaving the Shenyang area is shown on Figure 3.8. Shortly after leaving the Beijing area, plume began ascending and continued to do so as it crossed the Sea of Japan and traveled northward toward the Bering Sea. The plume reached its maximum height of ~3 km on March 16, 2001 at which point HYSPLIT4 predicted a sharp change in its trajectory from the north east to south east with a subsequent slow descend. Figure 3.8 shows that on Mach 18th the plume descended to the marine boundary layer.

Figures 3.9 shows the plume's position over the North Pacific Ocean on March 19, 2001, where it was last detected by the TOMS satellite after about 6 days of travel time over the Pacific Ocean. (Note that, during its transport, the plume crossed International Date Line, so the TOMS AI image on March 19, 2001 actually corresponds to ~22 UTC of March 18, 2001 on the HYSPLIT4 trajectory).

Moderate Resolution Imaging Spectrometer (MODIS) data and the modeling results of NOAA-CIRES Climate Diagnostic Center suggest that on March 19, 2001 the plume got embedded either in or near a precipitating low-pressure system, which likely strongly depleted the dust via wet deposition. Thus the simulation was stopped on March 19, 2001. Figure 3.8 shows that the general location where the dust plume probably encountered precipitation and was washed out. This location is somewhat south of HNLC waters of the subarctic North Pacific, in a region known as a transitional zone between Subarctic Current (southern boundary of Alaska Gyre) and North Pacific Current [Martin et al., 1989; Harrison, 1999]. Although this part of North Pacific Ocean is not considered an HNLC region, per se, it is suggested, that marine productivity in this transitional zone is also Fe limited [Moore et al., 2002] (see more discussion in Chapter 1).

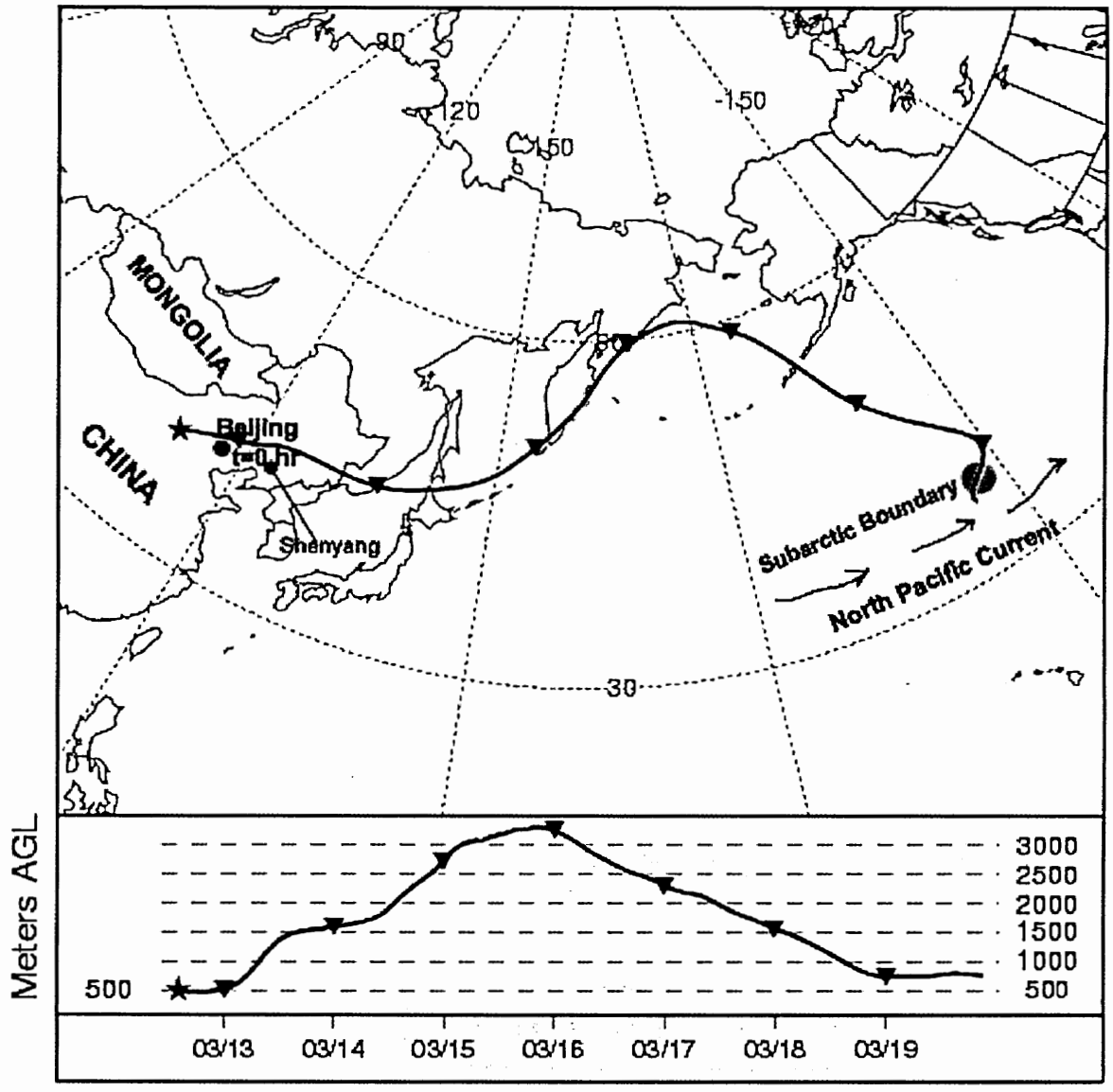

Figure 3.8 Possible trajectory for March 12, 2001 dust plume suggested by HYSPLIT4. Plume altitude is given in meters above ground level (AGL). The symbols are inserted at 24 hr intervals. Dark circle at the end of trajectory indicates the area where dust plume got embedded in precipitating low-pressure system.

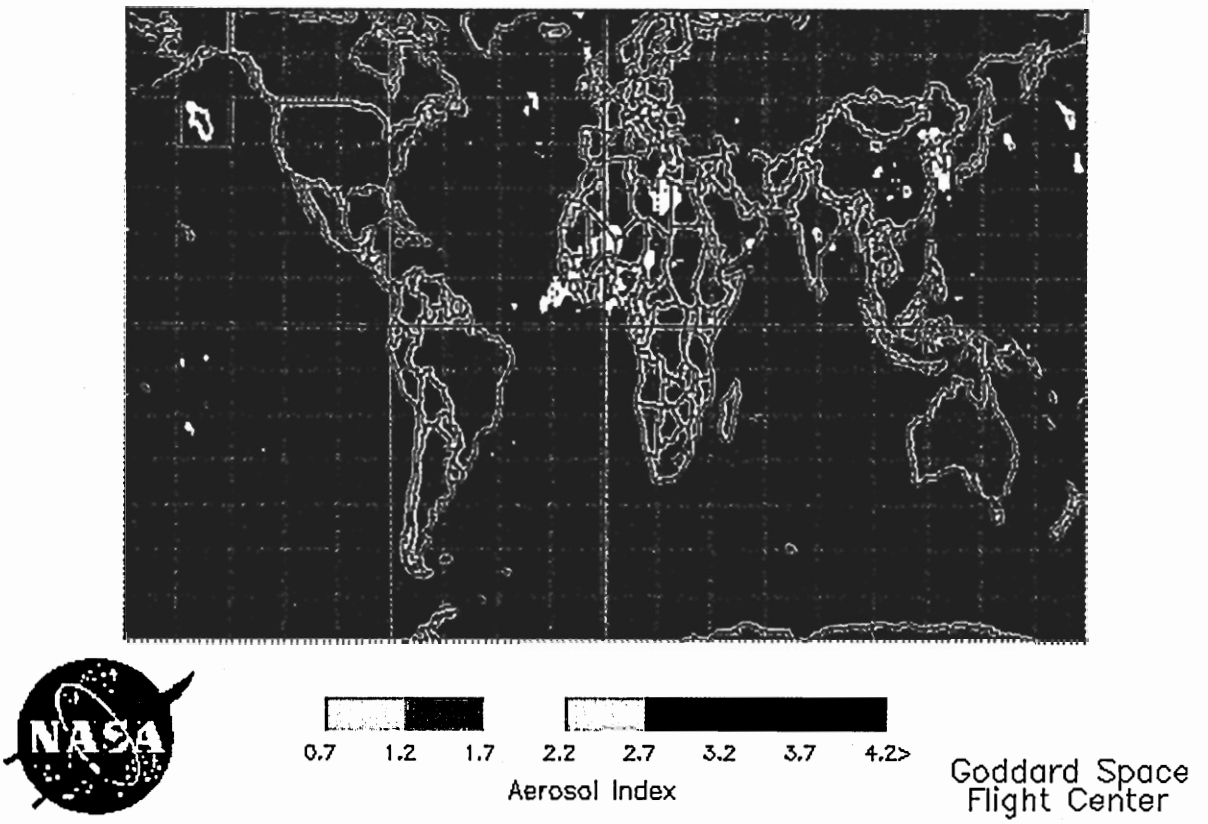

Figure 3.9 The earth probe TOMS aerosol index on March 19, 2001. The red square (coordinates: 160°W-140°W, 40°N-50°N) indicates the location of the plume over the North Pacific Ocean.

The March 12th dust episode was chosen for *Mid-Troposphere with Descent* simulation, because it: (1) was advected over Beijing metropolitan area at low-altitude providing sufficient opportunity to entrain air pollutants; (2) it followed the high-altitude trajectory over the North Pacific Ocean with subsequent descent to the marine boundary layer; and (3) ultimately reached an Fe-limited region of North Pacific Ocean, making the plume's chemical evolution relevant to the issue of dust Fe mobilization and its role in marine ecosystem productivity.

3.3 Species Simulated in Model

Table 3.1 lists the species simulated in our model along with information on the various chemical forms the species were allowed to attain. Note that each species "I" can have more than one chemical form and these forms can in turn be found in one of the three phases: (i) the gas phase, denoted by the subscript "g;" (ii) the aqueous phase within the aerosols, denoted by the subscript "aq;" and (iii) the solid phase within aerosols, denoted by the subscript "s."

Table 3.1 Species simulated in model

Symbol	Chemical forms allowed for species[1]
SO_2[2]	$(SO_2)_g$
S(VI)[3]	$(SO_4^{2-})_{aq}$, $(HSO_4^{2-})_{aq}$, $(FeSO_4^+)_{aq}$, $(AlSO_4^+)_{aq}$, $(CaSO_4)_s$, $(Na_2SO_4)_s$, $(NaHSO_4)_s$, $((NH_4)_2SO_4)_s$, $(NH_4HSO_4)_s$, $((NH_4)_3H(SO_4)_2)_s$
NO_x[2]	$(NO)_g$, $(NO_2)_g$
N(V)[4]	$(HNO_3)_g$, $(NO_3^-)_{aq}$, $(NH_4NO_3)_s$, $(NaNO_3)_s$
N(III)[5]	$(NH_3)_g$, $(NH_4^+)_{aq}$, $((NH_4)_2SO_4)_s$, $(NH_4HSO_4)_s$, $((NH_4)_3H(SO_4)_2)_s$, $(NH_4NO_3)_s$
Na[6], [7]	$(Na^+)_{aq}$, $(NaCl)_s$, $(NaNO_3)_s$, $(NaHSO_4)_s$, $(Na_2SO_4)_s$
Ca[7], [8]	$(Ca^{2+})_{aq}$, $(CaCO_3)_s$, $(CaSO_4)_s$
Fe[7]	$(Fe^{3+})_{aq}$, $(Fe(OH)^{2+})_{aq}$, $(Fe(OH)_2^+)_{aq}$, $(Fe(OH)_3^0)_{aq}$, $(Fe(OH)_4^-)_{aq}$, $(FeSO_4^+)_{aq}$, $(Fe(OH)_3)_s$
Al[9]	$(Al^{3+})_{aq}$, $(Al(OH)^{2+})_{aq}$, $(Al(OH)_2^+)_{aq}$, $(Al(OH)_3^0)_{aq}$, $(Al(OH)_4^-)_{aq}$, $(AlSO_4^+)_{aq}$
Dust[10]	See Sections 3.2.1.
Fine Aerosol Mode[6]	$[PM]_f$, the mass concentration ($\mu g\ m^{-3}$) of fine aerosols calculated as the sum of the concentrations of fine-mode S(VI), N(III) and N(V)
Coarse Aerosol Mode	$[PM]_c$, the mass concentration ($\mu g\ m^{-3}$) of coarse aerosols calculated as the sum of the concentrations of Dust, coarse-mode S(VI), N(III), and N(V), as well as mobilized, coarse mode Na, Ca, Fe, and Al.

(1) Subscript "g" denotes a gas-phase species, etc;
(2) Non-oxidative dissolution and condensation of SO_2 and NO_x(=NO+NO_2) on fine and coarse mode particles are neglected here;
(3) S(VI) is assumed to be nonvolatile;
(4) All species containing nitrogen in +5 oxidation state;
(5) All species containing nitrogen in -3 oxidation state;
(6) Concentration of K and Mg are expressed as equivalent Na (see text);
(7) Species are assumed to only arise from the dissolution of minerals from dust and therefore are only treated as being in the coarse aerosol mode;
(8) For all other Ca-containing compound (i.e., $Ca(NO_3)_2$), Ca is expressed as equivalent Na (see text);
(9) Under highly acidic conditions concentration of Al_{diss} is expressed as equivalent Na;
(10) Dust assumed to only be present in the coarse mode aerosol.

As indicated in Table 3.1, aerosols are assumed to have two size modes: (i) a coarse particle mode, dominated by mineral dust; and (ii) a fine particle mode, dominated by pollutants such as sulfate and nitrate. This separation reflects the contrasting formation mechanisms and thus chemical compositions that are typical of fine and coarse mode aerosols in the atmosphere: fine mode particles tend to arise from air pollution and other combustion processes either through direct emission or gas-to-particle conversion; while coarse particles are generally produced by mechanical processes such as soil erosion and sea-salt formation [Song and Carmichael, 1999].

Coagulation between the two modes is neglected in the model [Wexler et al., 1994] and thus mass transport between the coarse and fine modes only occurs through the gas phase. For simplicity, each mode is treated as being monodisperse. The fine-mode diameter, D_f is set at 0.12 μm, and the coarse-mode diameter, D_c is set at 1.7 μm. These diameters correspond to the peak diameters observed for these two modes during the ACE-Asia and TRACE-P experiments [Clarke et al., 2003].

3.4 Initial Plume Composition

Recall that time t = 0 in our model simulations corresponds to the starting point of the plume trajectory when, after the plume has already entrained an initial loading of air pollutants as well as Dust, it leaves the Beijing area and begins its long-range transport over the Pacific Ocean. The initial amounts of Dust and pollutants assumed to be in the plumes at t = 0 and used in the box model calculations are summarized in Chapters 4 and 5 and listed in Tables 4.1 and 5.1.

3.4.1 Initial Composition of Mineral Dust Transported in Plume

The initial mineral Dust content of the coarse particle mode is designed to grossly mimic that of the transportable fraction of gobi desert soils in Mongolia and northern China (i.e., the fraction of the soil particles that can be uplifted and transported over large distances by wind). It should be borne in mind, however, that the gobi deserts cover about a million sq km of north central China and Mongolia [Parungo et al., 1994] and the mineralogical composition of the soils changes considerably over this expanse [Claquin et al., 1999; Gong et al., 2003]. So, the dust composition assumed here should be considered illustrative. Sensitivity calculations are presented (in Chapter 4) to assess how reasonable variations in the assumed dust composition affect our calculations.

Measurements of mineral dust composition and mass-size distribution over the Yellow Sea and western North Pacific Ocean during ACE-Asia and TRACE-P suggest that the composition of mineral dust from East Asia is relatively invariant to the mineral dust loadings in the atmosphere [Clarke et al., 2003]. We therefore assume the same initial mineralogical dust composition for the Standard and Low Dust model simulations.

The U.S. Department of Agriculture (USDA) classification system classifies soil particles according to their size into three major textile classes: sand (2.0-0.05 mm), silt (0.05-0.002 mm), and clays (<0.002 mm) [Soil Survey Staff, 1998]. In general, both the mineral composition and transportable fraction of each class can vary significantly from the others [Leinen et al., 1994]. The mineralogical composition of the mineral dust produced from a given soil can be obtained using the following formula:

$$X_i^{air} = \frac{X_i^{sand}\beta_{sand}F_{sand} + X_i^{silt}\beta_{silt}F_{silt} + X_i^{clay}\beta_{clay}F_{clay}}{\beta_{sand}F_{sand} + \beta_{silt}F_{silt} + \beta_{clay}F_{clay}} \qquad (3.1)$$

where X_i^{air} is the weight percent of mineral "i" in the mineral dust transported in the atmosphere, X_i^{sand}, X_i^{silt} and X_i^{clay} are the weight percents of mineral "i" in sand, silt and clay fractions of the soil, respectively, β_{sand}, β_{silt}, and β_{clay} are the transportable fractions of sand, silt, and clay in the surface soil, respectively, and F_{sand}, F_{silt}, F_{clay} are the weight percent of sand, silt, and clay in the surface soil, respectively. It can be easily seen from Equation (3.1) that for the soils containing only one type of textural-classes, the mineralogical composition of the transportable fraction is exactly equal to the mineralogical composition of the soil. However, if more than one textural class is present, than mineralogical composition of the transportable fraction of the soil is determined by the magnitudes of β and F.

The surface soils of gobi deserts have been found to be about 50% sand, 30% silt, and 20% clay [Webb et al. 2000] (i.e., $F_{sand} = 0.5$, $F_{silt} = 0.3$ and $F_{clay} = 0.2$). However, sand particles are relatively large, are difficult to uplift and tend to be rapidly removed from the atmosphere by gravitational settling, and thus, $\beta_{sand} \sim 0$ and the transportable fraction is generally limited to the clay and silt fractions [Duce, 1995; Tegen and Fung, 1994; Ginoux et al., 2001]. Moreover, measurements of the size spectra of mineral dust aerosols [e.g. Prospero and Bonatti, 1969; Clarke et al., 2003] show that during a dust storm, the mass of clay-containing particles (with diameter, D_p between 0.2-2 μm) is generally 1-2 orders of magnitude smaller than mass of silt-containing particles (D_p between 2 to 50 μm). We therefore assume $\beta_{clay} = 0.1$ and $\beta_{silt} = 1$.

Table 3.2 lists our estimates of the weight percent concentrations of the key minerals in the silt and clay fractions of gobi desert soils obtained from a synthesis and

Table 3.2 Concentration of major minerals in the soil and clay fractions of surface soils in the gobi deserts and in mineral dust originating from these soils (% by weight)

Mineral	In soil [1]		In mineral dust and used as initial condition for model simulation [2]
	in silt	% in clay	
Anhydrite $CaSO_4$	6	0	6
Calcite $CaCO_3$	12	0	11
Albite $NaAlSi_3O_8$	18	8	17
Microcline $KAlSi_3O_8$	8	5	8
Illite [3] $K_{0.6}Mg_{0.25}Al_{2.3}Si_{3.5}O_{10}(OH)_2$	18	42	20
Smectite/ Montmorillonite [3] $Na_{0.6}Al_{1.4}Mg_{0.6}Si_4O_{10}(OH)_2 \cdot 4H_2O$	7	15	8
Hematite [4] Fe_2O_3	5	8	5
Quartz SiO_2	21	10	20
Kaolinite $Al_2Si_2O_5(OH)_4$	5	12	5
TOTAL	100	100	100

(1) The mineralogical composition of silt and clay in gobi desert soils listed here is largely based on the data from Hseung and Jackson [1952], Leinen et al. [1994], and Claquin et al. [1999], except as noted below;

(2) Calculated using Equation (3.1) assuming $F_{silt} = 0.3$, $F_{clay} = 0.2$, $\beta_{silt} = 1$, and $\beta_{clay} = 0.1$;

(3) The chemical composition of illite and montmorillonite depends on the extent to which Si and Al are replaced by other cations such as Na, K, and Mg [Wonik, 2001; Deer et al., 1998]. The compositional formulas for illite and montmorillonite used here were determined by keeping the fundamental unit of the structure (so-called 2:1 layered structure) and adding in Na, K, and Mg to the minerals so that the average overall concentration of Na, K, and Mg in gobi desert soils was equal to 2.1%, 1.9%, and 0.9%, respectively [Nishikawa et al., 1999]. It should be noted that the resulting compositions used here for illite and montmorillonite fall within the range of compositions typically observed for these minerals [Wonik, 2001; Deer et al., 1998];

(4) The weight percents for hematite in silt and clay was obtained by assuming that hematite is the only mineral containing significant amounts of Fe (see discussion in Section 3.4.9), and requiring that the weight percent of Fe in mineral dust was 3.5% in accordance with the observations of mass [Taylor and McLennan, 1985; Duce and Tindale, 1991]. Since Fe (II) can substitute for Mg and Fe(III) for Al in some clay silicates [Coey, 1988], the assumption that hematite is the only Fe-containing mineral in soils is not strictly valid. Nevertheless, the Fe content in clay minerals is usually

small [Murad and Fischer, 1988] and thus for the purposes of these illustrative calculations can be neglected.

Table 3.3 Composition of key elements in mineral dust assumed for model simulations (% weight)

Element	% by weight
Al	8.1
$Ca_{calcite}$	4.4
$Ca_{anhydrite}$	1.8
Fe	3.5
K	2.4
Na	1.7
Mg	0.5

analysis of data on gobi desert soils and dust in the literature. Also shown are the resulting mineral abundances in mineral dust, derived from Equation (3.1). Table 3.3 presents the percent weight abundances of various key elements in mineral dust that result from the mineral abundances listed in Table 3.2.

3.5 Mass Balance Equations for Determining Species' Concentrations

Within the model, the concentrations of relevant gas- and particulate-phase species in the advecting plume are determined by solving a system of coupled continuity equations. In its most general form, this equation is:

$$\frac{d[I]}{dt} = P_i - D_i - \alpha_{dep}[I] F_{frac} - \alpha_{dil}([I] - [I_{amb}]) \qquad (3.2)$$

where [I] is the concentration of species "I" within the plume (in units of mole/m^3), P_i and D_i are in-plume production and destruction rates for "I" species (in units of mole/m^3/s), α_{dil} is a first-order rate constant for dilution of the plume due to mixing with ambient air, and I_{amb} is the assumed ambient concentration of species "I," α_{dep} is a first-order rate constant for loss from the plume of species contained within coarse mode aerosols due to dry deposition, F_{frac} is the fraction of species "I" contained within coarse mode aerosols. (Note that fine particles are assumed to not have a significant deposition velocity and thus the components of this mode are not lost via an α_{dep}-like parameterization.)

It should be noted that Equation 3.2 ignores removal of gas-phase and particle species via wet removal. However, this should not represent a significant problem for the model calculations presented here, since the plumes we consider did not encounter precipitation events during the time intervals simulated by the model. Indeed, the trans-Pacific transport of dust from East Asia is not usually associated with wet removal [Husar et al., 2001].

Tables 3.5, 3.6, 3.7, 3.8 and 3.9 list the constants used to simulate the relevant gas-phase, heterogeneous and aqueous-phase reactions and equilibria that form the basis for calculating the P_i and D_i terms in Equation (3.2). A more detailed discussion of the specific mass balance equation used for each of the species listed in Table 3.1 follows below.

Table 3.4 Heterogeneous and gas phase reactions included in model

№	Reaction	Rate constant	Units	Source/note
RG1	$SO_2+OH(g) \xrightarrow{M} H_2SO_4+\ldots$ (1)	$k_0=3.0\times10^{-31}\times(300/T)^{3.3}$ $k_\infty=1.5\times10^{-12}$	$cm^6molecule^{-2}s^{-1}$ $cm^3molecule^{-1}s^{-1}$	Sander et al. [2003]
RG2	$SO_2 \xrightarrow{dust} SO_4^{2-}(aq)$	$(9\pm4)\times10^{-8}$	$m^3\mu g^{-1}s^{-1}$	Herring et al. [1996]
RG3	$NO_2+OH \xrightarrow{M} HNO_3(g)$ (1)	$k_0=2.5\times10^{-30}\times(300/T)^{4.4}$ $k_\infty=1.6\times10^{-11}\times(300/T)^{1.7}$	$cm^3molecule^{-1}s^{-1}$	Sander et al. [2003] /See text
RG4	$NO_2 \xrightarrow{dust} NO_3^-(aq)$	$(10\pm10)\times10^{-8}$	$m^3\mu g^{-1}s^{-1}$	Herring et al. [1996]
RG5	$NO_2+O_3 \xrightarrow[aerosol]{night} 2HNO_3(aq)$	$1.2\times10^{-13}\times\exp(-2450/T)$	$cm^3molecule^{-1}s^{-1}$	
RG6	$NO+O_3 \rightarrow NO_2+O_2$	$2.0\times10^{-12}\times\exp(-1400/T)$	$cm^3molecule^{-1}s^{-1}$	Sander et al. [2003]
RG7	$NO_2+h\nu \rightarrow NO+O$		s^{-1}	See text

(1) The rate coefficient for this reaction is obtained as follows:

$$k(T)=\left\{\frac{k_0(T)[M]}{1+k_0(T)[M]/k_\infty(T)}\right\}0.6^{\left\{1+[\log_{10}(k_0(T)[M]/k_\infty(T))]^2\right\}^{-1}}$$

Table 3.5 Additional aqueous-phase reactions added to modified version of ISORROPIA and their equilibrium constants

№	Equilibrium reaction	Equilibrium constants[(1)]				
		K^0 (298.15K)	*a*	*b*	units	Source
RAQ1	$CO_2(aq) \rightleftharpoons CO_2(g)$	3.404×10^{-2}	8.1858	-28.9307	mol/kg/atm	Meng et al. [1995]
RAQ2	$HCO_3^- + H^+ \rightleftharpoons CO_2(aq)$	4.299×10^{-7}	3.0821	31.8139	mol/kg	Meng et al. [1995]
RAQ3	$CO_3^{2-} + H^+ \rightleftharpoons HCO_3^-$	4.678×10^{-11}	5.9908	38.8440	mol/kg	Meng et al. [1995]
		K_{eq}				
RAQ4	$CaSO_4 \cdot 2H_2O(s) \rightleftharpoons Ca^{2+}(aq) + SO_4^{2-}(aq) + 2H_2O$	4.319×10^{-5}			mol^2/kg^2	Meng et al. [1995]
RAQ5	$Fe(OH)_3(s) + 3H^+ \rightleftharpoons Fe^{3+} + 3H_2O$	9.1×10^{3}			mol/kg	Stumm and Morgan [1981]
RAQ6	$Fe^{3+} + SO_4^{2-} \rightleftharpoons FeSO_4^+$	1.9×10^{4}			mol/kg	Millero et al. [1995]
RAQ7	$FeCl^{2+} \rightleftharpoons Fe^{3+} + Cl^-$	1.9×10^{1}			mol/kg	Millero et al. [1995]
RAQ8	$Fe^{3+} + H_2O \rightleftharpoons FeOH^{2+} + H^+$	6.46×10^{-3}			mol/kg	Stumm and Morgan, 1981
RAQ9	$Fe^{3+} + 2H_2O \rightleftharpoons Fe(OH)_2^+ + 2H^+$	2.14×10^{-6}			mol/kg	Stumm and Morgan [1981]
RAQ10	$Fe^{3+} + 3H_2O \rightleftharpoons Fe(OH)_3^0 + 3H^+$	1.59×10^{-12}			mol/kg	Millero et al. [1995]
RAQ11	$Fe^{3+} + 4H_2O \rightleftharpoons Fe(OH)_4^- + 4H^+$	2.51×10^{-22}			mol/kg	Stumm and Morgan [1981]
RAQ12	$Al(OH)_3(s) + 3H^+ \rightleftharpoons Al^{3+} + 3H_2O$	1.7×10^{10}			mol/kg	Lindsay [1979]; Bi et al. [2001a]
RAQ13	$Al^{3+} + SO_4^{2-} \rightleftharpoons AlSO_4^+$	1.0×10^{3}			mol/kg	Bi et al. [2001a]
RAQ14	$Al^{3+} + H_2O \rightleftharpoons AlOH^{2+} + H^+$	1.0×10^{-5}			mol/kg	Bi et al. [2001a]
RAQ15	$Al^{3+} + 2H_2O \rightleftharpoons Al(OH)_2^+ + 2H^+$	1.0×10^{-10}			mol/kg	Bi et al. [2001a]
RAQ16	$Al^{3+} + 3H_2O \rightleftharpoons Al(OH)_3^0 + 3H^+$	1.0×10^{-15}			mol/kg	Lindsay [1979]; Stumm and Morgan [1981]
RAQ17	$Al^{3+} + 4H_2O \rightleftharpoons Al(OH)_4^- + 4H^+$	1.0×10^{-23}			mol/kg	Bi et al. [2001a]

(1) For RAQ1, RAQ2, and RAQ3

$$K_{eq} = K^{\circ}\exp\left\{a\left(\frac{T_o}{T}-1\right)+b\left(1+\ln\left(\frac{T_0}{T}\right)-\frac{T_0}{T}\right)\right\}, \text{ where } T_0 = 298.15K;$$

All other K_{eq}'s assumed to be temperature independent and are based on experimental data at 298 K.

Table 3.6 Equilibria describing the dissolution/precipitation of minerals contained in dust

№	Equilibrium reaction	Equilibrium constants[1]	
		K_{eq} (mol^2/kg^2)	Source/note
REQ1	$Calcite \rightleftharpoons Ca^{2+} + CO_3^{2-}$	4.959×10^{-9}	Meng et al. [1995]
REQ2	$Albite + 4H^+ + 4H_2O \rightleftharpoons \Leftrightarrow Na^+ + Al^{3+} + 3H_4SiO_4^0 \rightleftharpoons$	1.6×10^3	Lindsay [1979]
REQ3	$Microcline + 4H^+ + 4H_2O \rightleftharpoons K^+ + Al^{3+} + 3H_4SiO_4^0$	1×10^1	Lindsay [1979]
REQ4	$Illite + 6H^+ + 4H_2O \rightleftharpoons 0.4K^+ + 0.25Mg^{2+} + 1.7Al^{3+} + 4H_4SiO_4^0$	2.24×10^{10}	Lindsay [1979]
REQ5	$Smectite + 4H^+ \rightleftharpoons 0.8Na^+ + 0.4Mg^{2+} + 0.8Al^{3+} + 4H_4SiO_4^0$	4.79×10^2	Lindsay [1979]
REQ6	$Kaolinite + 6H^+ \rightleftharpoons 2Al^{3+} + 2H_4SiO_4^0 + H_2O$	2.8×10^5	Lindsay [1979]
REQ7	$Hematite + 6H^+ \rightleftharpoons 2Fe^{3+} + 3H_2O$	4.4×10^{-1}	Blesa et al. [1994]

(1) All K_{eq}'s are for 298 K.

Table 3.7 Constants used to calculate mineral dissolution/precipitation rates using Equation (3.24)

№	Mineral	Rate constant K_r ($mol_{mineral\ dissolved}/m^2/sec$)	m	A_i ($m^2\ g^{-1}$)	W_i g(mineral) /g(dust)	Source
RS1	Calcite	$7.0x10^{-2}$ exp[1200(1/298-1/T)]	1	0.1	11	Morse and Arvidson [2002]; Alkattan et al. [1998]; Chou et al. [1988]; Sjöberg [1976]
RS2	Albite	$2.4x10^{-10}$exp[7200(1/298-1/T)]	0.5	1.0	17	Blum and Stillings [1995]; Hodson [1999]
RS3	Microcline	$2.0x10^{-10}$exp[6600(1/298-1/T)]	0.5	1.0	8	Blum and Stillings [1995]; Hodson [1999]
RS4	Illite	$1.3x10^{-11}$exp[6700(1/298-1/T)] (1)	0.39	90	20	Nagy [1995]; Tessier [1990]; Skopp [2000]
RS5	Smectite	$8.1x10^{-12}$exp[6700(1/298-1/T)] (1)	0.3	300	8	Nagy [1995]; Tessier [1990]; Skopp [2000]
RS6	Kaolinite	$4\ x10^{-11}$exp[6700(1/298-1/T)]	0.1	20	5	Carroll and Walther [1990]; Nagy [1995]; Skopp [2000].
RS7	Hematite	Stage I (0 to 0.8% of total oxide dissolved) $4.4x10^{-12}$exp[$9.2x10^3$(1/298-1/T)]	0.5	100	5	Azuma and Kametani [1964]; Blesa et al. [1994]; Cornell and Schwertmann [1996]; Zinder et al. [1986]; Skopp [2000]
		Stage II (0.8 to 40% of total oxide dissolved) $1.8x10^{-11}$exp[$9.2x10^3$(1/298-1/T)]				
		Stage III(40 to 100% of total oxide dissolved) $3.5x10^{-12}$exp[$9.2x10^3$(1/298-1/T)]				

(1) Average activation energy for kaolinite [Carroll and Walter, 1990] is used.

Table 3.8 Average values of q-parameter for the species used in model (apart from those in ISORROPIA)

Species	q	Source/Note
$FeCl_3$	0.424	(1)
$Fe(OH)Cl_2$	6.04	(1)
$Fe(OH)_2Cl$	7.05	(1)
$FeSO_4Cl$	7.05	(2)
$AlCl_3$	1.92	Kusik and Meissner [1978]
$MgCl_2$	2.9	Kusik and Meissner [1978]
$Fe_2(SO_4)_3$	0.43	(3)
$Al_2(SO_4)_3$	0.369	Kusik and Meissner [1978]
$MgSO_4$	0.15	Kusik and Meissner [1978]
$Fe(NO_3)_3$	1.51	(4)
$Al(NO_3)_3$	1.51	(4)
$Mg(NO_3)_2$	2.32	Kusik and Meissner [1978]

(1) Parameters for Fe(III) chlorides were calculated from Table 4 of Millero et al. [1995] by using definition of mean binary activity coefficient (γ_{ij}) for a single-salt solution containing an i-j ion pair: $\gamma_{ij}^{\nu_i+\nu_j} = \gamma_i^{\nu_i} \cdot \gamma_j^{\nu_j}$ where ν_i and ν_j are stoichiometric coefficients [Robinson and Stokes, 1959]. After the value of activity coefficient for the electrolyte was determined at some temperature and ionic strength the associated parameter q was calculated using Kusik and Meissner [1978] equations;

(2) Following Millero et al. [1995] same activity coefficients for $FeSO_4Cl$ and $Fe(OH)_2Cl$ were used;

(3) Value for $Cr_2(SO)_4$ from Kusik and Meissner [1978] was used;

(4) Value for $Cr(NO_3)_3$ from Kusik and Meissner [1978] was used.

3.5.1 Mass Balance for Dust and Estimation of Alpha Terms

Dust has no in-plume production and destruction terms and a negligible ambient concentration, and thus applying Equation (3.2) to Dust we obtain:

$$d[Dust]/dt = -\alpha_{dep}\,[Dust] - \alpha_{dil}\,[Dust] \qquad (3.3)$$

As described below, we can use this equation in combination with observations of Dust concentrations during the dust storm of April 9, 2001 (discussed in the *Boundary Layer* simulation) to estimate the values for α_{dep} and α_{dil}.

3.5.1.1. *Parameterization for Deposition:* Measurements and modeling results of dust transport show that the size composition of dust particles close to the source is non-uniform and dominated by the relatively large particles with diameter, $2 < D_p \leq 20$ μm [Tegen and Fung, 1994; Ginoux et al., 2001; Zender et al., 2003]. (Particles with the diameter > 20 μm rapidly fall out of the plume [c.f., Tegen and Fung, 1994] and therefore, as discussed earlier, are not considered in the model as part of the transportable dust fraction.) As the mineral dust advects, however, the larger particles settle out (i.e., they are deposited), leaving behind the smaller sized particles in the plume [Arimoto et al., 1997]. Thus we would expect α_{dep} to decrease as a function of transport time. To account for this variation, we assume that α_{dep} has the following form:

$$\alpha_{dep} = C_{dep} \cdot \xi(t) \qquad (3.4)$$

where C_{dep} is a constant determined from the observations (see discussion in Appendix B) and $\xi(t)$ is a time-dependant unitless parameter that varies inversely with the average settling velocity of the coarse particles that remain in the plume at time t. (The formula used in the model for $\xi(t)$ is derived in Appendix B.)

3.5.1.2. *Parameterization for Dilution: In general as* dust plumes are advected, they get dispersed under the action of turbulent velocity fluctuations. The rate at which plume will expand depends on its size relative to the length scales of turbulent motion [Seinfeld and Pandis, 1998; Blackadar, 1998]. The maximum plume growth (or dilution) usually occurs when the plume size is comparable with the scale of the turbulent eddies with highest kinetic energies; i.e., several hundreds of meters to tens of kilometers [Tennekes and Lumley, 1972]. In this stage, dilution is dominated by rapid lateral dispersion and growth. Plumes from dust storms generally reach this size within a few hrs of transport time from their sources). When the size of plume increases still further, the rate of dilution slows, as turbulent eddies are now only diluting the plume through entrainment of fresh air at the plume's boundaries. The rate of the plume dilution in this final stage becomes inversely proportional to the square root of the plume transport time [Csanady, 1973; Blackadar, 1998].

According to the composite satellite images of the dust cloud passage, by the time dust plumes get advected to the Beijing area (the initial location for the model simulations), they have already expanded beyond the size of a tens of kilometers (see Figures 3.4 and 3.10) and further lateral dispersion of the plume appears to be quite slow (Figures 3.6 a,b). So, in the model, plume dilution is treated using the following equation:

$$\alpha_{dil} = \frac{C_{dil}}{\sqrt{t}} \tag{3.5}$$

where C_{dil} is a constant determined from the observation (see discussion in Appendix B) and t is the plume transport time.

3.5.1.3. *Derivation of Constant for Deposition and Dilution:* First note, that that integration of Equation (3.3) yields:

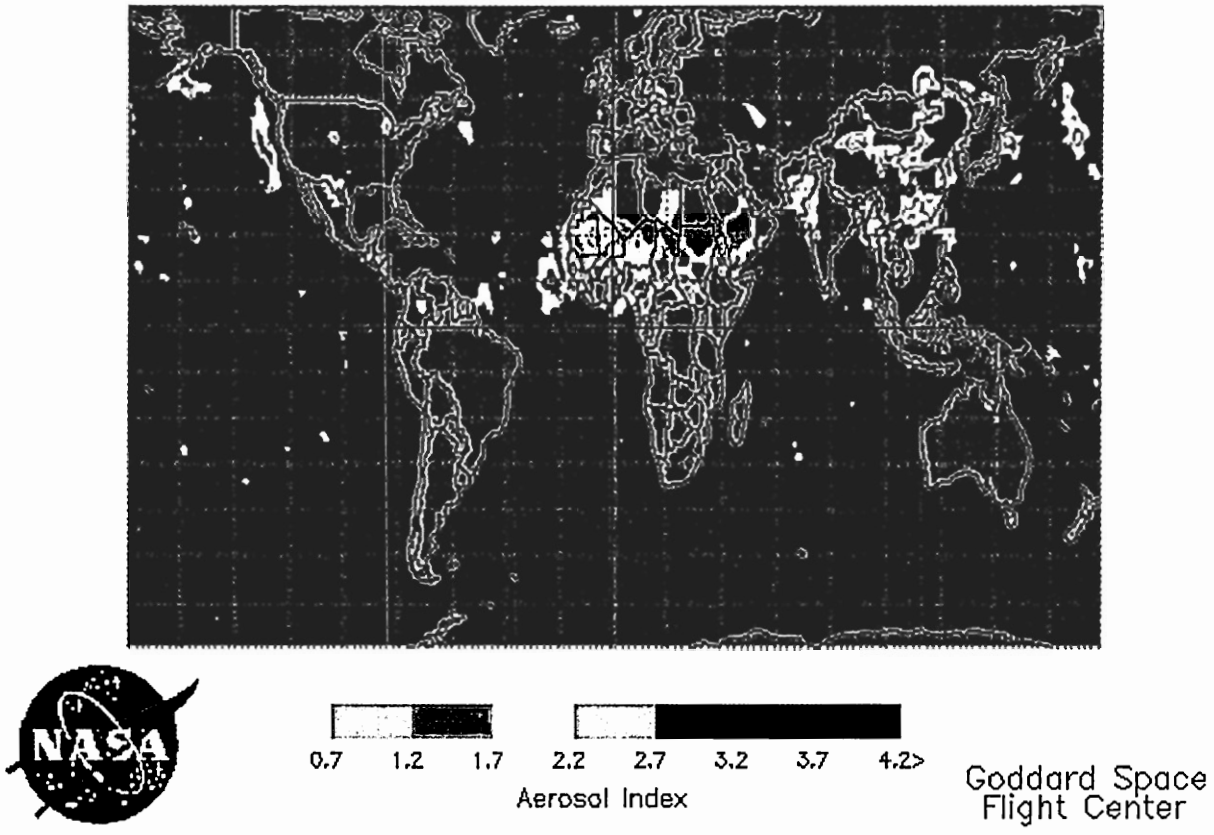

Figure 3.10 The earth probe TOMS aerosol index on April 7, 2001.

$$\text{Dust}(t) = \text{Dust}(0) \cdot \exp\{-\int(\alpha_{dep} + \alpha_{dil})dt\} \quad (3.6)$$

and substitution of Equations (3.4) and (3.5) into Equation (3.6) yields

$$\text{Dust}(t) = \text{Dust}(0) \cdot \exp\{-\int(C_{dep}\xi(t) + C_{dil}/\sqrt{t})dt\} \quad (3.7)$$

To derive values for C_{dep} and C_{dil}, recall that the average mineral dust concentration at Beijing on April 10, 2001 was about $700\,\mu g/m^3$. On the other hand, an average Ca^{2+} concentration of 18.7 $\mu g/m^3$ was measured on board the NCAR C-130 aircraft between 2:00 and 3:00 UTC on April 11, 2001 over the Yellow Sea at latitude 33°N-37°N and longitude 124°E (and an altitude of about 200m). According to back trajectory analysis, the flight track at this point was intercepting the same dust-laden plume that had been over Beijing some 18 hours earlier on April 10. If we assume that all of the Ca^{2+} measured on board of the C-130 was associated with the dust from the gobi deserts (see Chapter 2) and a weight percent concentration of Ca in dust of 6.2% (see Table 3.3, as well as Song and Carmichael [2001] and Zhang et al. [2003]), then the total concentration of Dust at the time of the C-130 sampling was about $300\,\mu g/m^3$. In other words, deposition and dilution processes caused roughly 60% reduction of the mineral dust plume concentration during first 18 hrs of plume transport time.

To estimate the relative contribution of the two processes, we consider the measurements of Tsunogai et al. [1985]. By analyzing weekly aerosol samples collected for two years at six stations located in the western North Pacific Ocean, these investigators observed that within dust plumes advecting from East Asia, dust concentrations generally decreased at about twice the rate of ^{210}Pb concentrations. If we

assume that ^{210}Pb (being a proxy for anthropogenic aerosols) is carried in the fine particle mode and thus behaves similar to that of gaseous species, then it follows that decrease in ^{210}Pb concentration is caused by dilution alone while the loss of Dust is caused be dilution and deposition.

Using the two sets of observations in concert with Equations (3.7), the values for C_{dep} and C_{dil} can be derived using a simple iterative scheme:

$$C_{dep} = 9.2x10^{-6}\ sec^{-1} \quad \text{and} \quad C_{dil} = 7.8x10^{-4}\ sec^{-1/2} \tag{3.8}$$

As different trajectory dust passages (i.e., boundary layer vs. mid-troposphere) can be characterized by different rates of dust deposition and dilution, an independent check of C_{dep} and C_{dil} values can be obtained from observations of the plume used in the *Mid-Troposphere* simulations. The NCAR C-130 aircraft during ACE-Asia Flight 5 intercepted this plume over the Sea of Japan between 8:00 - 9:00 UTC on April 8, 2001. Trajectory analysis suggests that the plume had been over Beijing some 30 hours earlier. Using this transport time, an initial Dust concentration of 1500 $\mu g/m^3$ (seeTable 3.2), and the C_{dep} and C_{dil} values given in Equation (3.8), the model predicts a Dust value at the time and location of the C-130 observations of 510 $\mu g/m^3$. This value is reasonably consistent with the average dust concentration measured on board the C-130 of 550 $\mu g/m^3$ [Huebert et al., 2003]. So, unless noted otherwise, our model simulations use the values for C_{dep} and C_{dil} listed in Equation (3.8). In Chapter 4 sensitivity calculations are carried out to estimate how reasonable variations in deposition and dilution parameterization can affect the model calculations.

3.5.2 SO_2 Mass Balance

In addition to dilution, in the model SO_2 is assumed to be removed from the plume via a homogeneous, gas-phase reaction with the free radical OH; i.e.,

$$\text{(RG1)}\ SO_2 + OH \rightarrow \text{multistep} \rightarrow (SO_4^{2-})_{(aq)}$$

as well as via a heterogeneous reaction with mineral dust; i.e.,

$$\text{(RG2)}\ SO_2 + \text{Dust} \rightarrow (SO_4^{2-})_{(aq)}$$

Thus, for SO_2 Equation (3.2) becomes

$$\frac{d[SO_2]}{dt} = -k_{G1} \cdot [OH][SO_2] - k_{G2} \cdot [\text{Dust}][SO_2] - \alpha_{dil}([SO_2] - [SO_2]_{amb}) \qquad (3.9)$$

where [Dust] is the dust concentration in $\mu g\ m^{-3}$, $[SO_2]$ and [OH] are the SO_2 and OH concentrations in molecules cm^{-3}, k_i are the rate constants for reactions "i" (see Table 3.4), and $[SO_2]_{amb}$, the background concentration of SO_2 over the remote Pacific is assumed to 50 pptv [Thornton et al., 1997; Andronache et al., 1997].

The OH concentration in our simulations is specified as a function of time of day following Liu et al. [2001]:

$$[OH] = [OH_{min}] + [OH_{max}]\exp\left(-\frac{z}{H_{OH}}\right)[\sin(\tfrac{\pi}{24}t)]^n \qquad (3.10)$$

where $[OH_{min}]$ is the nighttime minimum OH concentration, set to be $5x10^4$ molecules/ cm^3, $[OH_{max}]$ is the daytime maximum OH concentration, set to be $5x10^6$ molecules/cm^3, H_{OH}=6.9 km is a scale height and n is set to be 6. This parameterization yields a 24 hour averaged [OH] of ~1 x 10^6 molecules cm^{-3} for $\leq$ 5km altitude, which is consistent with model calculated TRACE-P mission averaged [OH] concentration for 25-45°N [Davis et al., 2003]. In addition, at an altitude of 1 km, this OH concentration in combination with

the value for k_{G1} listed in Table 3.4 produces a 24-hour averaged SO_2 oxidation rate of 0.45%/hr; in reasonable agreement with that calculated by Xiao et al. [1997] for 30°N.

The detailed mechanism for SO_2 oxidation on dust particles remains uncertain [Goodman et al., 2001]. In our model simulations, we assume that (RG2) is controlled by a quasi-second order kinetic relationship with the rate constant derived from an analysis of SO_2 oxidation by mineral dust in the plumes from Kuwaiti oil fires [Ferek et el., 1992; Herring et al., 1996]. Since mean concentrations of air pollutants and desert dust in these plumes were similar to ones observed during the springtime Asian outflow (i.e., TRACE-P Flight 13 and ACE-Asia Flights 5 and 6 described above), we believe that this approach should produce reasonable results. Moreover, Garrett et al. [2003] showed that the SO_2 uptake coefficient calculated from Herring et al. [1996] parameterization is within the range reported by Ullerstam et al. [2002] for SO_2 uptake by mineral dust. Sensitivity calculations are also presented to assess how reasonable variations in k_{G2} affect the model simulations.

3.5.3 S(VI) Mass Balance and Speciation

Sulfate or S(VI) is treated in the model as a nonvolatile species (see Table 3.1) that can either reside in fine or coarse mode particles. It is produced from the oxidation of SO_2 via reactions (RG1) and RG2). Production via (RG1) can lead to S(VI) in either fine or coarse mode particles, while production via (RG2) only results in S(VI) production in coarse mode particles. The fraction of S(VI) produced via (RG1) that is deposited into the fine and coarse modes is in turn determined by the relative surface areas contained in the two modes.

Assuming a negligibly small concentration for S(VI) in the background atmosphere, the mass balance equations for S(VI) in each of the modes become:

$$\frac{d[S(VI)]_c}{dt} = k_{G1} \cdot [OH][SO_2][\frac{S_c}{S_f + S_c}] + k_{G2} \cdot [Dust][SO_2] - (\alpha_{dil} + \alpha_{dep})[S(VI)]_c \quad (3.11a)$$

and

$$\frac{d[S(VI)]_f}{dt} = k_{G1} \cdot [OH][SO_2][\frac{S_f}{S_f + S_c}] - \alpha_{dil}[S(VI)]_f \quad (3.11b)$$

where the "c" and "f" subscripts are used to denote the fine and coarse modes, respectively, and S_{mode} is the surface area of the relevant particle mode (in units of $\mu m^2/m^3$). Since, as discussed above, we assume each mode to be monodisperse, S_{mode} is given by

$$S_{mode} = \frac{6 \cdot PM_{mode}}{\rho_{mode} \cdot D_{mode}} \quad (3.12)$$

where $[PM]_{mode}$ is the concentration (in $\mu g\ m^{-3}$) of the relevant mode, ρ_{mode} is the mode's density, and D_{mode} is the mode's nominal diameter (i.e., 0.12 and 1.7 μm for the fine and coarse modes, respectively). If we assume that $\rho_f = \rho_c$, then,

$$[\frac{S_f}{S_f + S_c}] = \frac{1.7\,PM_f}{1.7\,PM_f + 0.12\,PM_c} \quad (3.13a)$$

and

$$[\frac{S_c}{S_f + S_c}] = \frac{0.12\,PM_c}{1.7\,PM_f + 0.12\,PM_c} \quad (3.13b)$$

3.5.3.1 *S(VI) speciation:* As indicated in Table 3.1, S(VI) within the fine and coarse modes is distributed among 10 possible different solid or aqueous-phase species. The relative amounts of each of these species are determined somewhat differently in the two modes. Within the fine particle mode, the speciation of S(VI) is determined by the

thermodynamic module discussed in Section 3.6. Within the coarse particle mode, on the other hand, where Ca^{+2} from the dissolution of calcite can be present, the solution is first tested for supersaturation with respect to gypsum ($CaSO_4 \cdot 2H_2O$). If the solution is supersaturated, an appropriate amount of S(VI), along with Ca^{+2} is removed from the solution. The remaining S(VI) is then speciated using the thermodynamic module described in Section 3.6.

3.5.4 NO_x Mass Balance and Speciation

As in the case of SO_2, NO_x is removed in the model via

$$\text{(RG3)}\ NO_2 + OH \xrightarrow{M} HNO_{3(g)}$$

as well as via a heterogeneous reaction with mineral dust; i.e.,

$$\text{(RG4)}\ NO_2 + \text{Dust} \rightarrow (NO_3^-)_{(aq)}$$

In addition, it is assumed that the reaction between NO_2 and O_3 (which yields NO_3) ultimately leads to the production of N(V) at night [Munger et al., 1998]; i.e.,

$$\text{(RG5)}\ NO_2 + O_3 \rightarrow NO_3 + O_2 \rightarrow \text{multistep at night} \rightarrow N(V)$$

The mass balance equation for NO_x is thus given by

$$\frac{dNO_x}{dt} = -k_{G3}[OH][NO_2] - k_{G4}[Dust][NO_2] - 2 \cdot k_{G5}[NO_2][O_3]\Big|_{night} - \\ -\alpha_{dil}([NO_x] - [NO_x]_{amb}) \qquad (3.14)$$

where $[O_3]$ and $[NO_x]_{amb}$ are set at 40 ppbv and 50ppt [Talbot et al., 1997; Kondo et al., 1997], respectively. As in the case of SO_2, the rate of loss of NO_2 on Dust using a second order kinetic relationship with a rate constant from Herring et al. [1996].

3.5.4.1 *NO_x speciation:* NO_x is comprised of two gas-phase species: NO and NO_2. The relative concentration of NO and NO_2 in the remote troposphere is by a photostationary state between three reactions:

$$\text{(RG6)}\quad NO + O_3 \rightarrow NO_2 + O_2$$

$$\text{(RG7)}\quad NO_2 + h\nu \rightarrow NO + O$$

and

$$\text{(RG8)}\quad NO + RO_2 \rightarrow NO_2 + RO$$

where RO_2 denotes a peroxy radical. However, modeling results indicate that the NO oxidation rate by peroxyl radicals in the springtime over the western North Pacific is considerably smaller than its oxidation by ozone via (RG6) [Crawford et al., 1997]. Thus, the partitioning of NO_x between NO and NO_2 can be approximated by

$$[NO_2]/[NO] = k_{G6}[O_3]/J_{G7} \tag{3.15}$$

where J_{G7} is derived from the model of Crawford et al. [1997].

3.5.5 N(V) Mass Balance and Speciation

Unlike S(VI) which is nonvolatile, N(V) can exist in the gas-phase as HNO_3 and as a result, N(V) that is initially in one particulate mode can volatize and recondense on the other mode. This makes it necessary to use one single mass balance equation for N(V):

$$\frac{d[N(V)]}{dt} = k_{G3}[OH][NO_2] + k_{G4}[Dust][NO_2] + 2 \cdot k_{G5}[NO_2][O_3]\Big|_{night} - \alpha_{dep}[N(V)] \cdot F_{frac} - \alpha_{dil}[N(V)] \tag{3.16}$$

where F_{frac} is calculated using the following equation:

$$F_{frac} = \frac{[N(V)]_{coarse}}{[N(V)]_{fine} + [N(V)]_{coarse} + [HNO_3]_g} \quad (3.17)$$

and it is assumed that the ambient N(V) concentration is negligible.

3.5.5.1 *N(V) speciation:* The partitioning of N(V) between the gas-phase and the two particulate matter modes, and speciation of N(V) within each of the modes are determined in the model using the thermodynamic module, as described in Section 3.6.

3.5.6 N(III) Mass Balance and Speciation

N(III) consists of gas-phase NH_3 and the various dissolved and solid forms of ammonium that can exist in the fine and coarse particle modes. While NH_3 can be oxidized by OH, the reaction is slow; the tropospheric lifetime of NH_3 due to its reaction with OH is estimated at about 3 months [Warneck, 1988], and this is considerably longer than the plume transport time of several days considered here. So this reaction can be neglected in our calculation. The mass balance equation for N(III) then becomes, in-plume production or destruction terms for N(III) were not included in the model. For the mass balance of N(III) we have:

$$\frac{d[N(III)]}{dt} = -\alpha_{dep}[N(III)] \cdot F_{frac} - \alpha_{dil}([N(III)] - [N(III)]_{amb}) \quad (3.18)$$

where F_{frac} shows relative abundance of particulate phase NH_4^+ in a coarse mode and $[N(III)]_{amb}$=50 ppt is background concentration of ammonia over the remote Pacific [Dentener and Crutzen, 1994].

3.5.6.1 *N(III) speciation:* The partitioning of N(III) between the gas-phase and the two particulate matter modes, and speciation of N(III) within each of the modes are determined in the model using the thermodynamic module, as described in Section 3.6.

3.5.7 Mass Balance for Coarse-Mode Mobilized Na

The concentration of mobilized Na in the coarse mode aerosol is of interest because it can influence the pH of the coarse mode, and thus the dissolution of Fe, which, because it arises from dust, is only in the coarse mode. Dissolved Na in the coarse mode can arise from the dissolution of the Na-containing minerals in dust; as described in Section 3.3 these minerals are albite and smectite. Thus, if we neglect the coagulation of coarse-mode, dust-containing particles with sea-salt, and assume a negligible ambient coarse-mode Na concentration, the mass balance for dissolved, coarse mode Na can be written as:

$$\frac{d[Na]_c}{dt} = WNa_{alb} \cdot R_{alb}^{net} \cdot [Dust] + WNa_{smt} \cdot R_{smt}^{net}[Dust] - (\alpha_{dil} + \alpha_{dep})[Na]_c \qquad (3.19)$$

where $[Na]_c$ is total concentration (in units of mole/m^3) of mobilized coarse-mode Na (and excludes Na that is bound in albite and smectite minerals); WN_{alb} and WNa_{smt} are the molar fractions of Na in albite and smectite (i.e., 1 and 0.6, respectively); and R_{alb}^{net} and R_{smt}^{net} are the dissolution rates (in units of moles/g of dust/s) of albite and smectite, respectively. The formulation and methodology used to calculate mineral dissolution rates are discussed in Section 3.5. The speciation of dissolved coarse mode Na is determined using the thermodynamic module discussed in Section 3.6.

Mass balance equations for coarse-mode, dissolved K and Mg are similar to Na and are not specifically discussed. K and Mg are speciated in the model by first converting them to equivalent concentrations of Na and then speciating the Na.

3.5.8 Mass Balance and Speciation for Mobilized, Coarse-Mode Ca

In principle, Ca can be mobilizes in the coarse mode from the dissolution of two dust-containing minerals: calcite and anhydrite [Hseung and Jackson, 1952]. However, in view of the evidence of gypsum precipitation in mineral aerosols during their long-rage transport [Zhou and Tazaki, 1996; Mori et al., 1998; Böke et al., 1999; Kim and Park, 2001; Arimoto, 2001], we only consider calcite dissolution as a potential source of mobilized Ca. The mass balance for mobilized, coarse-mode Ca then takes the following form:

$$\frac{d[Ca]_c}{dt} = WCa_{cal} \cdot R_{cal}^{net} \cdot [Dust] - (\alpha_{dil} + \alpha_{dep})[Ca]_c \qquad (3.20)$$

where $[Ca]_c$ is total concentration of mobilized, coarse-model Ca (and excludes Ca bound in calcite and gypsum); WCa_{cal} is the number of moles of Ca contained in a mole of calcite (i.e., 1); and R_{cal}^{net} is calcite dissolution rate (expressed in units of moles of calcite dissolved/g of dust/s).

3.5.8.1 *Ca speciation:* The speciation of mobilized, coarse-mode Ca is determined in a two-step process. First, if the solution is supersaturated with respect to gypsum, Ca^{+2} along with an appropriate amount of S(VI) is removed (i.e., precipitate out) from solution, and then the remaining Ca is converted to an equivalent concentration of Na and speciated using the thermodynamic module (see Section 3.6).

3.5.9 Mass Balance and Speciation For Mobilized, Coarse-Mode Fe

In our model, Fe from dust within the coarse mode is mobilized through the dissolution of hematite. The mass balance equation for this species is therefore

$$\frac{d[Fe]_c}{dt} = WFe_{hem} \cdot R_{hem}^{net} \cdot [Dust] - (\alpha_{dil} + \alpha_{dep})[Fe]_c \qquad (3.21)$$

where $[Fe]_c$ is the concentration of mobilized, coarse-mode Fe, WFe_{hem} is the number of moles of Fe in a mole of hematite (2); and R_{hem}^{net} is the hematite dissolution rate (moles of hematite dissolved/g of dust/s).

3.5.9.1 *Fe speciation:* The acid dissolution of Fe from hematite will initially give rise to dissolved iron in the +3 oxidation state; i.e. Fe(III). In principle, subsequent reactions (e.g., triggered by photons and/or catalysts) can give rise to Fe(II) and both Fe(III) and Fe(II) can coexist in solution [Behra and Sigg, 1990; Sedlak and Hoigné, 1993; Blesa et al., 1994; Cornell and Schwertmann, 1996]. Because of the high concentration of oxidants in the atmosphere, Fe(II) tends to be thermodynamically unstable in atmospheric particulate matters and thus maintenance of Fe(II) in dust-containing aerosols requires continual cycling of Fe between the two oxidation states [Behra and Sigg, 1990; Zhu et al., 1993; Siefert et al., 1996]. The possible reaction scheme for the Fe(II)/Fe(III) cycling in ambient aerosols should perhaps include photochemistry, aqueous sulfite ions (SO_3^{2-}), aldehydes, radicals ($HO_2^{\cdot}/O_2^{-}$, $RO_2^{\cdot}$), Cu(I), hydrogen peroxide (H_2O_2) and some organic reductants (oxalate, ascorbate) [Behra and Sigg, 1990; Sedlak and Hoigné, 1993; Hislop and Bolton, 1999; Balmer and Sulzberger, 1999]. Photochemical/chemical cycling between Fe(III) and Fe(II) are not included in our model calculations, and thus $[Fe]_c$ is given by the total concentration of Fe(III) species in the aerosol coarse mode not associated with hematite. (Although Fe(II) has much higher solubility [Cornell and Schwertmann, 1996], consideration of only ferric complexes should not affect considerably DIF of mineral dust when solution remains under-saturated with respect to

Fe(III). It is shown below that for most of the simulated cases deliquesced mineral dust solution remained under-saturated with respect to Fe(III) and formation of $Fe(OH)_3(s)$ was not observed.)

Iron hydrolysis (even when restricted to Fe(III)) is rather complex [Blesa et al. 1994; Brandt and Eldik, 1995; Millero et al., 1995; Cornell and Schwertmann, 1996] and some simplifications have been made to keep the calculations tractable. In the model, I assume that $[Fe]_c$ can take six different aqueous-phase forms, as well as one amorphous precipitate; i.e.,

$$[Fe]_c = (Fe^{3+})_{(aq)} + (FeOH^{2+})_{(aq)} + (Fe(OH)_2^+)_{(aq)} + (Fe(OH)_3^0)_{(aq)} + (Fe(OH)_4^-)_{(aq)} + \\ + (FeSO_4^+)_{(aq)} + (Fe(OH)_3)_{(s)} \qquad (3.22)$$

Note that, the Fe^{3+} ion in solution actually contains six water molecules in its coordination spheres (i.e., $[Fe(H_2O)_6]^{3+}$) [Stumm and Morgan, 1981]. However, for simplicity, I simply refer to it here as Fe^{3+}. The higher, polymeric iron hydroxide complexes, such as $Fe_2(OH)_2^{4+}$, $Fe_{12}(OH)_{34}^{2+}$, are not considered in the model, as their concentrations only become significant at much higher concentrations of Fe(III) then those encountered in our calculations [Blesa et al., 1994; Millero et al., 1995]). Out of the several possible inorganic complexes that Fe(III) can form (i.e., $FeSO_4^+$, $FeHSO_4^{2+}$, $Fe(SO_4)_2^-$, $FeCl^{2+}$, FeF^{2+}), we only include $FeSO_4^+$, as other inorganic form of Fe(III) appear to be less important under our model conditions [Dousma et al., 1979; Millero et al., 1995].

Using the assumption about the absence of metastable supersaturation with respect to $Fe(OH)_3(s)$, at every time step the total Fe(III) concentration allowed to be present in a solution is calculated based on equilibrium constant of RAQ6 (Table 3.5),

and pH and ionic strength of the solution. Since the establishment of hydrolysis equilibria between all Fe(III) species in Table 3.5 is usually very fast [Stumm and Morgan, 1981], the relative concentrations of each of the species appearing in Equation (3.22) is determined by using appropriate equilibrium constants, pH and ionic strength of the solution.

3.5.10 Mass Balance and Speciation For Mobilized, Coarse-Mode Al

In acidic solutions, elevated concentrations of dissolved Al can increase acid neutralizing capacity (ANC) and act as pH buffer [Sullivan, et al., 1989; Bi et al., 2001a; 2001b]. Al-buffering effect in the model is calculated by determining total concentration of mobilized Al in the coarse mode and its subsequent speciation in hydroxo and inorganic complexes. Mass balance for dissolved Al is calculated using the following equation:

$$\frac{d[Al]_c}{dt} = \sum_i WAl_i \cdot R_i^{net} \cdot [Dust] - (\alpha_{dil} + \alpha_{dep})[Al]_c \qquad (3.23)$$

where $[Al]_c$ is the concentration of mobilized, coarse-mode Al, *i* represents each of the Al-containing minerals from dust include in our model (i.e., albite, microcline, illite, smectite, and kaolinite), WAl_i is the number of moles of Al in a mole of each of the aluminum-containing minerals (1, 1, 2.3, 1.4, and 2, respectively), and R_i^{net} is dissolution rate of each of mineral "i" (moles of mineral dissolved/g of dust/s).

3.5.10.1 *Al speciation:* Speciation of mobilized Al is determined by invoking equilibrium between all monomeric Al-hydroxo and Al-sulfate (i.e., $AlSO_4^+$) complexes [Bi et al., 1995]:

$$[Al]_c = Al^{3+} + \sum_{1}^{n} \left(Al(OH)_n\right)^{3-n} + (AlSO_4^+)_{(aq)} + (Al(OH)_3)_{(s)}, \quad \text{where n=1,2,3,4} \qquad (3.24)$$

For model simplicity, polynuclear Al-hydoxides (i.e., $Al_2(OH)_2^{4+}$, $Al_3(OH)_4^{5+}$) and other Al-inorganic complexes [Bi et al., 1995] were not taken into account.

The relative concentrations of $[Al]_c$-species is determined at each time step by assuming a steady state between the reactions in Table 3.5 involving Al species while assuring the absence of supersaturation with respect to $(Al(OH)_3)_{(s)}$. The impact of these various Al-species on pH and liquid water content is then simulated by converting each species to an equivalent concentration of Na (i.e., all Al-containing species with a charge of +1 is equivalent to one Na ion, species with a charge of +2 correspond to two Na ions, etc), and then calculating the subsequent speciation of Na using the thermodynamic module (see 3.6).

3.6 Mineral Dissolution Kinetics

In this work I consider the dissolution of 7 minerals contained in dust: calcite, albite, microcline, illite, smectite, kaolinite and hematite. The stoichiometry and equilibrium constants for the dissolution/precipitation of each of these minerals are provided in Table 3.6.

To calculate R_i^{net}, the rate of dissolution of mineral "i," we adopt the formulation of Lasaga et al. [1994]:

$$R_i^{net} = K_r(T)\, a(H^+)^m\, f(\Delta G_r)\, A_i\, W_i \qquad (3.25)$$

where R_i^{net} has units of moles of mineral dissolved per gram of dust per s and is positive when the mineral is dissolving and negative when precipitating, K_r has units of mole

dissolved/m^2 of mineral/s and is a function of temperature, T, $a(H^+)$ is the H^+ activity, m is an empirical parameter, f is a function of Gibbs free energy, ΔG_r, and accounts for the variation of the rate with deviation from equilibrium [Cama et al., 1999], A_i is the specific surface area of mineral in units of m^2/g of mineral, and W_i is the weight fraction of the mineral in dust in units of g of mineral/g of dust. Values for K_r, m, A_i, and W_i for each of the mineral-dissolution reactions considered here are listed in Table 3.7.

The function f is in turn given by:

$$f(\Delta G_r) = [1 - \exp(n\Delta G_r/RT)] \tag{3.26}$$

where

$$\Delta G_r = RT\ln(Q/K_{eq}) \tag{3.27}$$

and Q is the reaction activity quotient (i.e., the ratio of the product of the reactants over and the product of the species produced), K_{eq} is the equilibrium constant (given in Table 3.5), and n is an empirical parameter (assumed here, for simplicity, to be 1). Note that Q/K_{eq} describes the state of saturation of the solution with respect to a solid, so that when $Q/K_{eq}>1$ the solution is oversaturated with respect to solid and $R_i^{net} < 0$, and when $Q/K_{eq} <1$ the solution is undersaturated and $R_i^{net} > 0$ [Stumm and Morgan, 1981]). Moreover, when n=1, the formulation reduces to the form for a single rate-limiting elementary reaction [Burch et al., 1993].

3.6.1 Hematite Dissolution Kinetics

Because of the complexity of hematite dissolution, as well as its importance to our modeling study, some further discussion of this process is in order. The formulation for hematite dissolution adopted here was derived from the data illustrated in Figure 1 of

Azuma and Kametani [1964]. As indicated in Table 3.7, rates are calculated for three stages of hematite dissolution: the first stage, which is characterized by relatively slow dissolution, is applicable to the dissolution of the first 0.8% of the oxide's mass; the second stage, with an accelerated dissolution rate likely associated with the digestion of the oxide phase [Gorichev et all., 1976]), is applied when the mass of oxide dissolution ranges from 0.8 to 40%; and the third stage is applied when the dissolved mass is > 40%, as dissolution approaches completion [Azuma and Kametani, 1964]. In such case of dissolution, when the stages of dissolution process always remain the same the rate is controlled only by one stage and not the combination of several [Gorichev et all., 1976].

3.7 Thermodynamic Module

Once the concentrations of the major species listed in Table 3.1 have been determined at a given time step using the Equations described in Section 3.4, these species must be subdivided into their various possible chemical forms. This is accomplished in the model by invoking thermodynamic equilibrium between the gas-phase and the two aerosol modes using a modified form of ISORROPIA [Nenes et al. 1998].

ISORROPIA is a numerical module which calculates the equilibrium solid-, aqueous- and gas-phase concentrations of relevant species along with the liquid-water content of a single mode particle phase as a function of ambient relative humidity and temperature while accounting for multicomponent activity coefficients and other solution non-idealities. In the model there are two independent aerosol modes (e.g., fine and coarse). To calculate the equilibrium state between the gas-phase and these two aerosol

modes, I iteratively run ISORROPIA for each mode separately until a self-consistent set of gas-phase concentrations is obtained for both modes.

ISORROPIA provides options to treat the particles as being in a thermodynamically stable state, where particles can be solid, liquid or both, or in a metastable state, where particles are always an aqueous solution. Unless otherwise specified, the metastable-state option has been adopted in the simulations.

The standard version of ISORROPIA treats the sodium-ammonium-chloride-sulfate-nitrate-water gas/aerosol system. To simulate the chemistry of mineral dust and mobilization of Fe additional species and reactions must be considered. I therefore have modified ISORROPIA to explicitly include reactions involving gas-phase CO_2 and aqueous-phase carbonates and Fe-species. The additional reactions and equilibrium constants used for these processes are listed in Table 3.5. The effects of other crustal elements (i.e., Ca, Mg, K and Al) on chemical properties of the coarse-mode aerosols are modeled by converting them to the equivalent concentration of sodium. Moya et al. [2001] showed under relatively low concentration of particulate matter ISORROPIA performs well when crustal element concentrations, expressed as equivalent sodium, are used as an input. Such approach might encounter some difficulties when crustal material (particularly Ca) comprises a significant portion of total particulate matter. However, even under such conditions no significant errors in the amount of the dissolved Fe are expected, as the dissolution of hematite only takes place in highly acidic deliquesced mineral dust particles when most of the Ca^{2+} in the solution is bounded in the insoluble mineral, gypsum and has no direct effect on the properties of dust particles.

In order to include these additional reactions in ISORROPIA it was also necessary to calculate activity coefficients for the additional species involved in these reactions. We calculated binary activity coefficients for each new ion pair using the formulation of Kusik and Meissner [1978] and the q-parameters for each relevant salt listed in Table 3.8. Activity coefficients for $Fe(OH)_3^0$ and $Fe(OH)_4^-$ have been neglected; the former is assumed to be equal to 1 [Millero et al., 1995] and latter is only important for high pH values (pH> 8) not relevant to our problem. Activity coefficients for weak electrolytes (i.e., $H-HCO_3$ and H_2CO_3) and uncharged species (i.e., $CO_2(aq)$) were also omitted in this study, as such corrections are generally only for alkaline and neutral solutions. The multicomponent activity coefficients for the aerosol solutions were determined using the method of Bromley [1973].

CHAPTER 4

RESULTS OF LAGRANGIAN BOX MODEL CALCULATIONS

4.1 Introduction

The Lagrangian box model described in the previous chapter was used to simulate the chemical evolution of three different dust plumes having distinct advection paths with the following objectives: (1) to evaluate if the nominal amounts of anthropogenic air pollutants (particularly SO_2) found in the urban/industrial centers of East China are sufficient to acidify dust-containing plume and produce DIF of about 0.5-2%; (2) to study how variations in the amount of mineral dust and/or SO_2 contained in the advecting plumes can affect the DIF; and (3) to identify atmospheric parameters that can influence Fe mobilization rates in deliquesced mineral dust particles. The results of these simulations are presented below.

4.2 Initial Plume Composition

The initial amounts of Dust and pollutants assumed to be in the plumes at t = 0 are listed in Table 4.1. Plumes simulated under the Standard model conditions (Standard Dust/ Standard Pollution case) are designed to mimic typical large dust outflows from East Asia that are entrained with an initial loading of SO_2, NO_x, and O_3 characteristic of springtime concentrations measured in the Beijing metropolitan area [Song and Carmichael, 1999; 2001; Phadnis and Carmichael, 2000; Wang et al., 2001; Tan et al.,

2002;3, 2001], along with nominal amounts of SO_4^{2-} and NO_3^- and SO_4^{2-}, NO_3^- and NH_4^+ in the coarse and fine particle modes, respectively. Note, that in this chapter we assume all plumes have similar initial dust loading and chemical composition. This assumption greatly reduces number of variables in the model simulations and helps to better evaluate how varying atmospheric conditions and plume trajectories affect the DIF in these dust plumes. In Chapter 5, initial conditions more appropriate to the specific events simulated are used to estimate the amounts of dissolved Fe the plumes from these events might have delivered to the remote North Pacific Ocean.

Table 4.1 Initial chemical conditions adopted for model calculations

Parameter	
Coarse model aerosol composition	
Dust , ($\mu g/m^3$)(1)	700 (Standard Dust case); 100 (Low Dust case)
SO_4^{2-}, ($\mu g/m^3$)	0.5
NO_3^-, ($\mu g/m^3$)	0.5
Fine mode aerosol composition	
SO_4^{2-}, ($\mu g/m^3$)	3.5
NO_3^-, ($\mu g/m^3$)	3.0
NH_4^+, ($\mu g/m^3$)	2.5
Gas phase mixing ratios	
SO_2, (ppbv)	8.0 (Standard Pollution case); 30 (High Pollution case); 2.0 (Low Pollution case)
NO_x, (ppbv)	4.0
NH_3, (ppbv)	5.5
O_3 , (ppbv)	50

(1) The assumed initial composition of the dust is discussed in Section 3.4.1 and detailed in Table 3.3.

In addition to the Standard Dust and Pollution cases, we have carried out model simulations for a Low Dust case, a Low Pollution case, and a High Pollution case. The Low Dust case, with an initial dust concentration of 100 $\mu g\ m^{-3}$, is designed to explore the production of dissolved iron via acid mobilization during small dust outbreaks over the gobi deserts, a phenomenon that appears to occur far more frequently than the large dust storm events simulated in the Standard Dust cases [Tratt et al., 2001; Jordan et al., 2003a]. Initial SO_2 concentrations in the Low and High Pollution cases are adopted to explore how varying the level of the acidifying pollutants affects the production of dissolved Fe.

4.3 *Boundary Layer* Simulations

Figure 4.1 shows the model-calculated DIF as a function of time for Standard Dust/Standard Pollution and Low Dust/Standard Pollution cases of the *Boundary Layer* simulation. This figure demonstrates that, for the Standard Dust case, the model-calculated DIF after 5 days of plume travel-time remains to be insignificant. By contrast, for the Low Dust case, DIF is within the aforementioned 0.5 – 2 % range required for making acid mobilization of Fe a viable mechanism. Interestingly, even though the Low Dust case has less total Fe than the Standard Dust case, the Low Dust case produces a significantly higher concentration of dissolved Fe than that of the Standard Dust case by the end of the simulation period; i.e., 0.17 n mole/m^3 versus $2x10^{-8}$ n mole/m^3. As described below, the reason for this perhaps counterintuitive result lies in the amounts of acidifying pollutants in the plume relative to the buffering capacity of the mineral dust.

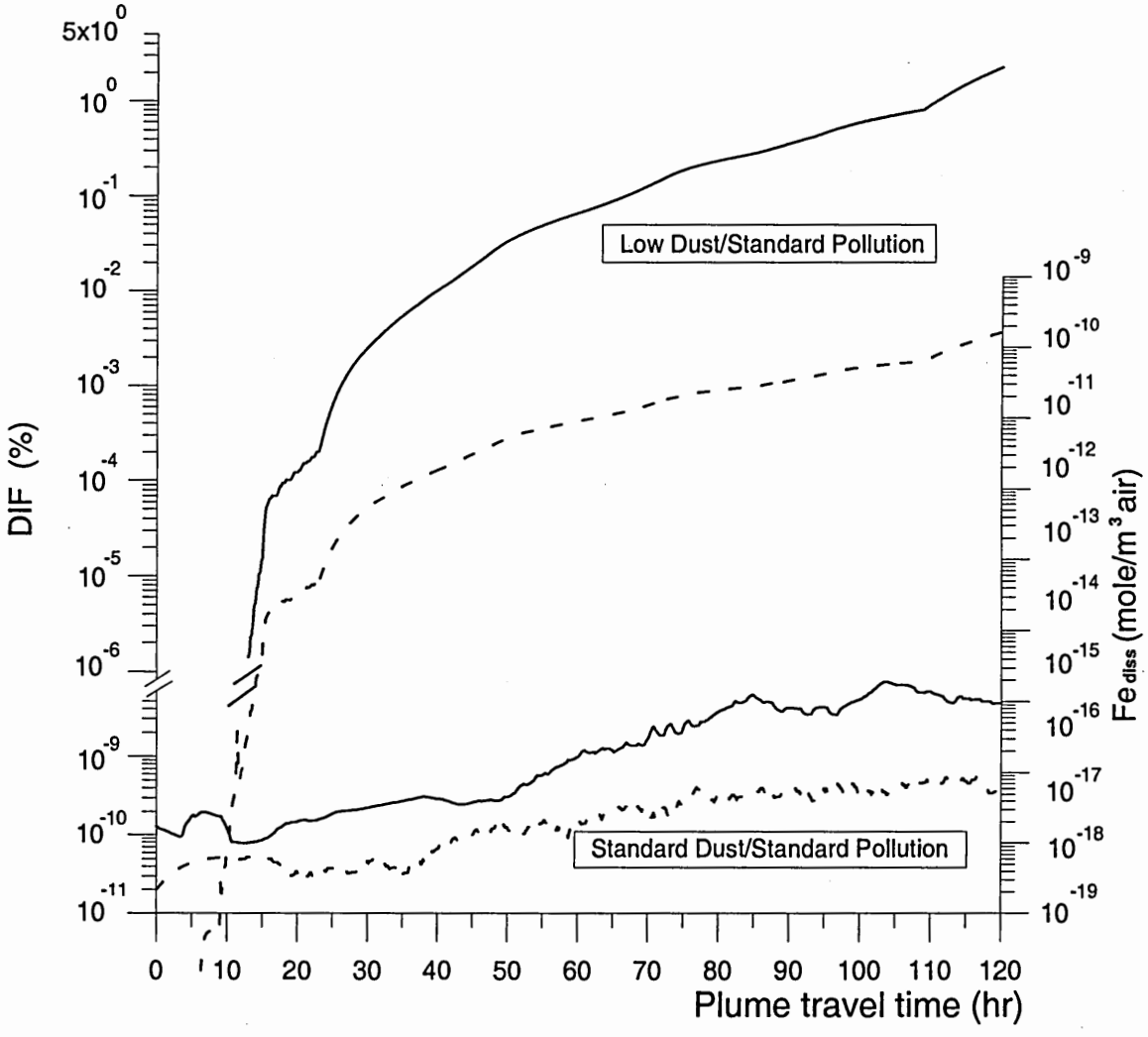

Figure 4.1 Dissolved Iron Fraction (solid line) and amount of dissolved Fe (dashed line) as a function of plume transport time for the *Boundary Layer* simulations.

4.3.1 *The pH of the mineral dust particles in Standard Dust case:* Figure 4.2 shows pH, hematite dissolution rates and [Acid], the total concentration of SO_4^{2-} and NO_3^- added per microgram of mineral dust from the Reactions RG1, RG2, RG4 and RG5 of Table 3.5 (in units of $\mu eq/\mu g$ dust), as a function of the plume transport time for Standard Dust Standard Pollution and Low Dust Standard Pollution cases of the *Boundary Layer* simulations. We see that while [Acid] increases rapidly for both cases, the mineral dust pH decreases only in the Low Dust case. The lack of acidification in the Standard Dust case despite the addition of [Acid] is caused by the buffering action of the $CaCO_3$ in the mineral dust. As acids are added to the particles, the excess acidity is then neutralized by the following multi-step, stoichiometric reactions:

(REQ1) $CaCO_3(s) \rightleftharpoons Ca^{2+}(aq) + CO_3^{2-}(aq)$

(RAQ4) $Ca^{2+}(aq) + SO_4^{2-}(aq) + 2H_2O \rightleftharpoons CaSO_4 \cdot 2H_2O(s)$

(RAQ3) $CO_3^{2-}(aq) + H^+ \rightleftharpoons HCO_3^-(aq)$

(RAQ2) $HCO_3^-(aq) + H^+(aq) \rightleftharpoons CO_2(aq) + H_2O$

(RAQ1) $CO_2(aq) \rightleftharpoons CO_2(g)$

In the Standard Dust case, the $CaCO_3$ concentration is relatively high and the acidic species deposited to the mineral dust particles are never sufficient to overcome the carbonate buffering. Thus the pH of the mineral dust in the Standard Dust case remains fairly constant, at a value characteristic of aqueous systems containing undissolved $CaCO_3$ [Lindsay, 1979]. Because of the high pH in this case, the model predicted rate of

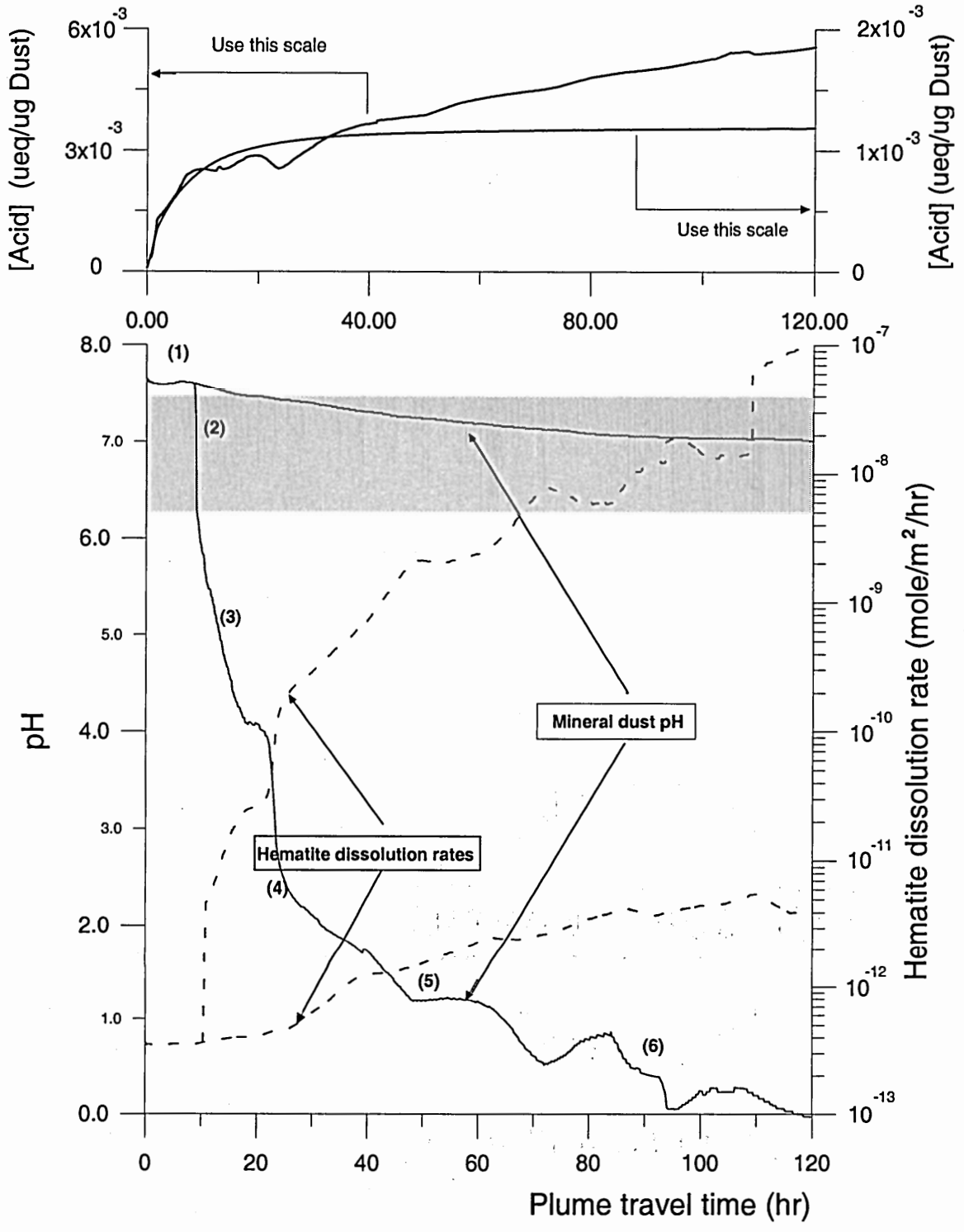

Figure 4.2 [Acid], pH and hematite dissolution rates for Standard Dust (red) and Low Dust (blue) cases of the *Boundary Layer* simulations. [Acid] is calculated by dividing total equivalent acidity of the dust plume (in units of μeq/m^3 air) by the mineral dust mass (in units of μg/m^3 air). The shaded area shows approximate range in hematite dissolution rates needed to mobilize 0.5 - 2 % of Fe in 3-5 days.

hematite dissolution is very small and, as indicated in Figure 4.1, DIF remains insignificant.

4.3.2 *The pH of the mineral dust particles in the Low Dust case:* For the Low Dust case, on the other hand, there is a relatively small amount of $CaCO_3$ present, the carbonate buffer is rapidly overwhelmed and the pH of the mineral dust begins to fall. However, inspection of Figure 4.2 reveals that the fall in pH is not monotonic but rather varies in a complicated manner involving six distinct segments. The first segment of the pH curve (labeled "(1)" in Figure 4.2) in the Low Dust case is similar to that of the Standard Dust case. During this segment, the dust particles still contain some undissolved $CaCO_3$ and the carbonate buffer is able to maintain the pH at ~ 7.5 in spite of the addition of acids. As a result, the hematite dissolution rate remains insignificantly small during this segment.

However, because of the relatively low concentration of dust in this case, the carbonate buffering capacity of the dust is overwhelmed after only a few hours. At that point, $CaCO_3$ has been completely dissolved, and the Ca has been precipitated as $(CaSO_4)_{(s)}$, while the carbonate has been volatized as CO_2. At this point, marked by the beginning of segment (2) in Figure 4-2, any further addition of acids will cause the pH to fall. Although hematite dissolution rate by more than 2 orders of magnitude during segment (2), it is still significantly lower than the range needed to mobilize of 0.5 - 2 % of Fe in mineral dust particles (shaded region on Figure 4.2).

The rapid decrease of pH during segment (2) continues until the pH reaches a value of about 5.5, when segment (3) begins. This segment is also characterized by falling pH, but at a somewhat reduced rate. This slower rate of pH change is caused by

the uptake of $(NH_3)_{(g)}$, whose solubility becomes significant for pH < 5.5. The uptake of $(NH_3)_{(g)}$ represents a source of alkalinity to the mineral dust, via

$$NH_3(g) \rightleftharpoons NH_3(aq) \tag{4.1}$$

$$NH_3(aq) + H_2O(aq) \rightleftharpoons NH_4^+(aq) + OH^-(aq) \tag{4.2}$$

$$2NH_4^+(aq) + SO_4^{2-}(aq) \rightleftharpoons (NH_4)_2SO_4(s) \tag{4.3}$$

$$NH_4^+(aq) + NO_3^-(aq) \rightleftharpoons NH_4NO_3(s) \tag{4.4}$$

and this slows the rate at which the mineral-dust pH falls.

By the time the mineral dust pH reaches a value of about 4, virtually all of the $(NH_3)_{(g)}$ has been consumed and the rate of pH decline increases again; i.e., segment (4). However, when the pH falls below 3 volatilization of nitrate from the mineral aerosol via

$$NO_3^-(aq) + H^+(aq) \rightleftharpoons HNO_3(g) \tag{4.5}$$

counters the addition of SO_4^{2-}, and the rate of pH decline slows again; i.e., segment (5).

At the end of segment (5), at a simulation time of about 40 hours, the pH has reached a value of ~1. As discussed in Chapter 2, the hematite dissolution rate at this pH is within the targeted range needed to produce significant quantities of dissolved Fe.

During the final segment (6), pH exhibits an undulating behavior varying from ~ 1 - 0.3. At these low pH–values, virtually all particulate nitrate has been volatilized and self neutralization reaction of sulfate via

$$H^+(aq) + SO_4^{2-}(aq) \rightleftharpoons HSO_4^-(aq) \tag{4.6}$$

acts as a new buffer against further declines in pH [Song and Carmichael, 1999]. The wave-like behavior of pH during this segment is caused by the variation in relative

humidity which in turn causes the liquid water content of the dust particle to vary (see RH variation for the *Boundary Layer* case in Figure 3.3).

Overall, the results described above suggest that the hypothesized acid mobilization mechanism driven by the addition of SO_2 pollution into advecting mineral dust plumes is viable (at least for plumes advecting within the boundary layer) provided the initial Dust concentrations are not too large. This limitation on the amount of Dust is explored further in the section below.

4.3.3 *Effect of varying SO_2:* In the previous section, it was shown that significant DIF is generated in the *Boundary Layer* simulation using the Low Dust Case, but not in the Standard Dust case. In Figure 4.3, we compare DIF's calculated for these two cases, with two additional cases: the Standard Dust Case with High Pollution, and the Low Dust Case with Low Pollution. Note while DIF remains small for the Standard Dust/Standard Pollution Case, it reaches the 0.5 – 2 % level for the Standard Dust/High Pollution Case. Similarly, while DIF reaches the targeted range for the Low Dust/Standard Pollution Case, it does not for the Low Dust/Low Pollution Case. These results suggests that the initial Dust level, in and of itself, is not the determinate of whether enough dissolved Fe can be generated in a dust plume. Instead it is the relative amounts of Dust and SO_2.

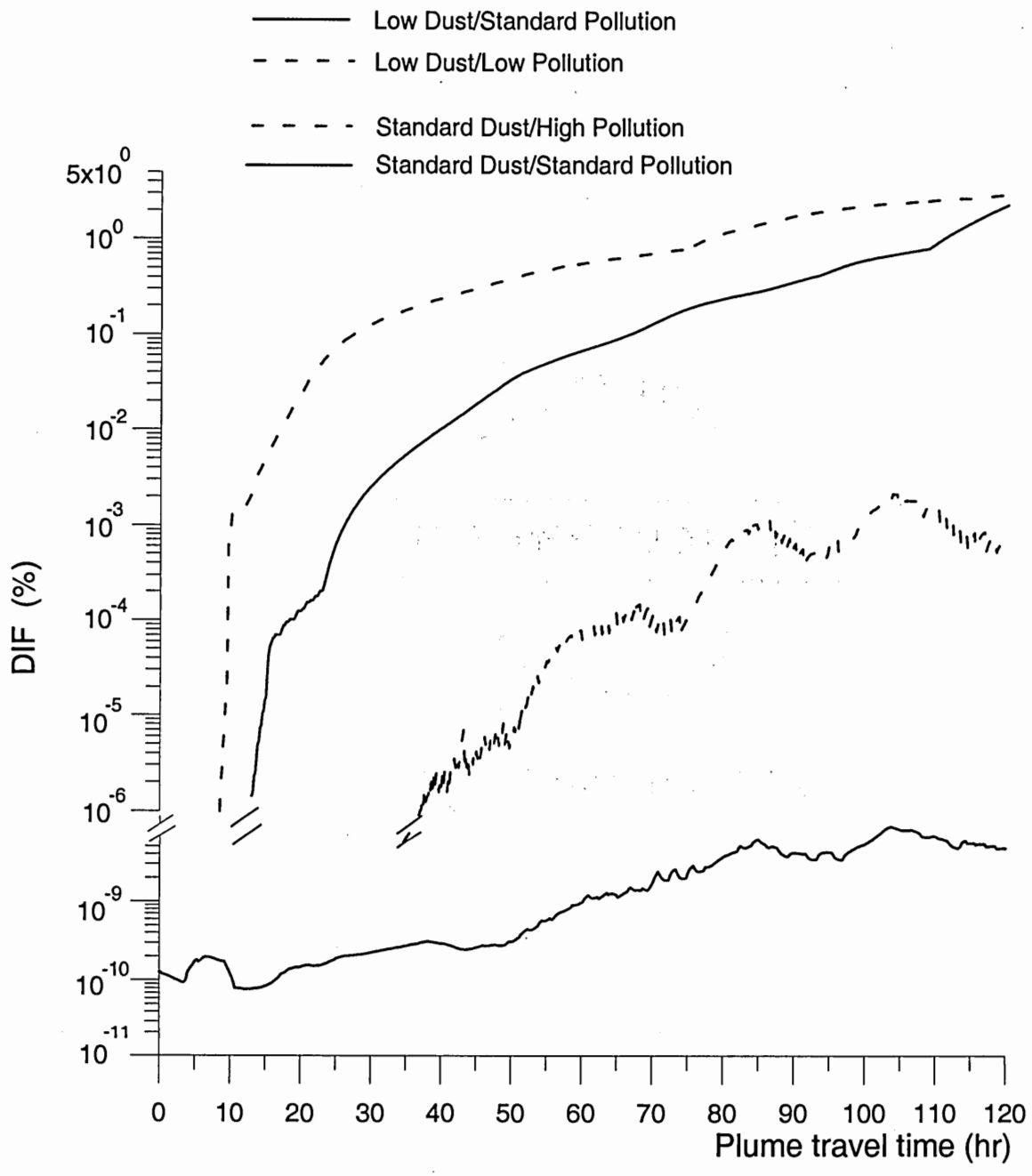

Figure 4.3 Dissolved Iron Fraction as a function of plume transport time for the *Boundary Layer* simulations.

The amount of SO_2 required to acidify dust plumes and generate DIF-values of 0.5 – 2% for Low Dust conditions (of the *Boundary Layer* simulations) are consistent with the Standard Pollution concentrations adopted in our model, which are in turn based on the pollutant concentrations typically encountered in the eastern cities of China [Song and Carmichael, 1999; 2001; Wang et al., 2001; Tan et al., 2002; Wild et al., 2003]. On the other hand, the SO_2 concentration required for the Standard Dust case is more than a factor of three higher than that used in the Standard Pollution case (see Table 4.1). These results suggest that under typical conditions, when average amounts of pollutants from industrial regions of East China get entrained into advecting mineral dust plumes, the generation of significant DIF-levels via acid mobilization will be limited to small plumes (sometimes referred to in the literature as puffs) generated from minor dust events – that are often not even characterized as storms. While the amount of dust carried in individual puffs is small compared to that carried in plumes from large storms, they are far more frequent and, in total, may actually carry more dust to the ocean than carried by the larger, less frequent plumes [Tratt et al., 2001; Jordan et al., 2003a].

However, this does not mean that plumes from large, intensive dust storms can never have significant DIF's from acid mobilization. TRACE-P and ACE-Asia airborne campaigns showed that the concentrations of SO_2 and related air pollutants in the East Asian dust-laden plumes advecting over the North Pacific Ocean can, on occasion, be several times higher than their typical values [Talbot et al., 2003]. The March 13, 2001 (see discussion in Chapter 5) and March 21, 2001 (discussed in Chapter 2) dust plumes are two examples of such high pollution dust episodes, with SO_2 mixing ratios almost an order of magnitude higher than its normal concentration in the springtime outflow.

4.4 *Mid-Troposphere* Simulations and the Effect of Temperature

Figure 4.4 illustrates the model-calculated DIF for the Low Dust/Standard Pollution and Standard Dust/Standard Pollution cases using the *Mid-Troposphere* simulations. This figure shows that similar to the *Boundary Layer* case (given in Figure 4.1), the model calculated DIF for Standard case of the *Mid-Troposphere* simulation is insignificant. As discussed above, this result can be explained by comparing the amounts of acidifying pollutants contained in the plume to the buffering capacity of mineral dust. For the Standard conditions of the *Mid-troposphere* simulations, [Acid] added to the mineral dust particles is not sufficient to overcome carbonate buffering and the model calculated DIF of the dust plume remains insignificant.

Figure 4.4 reveals that, despite the longer transport time, the value for the DIF in Low Dust/Standard Pollution case of the *Mid-Troposphere* simulation is also quite low; i.e., more than two orders of magnitude lower than that of the corresponding case for the *Boundary Layer* simulations. This result is somewhat unexpected, since the two simulations had similar initial plume compositions. So the strong contrast in DIF-values must arise from the different physical conditions encountered by the plumes. Inspection of Figure 3.3 indicates that the trajectories for the two plumes had two major differences: the *Mid-Troposphere* simulation had lower RH and T than that of the *Boundary Layer* case. To determine if either or both of these parameters could have caused the low DIF in the *Mid-Troposphere* simulations, two sensitivity calculations using the *Boundary Layer* /Low Dust case were carried out. In one, the RH was lowered by 25% and in the other T was reduced by 30 K. These changes, according to Figure 3.3, roughly correspond to the differences in RH and T that plumes encountered along their paths. The resulting DIFs as

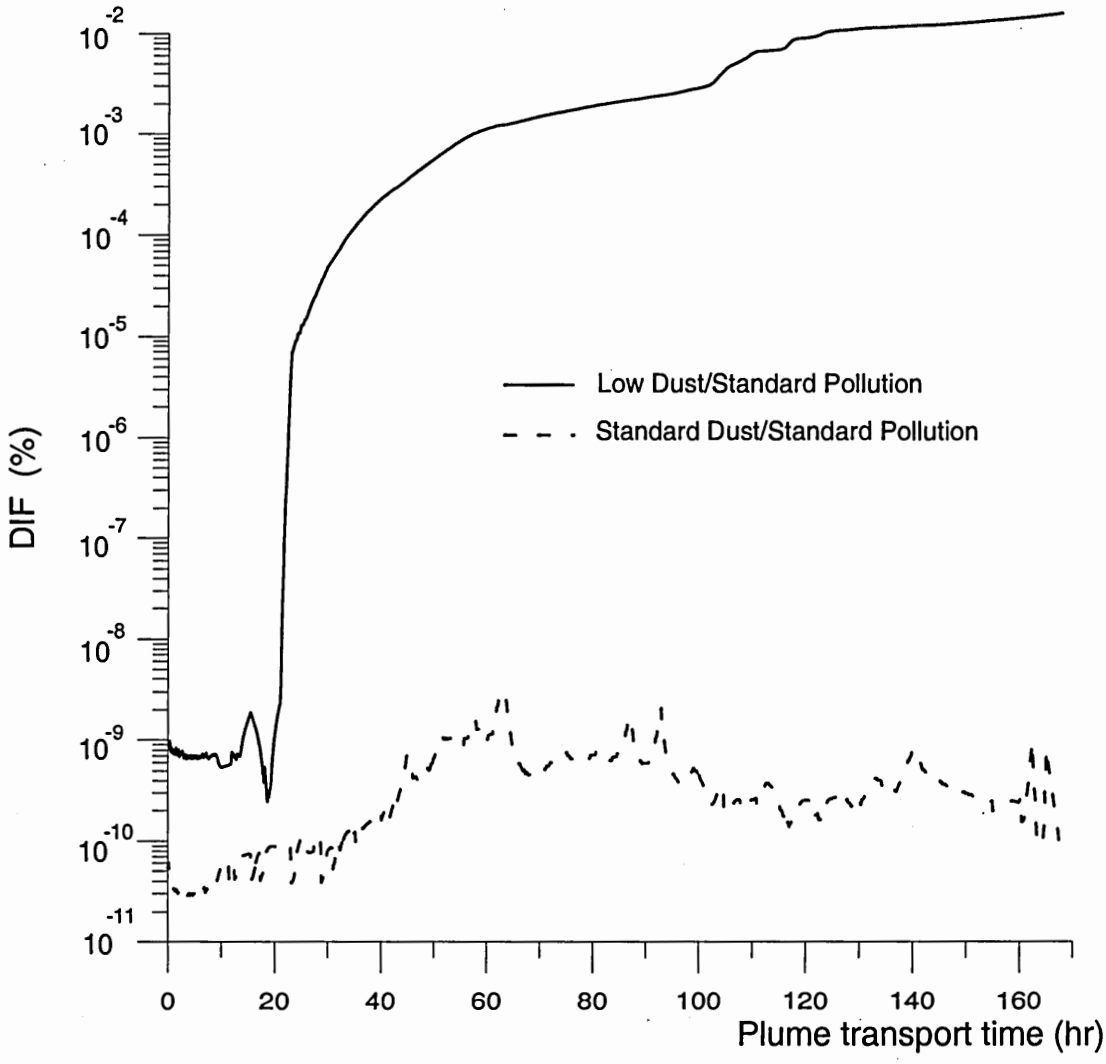

Figure 4.4 Dissolved Iron Fraction as a function of plume transport time for the *Mid-Troposphere* simulations.

a function of time are compared to the DIF-values calculated for the *Boundary Layer/* Low Dust case in Figure 4.5. Inspection of this figure reveals that varying RH had a small effect on the final DIF (in the opposite direction), while lowering temperature had a major effect; preventing the production of significant amounts of dissolved Fe. Indeed from Table 3.8 we can see that the hematite dissolution rate is a strong function of T; the lower temperatures of the *Mid-Troposphere* simulations produce dissolution rates that are one to two orders of magnitude lower than the rates calculated for *Boundary Layer* simulations at the same pH levels. And thus, negligible amounts of dissolved Fe are produced in the *Mid-Troposphere* simulation even though it adopts the same initial amounts of Dust and SO_2 as in the *Boundary Layer* simulations.

Increasing the initial SO_2 concentration does not make a significant difference; as discussed above, under highly acidic conditions self-neutralization of sulfate buffers deliquesced mineral particle pH and thereby prevents the pH from falling much below ~ 1. Sensitivity runs of the *Mid-Troposphere* simulation with SO_2 set at the High Pollution level (see below) or even several times higher than the High Pollution level (not shown) yield somewhat higher hematite dissolution rates, but rates still below the values needed to produce the required 0.5 - 2% of DIF.

It is believed that most of the dust from East Asia that is delivered to the HNLC waters of the subarctic North Pacific follows a high altitude trajectory similar to that used in the *Mid-Troposphere* simulations. However, model simulations presented above suggest that such trajectories are too cold to allow significant amounts of hematite dissolution even in the presence of adequate acidifying pollutants. In the sections below I

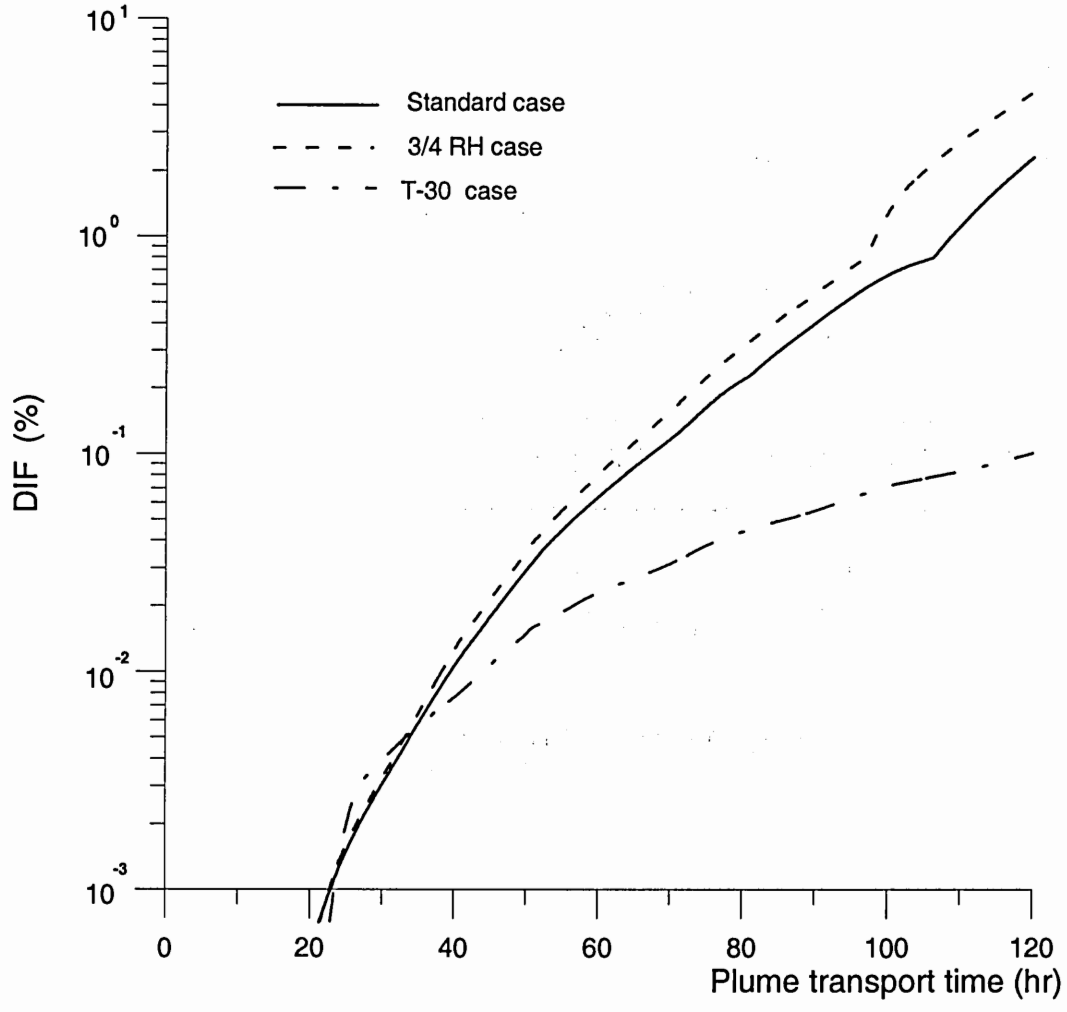

Figure 4.5 Dissolved Iron Fraction as a function of plume transport time for Low Dust Standard Pollution case of the *Boundary Layer* simulations. The ¾ RH denotes the model simulation in which relative humidity was reduced by 25% and in T-30 case the air temperature was lowered by 30K (see text for more details).

examine several possible mechanisms for producing significant amounts of dissolved Fe in plumes that follow a mid-tropospheric trajectory.

4.5 *Mid-Troposphere with Descent* Simulation

In Figure 4.6 we compare the DIF for the Low Dust/High Pollution case of the *Mid-Troposphere with Descent* simulation with the same case using the *Mid-Troposphere* simulation. This figure illustrates that out of two mid-troposphere dust passages DIF reaches the targeted 0.5 - 2% range only in the descending case, despite the similar initial plume compositions. (Although not illustrated here, similar DIF-levels are obtained for the Standard Dust/High Pollution case of the *Mid-Troposphere with Descent* simulation.) Inspection of Figures 3.5 and 3.8 reveals that after leaving the Asian continent both plumes ascended to the mid-troposphere altitudes. However, the plume simulated in the *Mid-Troposphere with Descent* case subsided to the warmer marine boundary layer while the plume simulated in the *Mid-Troposphere* case remained at higher altitudes with significantly colder temperatures. Based on these modeling results, it is proposed that significant amounts of Fe can be generated by acid mobilization in plumes that follow mid-tropospheric trajectories provided that these plumes experience subsidence back to the marine boundary layer over the remote North Pacific Ocean.

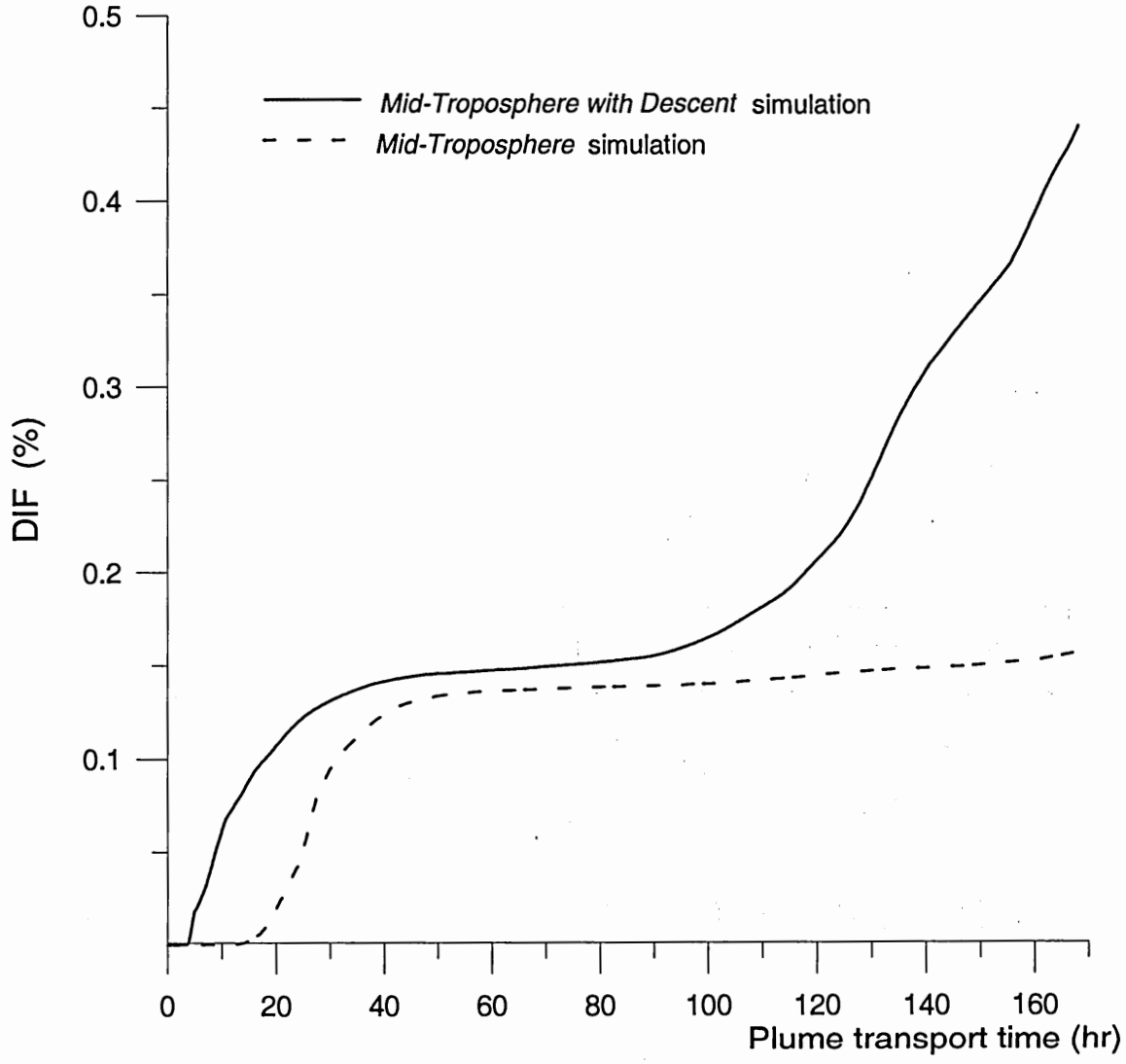

Figure 4.6 Dissolved Iron Fraction as a function of plume transport time for Low Dust/ Standard Pollution cases.

4.6 Additional Mechanisms Enhancing Fe Mobilization Rates

There are several processes that can potentially enhance Fe dissolution rates in advecting dust plumes but have not been included in the model. For example, laboratory studies suggested that sunlight can significantly accelerate hematite dissolution rates in sulfuric acid solutions, making photoinduced reductive dissolution an important mechanism for mobilizing Fe in acidic ambient aerosols [Simnad and Smoluchowski, 1955; Faust and Hoffman, 1986; Behra and Sigg, 1990; Zhuang et al., 1992a]. The presence of organic photo-sensitizers (i.e., oxalate, formate, acetate and continentally derived humic-like organic species) frequently measured in aerosols collected over the polluted areas [Zuo and Holgnè, 1992; Siefert et al., 1994; Havers et al., 1998] can further increase Fe mobilization rates in the presence of sunlight [Zinder et al., 1986; Siffert and Sulzberger, 1991; Pehkonen et al., 1993; Siefert et al., 1994; Blesa et al., 1994; Sulzberger and Laubscher, 1995; Voelker et al., 1997; Banwart et al., 1989; Chang and Matijević, 1983; Faust and Zepp, 1993; Jickells and Spokes, 2001].

In addition, it has been suggested that saltation bombardment (sand blasting) process, the main mechanism for dust uplift into the atmosphere [Gomes, 1990; Prospero, 1999; Ginoux et al., 2001], and the impact of wind-driven particles during their long-range transport can cause dislodgement of the fine particles [Prospero, 1999], increasing reactive surface area of dust and making Fe-III oxides more susceptible for acid dissolution.

Below I will carry out model simulations with increased Fe mobilization rates (by 5 to 10 times) to examine the possible effect of photochemistry and wind-driven physical processes on the DIF of the advecting dust plumes. Such enhancement of the

mobilization rates roughly corresponds to the suggested increase under the conditions similar to those encountered by the plumes simulated here.

Figure 4.7 shows the model-calculated DIF for Standard Dust/High Pollution cases using the *Mid-Troposphere* and *Mid-Troposphere with Descent* simulations. In both model calculations hematite dissolution rates during the daylight hours were raised 5 and 10 times. Interestingly, at the end of simulation period the resulting DIF is close to 0.5 - 2% range for the *Mid-Troposphere* case and even several times higher than this targeted range for *Mid-Troposphere with Descent* case. Therefore, photochemical reductive dissolution and wind-driven physical processes are proposed as additional mechanisms that can enhance Fe mobilization rates in acidic mineral dust plumes pursuing high altitude trajectory to HNLC waters of subarctic North Pacific Ocean.

Finally, recall that the model produced insignificant DIF's for all three model simulations (i.e., *Boundary-Layer*, *Mid-Troposphere* and *Mid-Troposphere with Descent*) in the Standard Dust/Standard Pollution case because there was an insufficient amount of acidity to overcome the carbonate buffer. Although not shown here, the model-calculated DIF-levels for these three cases remain insignificantly small even with enhanced hematite dissolution rates. If it is assumed that three dust trajectories discussed here capture the main advection routes for dust plumes from East Asia, it can be concluded that significant amounts of DIF can not be produced in mineral dust plumes by acid mobilization if the total concentration of acidic species deposited to the dust particle is not high enough to overcome carbonate buffering.

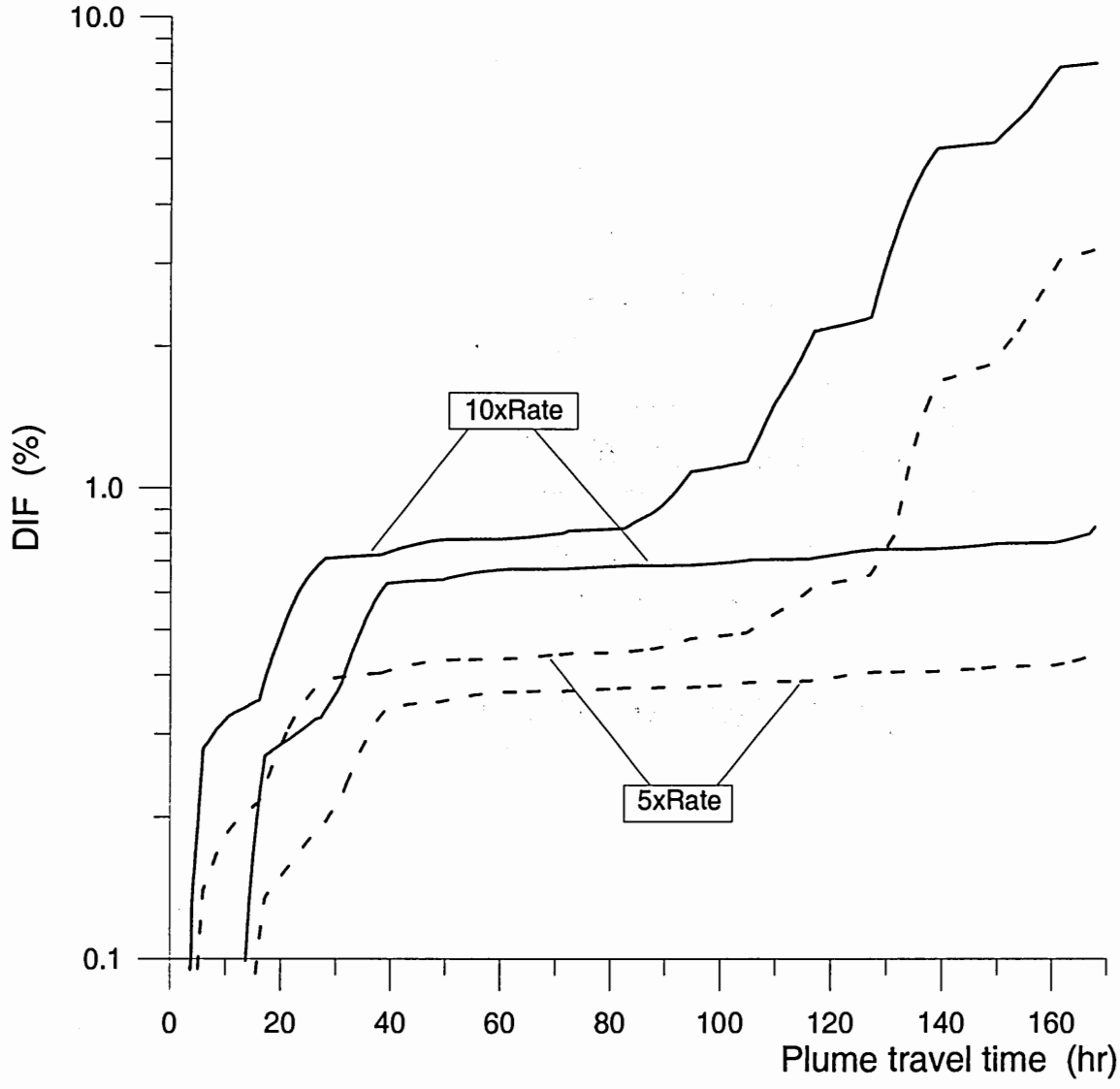

Figure 4.7 Dissolved Iron Fraction as a function of plume travel time for Standard Dust/High Pollution cases of *Mid-Troposphere* (blue) and *Mid-Troposphere with Descent* (red) simulations. The 5xRate and 10xRate cases denote the model simulations when hematite dissolution rate was raised by 5 and 10 times, respectively.

4.7 Model Sensitivity Analysis

In this section, sensitivity calculations are presented to illustrate how reasonable variations in the key model parameters affect DIF in the advecting mineral dust plume. Specifically, model sensitivities to the transport parameterization (i.e., C_{dep} and C_{dil}), the heterogeneous oxidation rates of trace gases, and the initial plume composition are examined. The control run and all tests have been carried out for the Low Dust/Standard Pollution case using the *Boundary Layer* simulation. The sensitivity test results, summarized in Table 4.2, reveal that within the range examined, variations in the key model parameters do not significantly affect model calculated DIF-values.

Table 4.2 Model sensitivities to different parameters

Parameter	Change in the parameter, (%)	Corresponding change in DIF, (%)
C_{dep}	+50	-40
	-50	+5
C_{dil}	+50	-28
	-50	+33
k_{G2} (1)	+45	+62
	-45	-82
k_{G4} (1)	+95	+2
	-95	-2
Wt % Ca (2)	+15	-45
	-15	+25

(1) The sensitivity of the modeling results to SO_2 and NO_x deposition rates are studied for the uncertainties in rate coefficients suggested by Herring et al. [1996];

(2) The sensitivity to the dust composition is tested by varying the weight % of Ca contained in the transportable fraction of the gobi desert soils. The range examined roughly corresponds to the highest and the lowest values suggested in the literature [Hseung and Jackson, 1952; Claquin et al., 1999; Chang et al., 1996; Song and Carmichael, 2001; Zhang et al., 2003]. Changes in the hematite content of the mineral dust are not considered, as (by the definition of DIF) it has no direct effect on the DIF-values of the advecting dust.

4.8 Conclusions

Numerical simulations of three dust-laden plumes emanating from the gobi deserts were presented in this chapter. The results suggest that incorporation of SO_2 into the advecting dust plumes and subsequent acidification of the dust through heterogeneous SO_2 oxidation can increase the acidity of deliquesced mineral dust particles to the levels required to make acid mobilization a viable mechanism for depositing dissolved Fe to the remote oceanic areas, provided some conditions are met.

According to the modeling results, the amount of SO_2 required to mobilize 0.5 - 2% of Fe in large dust storms is several times higher than the normal concentrations measured in urban/industrial cities of East China. Thus, it is proposed that the major fraction of the dissolved Fe generated by acid mobilization and transported to the surface waters of the North Pacific Ocean is contained in relatively small dust plumes (or puffs). However, large dust events that are accompanied by large additions of air pollutants, occasionally observed in China and off the coast of East Asia, can also attain the required 0.5 - 2% of DIF via acid mobilization. Therefore, while the role of the large dust episodes in the supply of dissolved Fe to the surface ocean waters should not be overlooked, the model results suggest that in future studies of the budget of mineral dust export from the Asian continent to the Pacific Ocean attention should also be directed towards evaluating the contributions of small dust outbreaks.

The model simulations carried out in this chapter have also suggested that low atmospheric temperatures encountered by the dust plums during the mid-troposphere transports can effectively reduce acid dissolution rate of hematite below the value required to produce 0.5 - 2% of DIF in advecting mineral dust plumes. Increased initial

SO_2 concentrations in this case did not make a significant difference. The subsidence of the dust plume to the marine boundary layer, the photochemical reductive dissolution of hematite and the increase of dust particle reactive surface area due to the wind-driven physical processes are proposed as additional mechanisms for mobilizing significant amounts of Fe in dust plumes following such high altitude trajectories to the HNLC waters of subarctic North Pacific Ocean. These findings suggest that inclusion of the detailed mechanism for the photochemical cycling of Fe in deliquesced mineral dust particles and parameterization for the possible change in reactive surface area during long-range atmospheric transport might be required in future models to better estimate fluxes of dissolved Fe to the surface waters of the North Pacific Ocean.

In the following section the model results in combination with the space-borne MODIS data are used to explore if the model-predicted amounts of Fe mobilized in dust plumes advecting to the Fe stressed regions of North Pacific Ocean can be correlated with the satellite-borne remote observations of changes in marine ecosystem productivity following passage of these plumes.

CHAPTER 5

EPISODIC DUST PASSAGE AND PHYTOPLANKTON BLOOMS IN NORTH PACIFIC OCEAN

5.1 Introduction

In this chapter, the results of the model calculations presented in the previous chapter (and their relevance to C-uptake and ocean productivity) are evaluated. I do this by testing if the model predicted amounts of dissolved Fe to have been deposited to the Fe-stressed regions of the North Pacific Ocean can be correlated with satellite-borne observations of changes in chlorophyll *a* levels following passage of the plume.

5.2 General Considerations

The waters of subarctic North Pacific can be divided into two distinct biogeochemical regions: the inshore (or coastal) and the offshore (or open ocean) regions [Boyd and Harrison, 1999]. The coastal ocean waters are characterized by the highest primary productivity rates in the Pacific Ocean. Productivity rates in the region tend to be well correlated with the ocean upwelling and riverine outflow, the two main mechanisms that provide fresh nutrients to the euphotic zone of these waters [Firme et al., 2003]. Because upwelling events are not constant, the phytoplankton community goes through intercalating bloom and relaxation events that can last up to 3 weeks [Dugdale and Wilkerson, 1989; Firme et al., 2003]. (Phytoplankton bloom areas are loosely defined as

the patches where total chlorophyll levels episodically increase by more than an order of magnitude over the waters of the surrounding area [Boyd et al., 1998; McDonald et al., 1999; Wells, 2003].) During the late spring and summer, when upwelling events are most intensive, chlorophyll *a* levels in the coastal ocean waters can increase to 2 mg/m^3 or even higher [Boyd and Harrison, 1999]. In the coastal region, diatoms are usually the dominant phytoplankton group and sedimentation is most likely the main removal mechanism of Particulate Organic Carbon (POC) [Boyd and Harrison, 1999].

By contrast, the open ocean area of subarctic North Pacific (that hosts one of the three HNLC regions discussed in Chapter 1) shows low seasonal variability in biomass production, despite the perennial presence of nutrients such as nitrate, phosphate and silicic acid. The year round chlorophyll *a* values in the offshore areas of subarctic North Pacific are about an order of magnitude lower (0.2 to 0.4 mg/m^3) than those of the costal waters [McDonald et al., 1999; Tsuda et al., 2003]. Moreover, algal biomass is dominated by nano and pico-planktonic communities, the main fate of which is believed to be pelagic recycling through the microbial food web [Boyd and Harrison, 1999].

The main reason for the strong difference in the primary productivities of these two regions appears to be the availability of the micronutrient Fe [Martin and Gordon, 1988; Martin et al., 1989; Martin et al., 1991a; Boyd and Harrison, 1999; McDonald et al., 1999; Tsuda et al., 2003; Nishioka et al., 2003]. While riverine outflow and the upwelling of sedimentary Fe are effective in delivering dissolved Fe to the coastal regions [Firme et al., 2003], they are not active in the offshore areas of the subarctic North Pacific. As noted earlier, the dominant source of bioavailable Fe in these later regions is most likely the transport and deposition of mineral dust from arid and semi-arid

regions of East Asia [Duce et al., 1991; Duce and Tindale, 1991; Jickells and Spokes, 2001; Watson, 2001].

Since the offshore waters of subarctic North Pacific are characterized by very low seasonality in phytoplankton primary production rates and the year round presence of all major nutrients except Fe (which is believed to be supplied predominantly through the atmosphere), this open ocean region is perhaps is the most appropriate area to examine the role of episodic aeolian dust deposition to marine ecosystem productivity.

In this chapter we examine the impact on local ocean productivity of two of the three dust episodes simulated in the Lagrangian model and discussed in the previous chapters: specifically, the episodes from the *Mid-Troposphere* and *Mid-Troposphere with Descent* simulations. Recall that the trajectories of both plumes brought them to the Fe stressed waters of the North Pacific Ocean (see Figures 3.5 and 3.8).

5.3 Initial Plume Composition and Corresponding Dust and DIF-Levels

In Chapter 4, the results of model calculations for the *Mid-Troposphere* and *Mid-Troposphere with Descent* simulations were presented using typical initial Dust and pollutants concentrations. In order to investigate the amount of Fe delivered to the North Pacific Ocean from the specific dust plumes simulated in these cases, it is necessary to rerun these simulations using initial concentrations appropriate for these episodes. Table 5.1 summarizes these initial values for Dust and pollutants. As discussed below, the initial values of Dust, SO_2, NO_x, and O_3 were set to match those measured during the ACE-Asia/TRACE-P ground-based and airborne missions. The initial NH_3 concentration, which was not measured during these missions, was based on the model-calculated

concentrations for Beijing during a March, 1994 dust storm [Song and Carmichael, 2001].

5.3.1 *Chemical composition of the plume used in Mid-Troposphere simulations:* In the *Mid-Troposphere* simulations the initial concentrations for Dust, SO_2, NO_x, and O_3 were assumed to be 1500 $\mu g/m^3$ and 6, 2, and 55 ppbv, respectively. As the dust plume used for *Mid-Troposphere* simulations was advected at high altitudes over Beijing, no direct measurement of the initial dust concentration is available. The initial value used here was assigned from the Navy Aerosol Analysis and Prediction System (NAAPS) modeling results [on the web at: http://www.nrlmry.navy.mil/aerosol/Case_studies/ aceasia/] for Beijing at ~06 UTC on April 7, 2001. Note that large initial Dust concentration of 1500 $\mu g/m^3$ for this simulation indicates that the dust plume for the *Mid-Troposphere* simulation was formed from an exceptionally large storm [Kurosaki and Mikami, 2003; Liu et al., 2003].

Initial concentrations of gas-phase SO_2, NO_x, and O_3 the *Mid-Troposphere* simulations were set at 8, 4 and 55 ppbv, respectively, to match the values observed over the Sea of Japan by the NCAR C-130 when it intercepted the dust-laden air-masses between 8:00 and 9:00 UTC on April 8, 2001. Note, that the low concentration of pollutants measured inside the plume by the C-130 aircraft (molar ratios of SO_4^{2-}/Ca^{2+} <0.3 and SO_2 mixing ratios less than 100 ppt [Huebert et al., 2003; Lee et al., 2003]) are consistent with the SeaWiFS image (see Figure 5.1) showing the plume used in our *Mid-Troposphere* simulations had a yellowish-brown color with some grayish-green regions; i.e., suggesting that the plume mainly consisted of mineral dust with a small amount of anthropogenic pollution [Kaufman et al., 2002]. Note, that availability of the in situ data

for the plume used in *Mid-Troposphere* simulations makes SeaWiFS image relatively unimportant; however, it is included here to show consistency between the airborne measurements and the satellite retrievals, so that SeaWiFS images can be used later to characterize mineral dust plumes when no direct measurements of the plume's chemical composition exists.

Table 5.1 Initial chemical conditions adopted for model calculations

Parameter	*Mid-Troposphere* simulations	*Mid-Troposphere with Descent* simulations
Coarse model aerosol composition		
Dust , ($\mu g/m^3$)(1)	1500	750
SO_4^{2-}, ($\mu g/m^3$)	0.5	0.5
NO_3^-, ($\mu g/m^3$)	0.5	0.5
Fine mode aerosol composition		
SO_4^{2-}, ($\mu g/m^3$)	3.5	3.5
NO_3^-, ($\mu g/m^3$)	3.0	3.0
NH_4^+, ($\mu g/m^3$)	2.5	2.5
Gas phase mixing ratios		
SO_2, (ppbv)	8.0	50
NO_x, (ppbv)	4.0	4.0
NH_3, (ppbv)	5.5	5.5
O_3 , (ppbv)	55	65

(1) The assumed initial composition of the dust is discussed in Section 3.4.1 and detailed in Table 3.3.

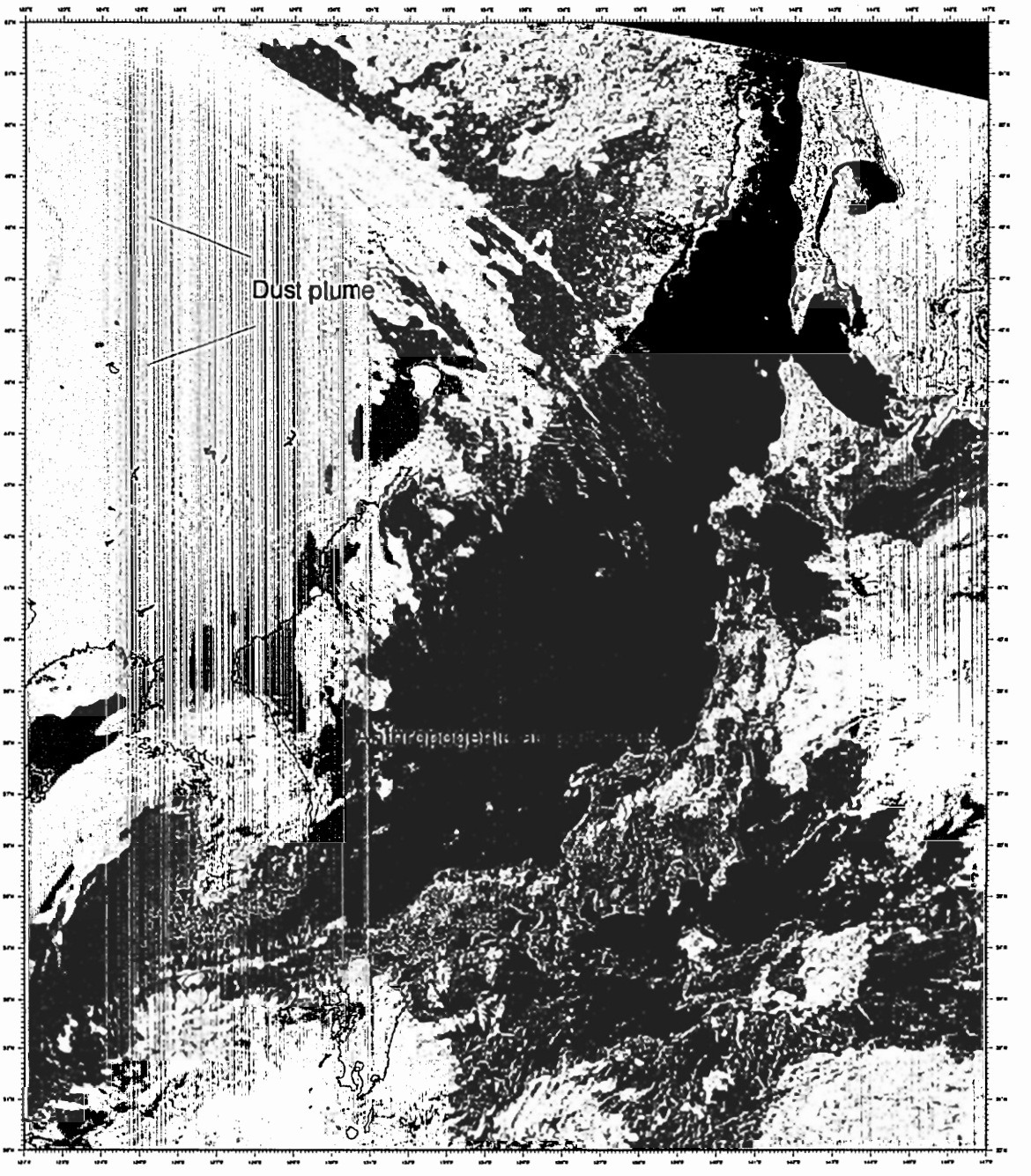

Figure 5.1 SeaWiFS image of eastward moving gobi-dust plume captured on April 8, 2001. The image is provided by the SeaWiFS Project, NASA/Goddard Space Flight Center, and ORBIMAGE; on the web at http://visibleearth.nasa.gov.

5.3.2 *Chemical composition of the plume used in Mid-Troposphere with Descent Simulations*: In the *Mid-Troposphere with Descent* simulations initial Dust and SO_2, NO_x, and O_3 concentration were assumed to be 750 $\mu g/m^3$ and 50, 4 and 65 ppbv, respectively. The initial boundary layer dust concentration is consistent with both filter-based ground level [Wild et al., 2003] and continuous lidar measurements [Chen et al., 2001] in Beijing on March 12 and March 13, 2001. The initial concentrations of SO_2, NO_x and O_3 for this case were approximated from Chinese air quality data reports for Beijing during the same time period [Wild et al., 2003]. This data shows that on March 12 and March 13, 2001 one day averaged SO_2 mixing ratio in Beijing reached 60 ppb, more than 5 times its nominal springtime concentration and the highest value reported during spring, 2001 [Wild et al., 2003]. Such high pollution episode is in agreement with the measurements of dual polarization lidar, showing the exceptionally high concentrations of anthropogenic air pollution aerosols in Beijing for that time period [Chen et al., 2001].

There are no in situ measurements for the gas-phase and particulate-phase composition of this plume; however, as dust was advecting inside the boundary layer of Beijing metropolitan area, the enrichment of dust with high mixing ratios of SO_2 is a reasonable assumption. The mixture of mineral dust with the elevated concentrations of anthropogenic air pollutants was also captured on SeaWiFS satellite image (see Figure 5.2), showing a yellowish-brown haze (dust) over the northeastern China mixed with high amount of grayish-green haze, proxy for the anthropogenic air pollutants [Kaufman et al., 2002].

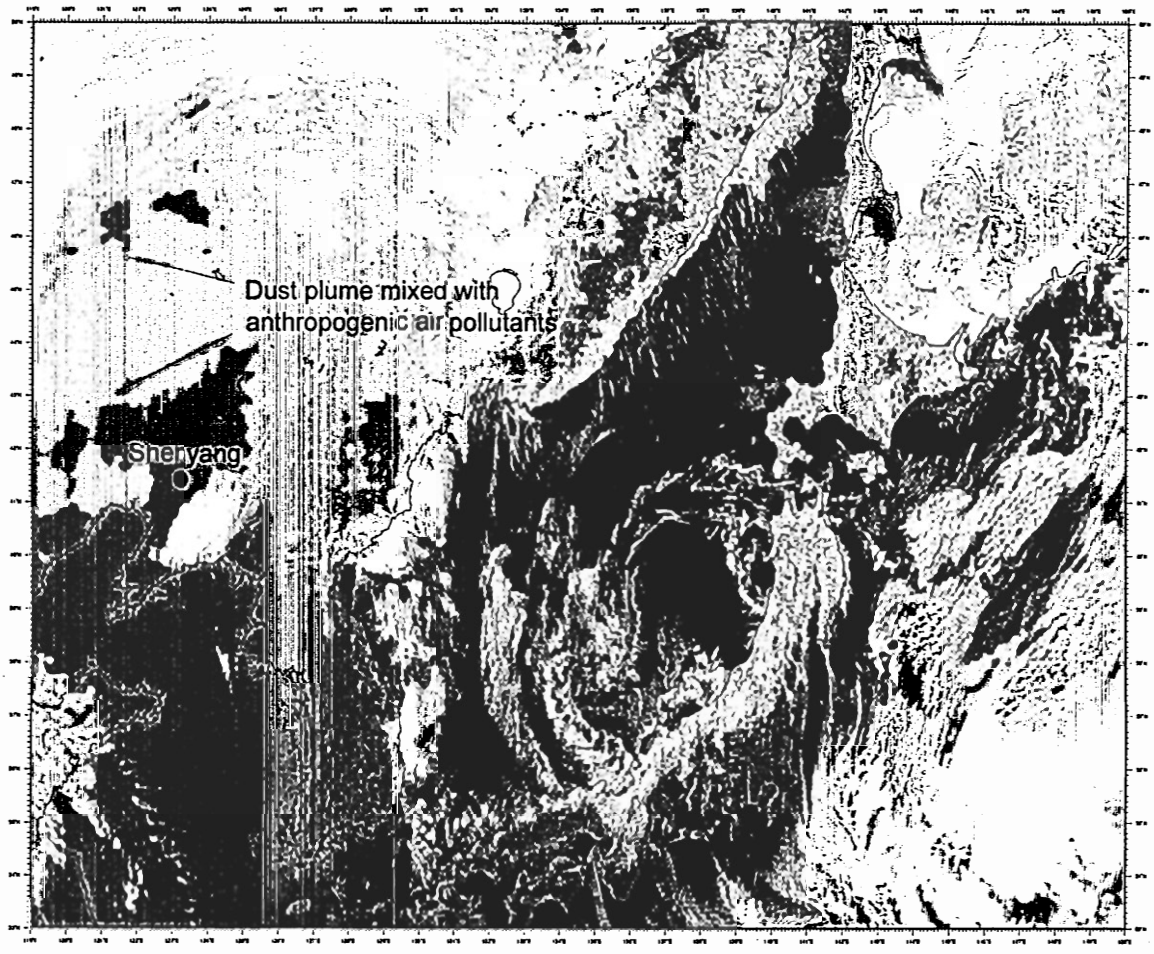

Figure 5.2 SeaWiFS image of north eastward moving gobi-dust plume captured on March 13, 2001. The image is provided by the SeaWiFS Project, NASA/Goddard Space Flight Center, and ORBIMAGE.

Comparison of Tables 4.1 and 5.1 shows that pollutant concentrations for the *Mid-Troposphere* simulations are consistent with the nominal springtime values typically measured in Beijing metropolitan area [Song and Carmichael, 1999; 2001; Wang et al., 2001; Tan et al., 2002; Wild et al., 2003]. The ground-based measurements conducted in Beijing [Wild et al., 2003] also show, while SO_2 mixing ratio used in *Mid-Troposphere with Descent* simulations is significantly higher than the average springtime concentration, it is not unreasonable. Such high concentrations of SO_2 were recorded in Beijing several times during winter early spring 2001.

5.3.3 *Resulting Dust and DIF*: Figure 5.3 shows the model-calculated Dust and DIF-levels as a function of time for the *Mid-Troposphere* and *Mid-Troposphere with Descent* simulations using these new sets of initial conditions and the enhanced hematite dissolution rates (due to photochemistry and wind-driven physical processes). Note that because the initial Dust concentration for the *Mid-Troposphere* simulation is quite large (i.e., 1500 $\mu g\ m^{-3}$), the initial SO_2 concentration (of 8 ppbv) is inadequate to overcome the carbonate buffer and as a result, the DIF remains insignificantly small. In the *Mid-Troposphere with Descent* simulation, on the other hand, the initial Dust concentration is more modest (i.e., 750 $\mu g\ m^{-3}$) and the initial SO_2 was quite large (i.e., 50 ppbv), and thus the DIF becomes quite significant reaching a maximum of 3.5% when the enhanced hematite dissolution rate was used. In the sections below, the results of these calculations will be used to estimate the Fe enhancements to the surface waters of the remote Pacific Ocean that might have resulted from these two dust episodes.

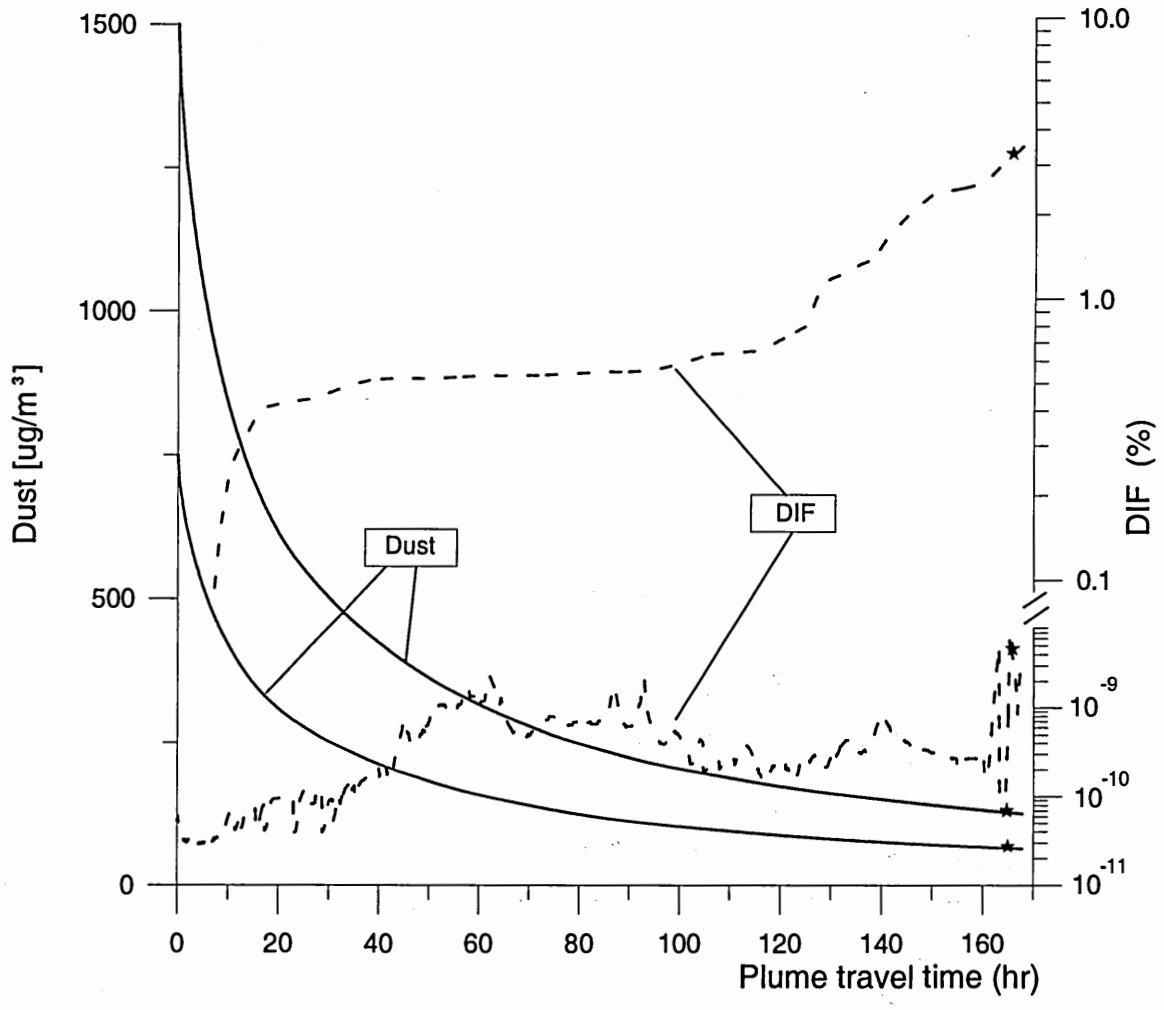

Figure 5.3 Model calculated Dust and DIF as a function of plume travel time for *Mid-Troposphere* (black) and *Mid-Troposphere with Descent* (red) simulations. Symbols on the graphs show the values that are used below to estimate the Fe enhancements to the surface waters of the remote Pacific Ocean.

5.4 How much Dissolved Fe was Delivered to the Ocean by the Dust Plumes?

Let $Dust_f$ and DIF_f denote the model-calculated dust concentration (in $\mu g/m^3$ air) and DIF-value in the plume when the plume reaches the Fe-stressed regions of the North Pacific Ocean. It then follows that $(Fe_{diss})_f$ the average concentration of the dissolved Fe in the plume in units of μ g Fe /m^3 of air is given by

$$(Fe_{diss})_f = 0.035*Dust_f*DIF_f \quad (5.1)$$

where 3.5% is the Fe content of the Asian dust [see Table 3.4, as well as Taylor and McLennan, 1985; Duce and Tindale, 1991]. Now, if H is the vertical height (in meters) of the dust plume, then $(N_{Fe\text{-}diss})_f$, total concentration of dissolved Fe in the dust column in μ g Fe/m^2 is:

$$(N_{Fe\text{-}diss})_f = 0.035*Dust_f*DIF_f*H \quad (5.2)$$

If, by some process such as rainout, this dust column is deposited onto the ocean and evenly distributed within the surface mixed layer, then concentration of the enriched Fe_{diss} (in units of mole/liter of seawater) in the patch should be given as:

$$[Fe]_{enrich} = 0.035 \cdot Dust_f \cdot DIF_f \cdot H/M_{Fe}/D/\rho \quad (5.3)$$

where M_{Fe} is gram-molecular weight of Fe (i.e., 56 g/mole), D is the ocean mixed layer depth (in m) and ρ is the density of seawater (~1000 kg/m^3). In deriving Equation (5.3), it is assumed that all of the mineral Fe mobilized in the dust plume stays in dissolved form after its deposition on the ocean surface. Such an assumption is supported by the Subarctic Pacific Iron Experiment for Ecosystem Dynamics Study (SEEDS) which showed that the major fraction of the dissolved Fe after its release in subarctic North Pacific Ocean waters is complexed by macromolecular organic colloids (operationally defined as size range between 1nm and 0.2 μm) [Nishioka et al., 2003]. Such binding

with natural organic ligands significantly increases the concentration of Fe in the infused patches above its inorganic solubility threshold and inhibits conversion of dissolved Fe to the particulate form [Kuma et al., 1996; Liu and Millero, 2002]. Recent studies suggest that much (but not all) of the Fe bonded to organic ligands is available to phytoplankton [Rue and Bruland, 1995; Maldonado and Price, 1999; Hutchins et al., 1999; Chen et al., 2003; Wells, 2003].

Using Equation 5.3 along with values calculated for $Dust_f$ and DIF_f for the two simulations using the Standard Dust/Standard Pollution cases (see Figure 5.3 and Table 5.2), it is estimated that the dust plume used in the *Mid-Troposphere with Descent* simulations enriched the surface ocean waters by ~ 0.07 to 0.4 nM of Fe. The range in values arises from the use of two values for DIF_f, the lower value using the DIF calculated in the Standard Model and the higher value using the DIF calculated with the hematite dissolution rate increased by a factor of 5 during the daytime hours to account for the possible enhancement in iron dissolution rate due to the photochemistry and the wind-driven physical processes. In comparison, a negligibly small Fe enrichment is calculated for the *Mid-Troposphere* simulation.

Table 5.2 Parameters used and calculated values for $[Fe]_{enrich}$, the surface ocean enrichment in dissolved Fe

Parameter	*Mid-Troposphere with Descent* case[1]	*Mid-Troposphere* case[1]	Source
$Dust_f$, final average dust concentration in plume ($\mu g/m^3$)	65	125	From the model
Average Fe content of dust, (%)	3.5	3.5	Taylor and McLennan [1985]; Duce and Tindale [1991]
DIF_f, final dissolved iron fraction of dust, (%)	3.5 (0.45)	$2x10^{-9}$ ($3x10^{-10}$)	From the model
D, ocean mixed layer depth, (m)	10-40	10-40	Maldonado et al. [1999]; Nishioka et al. [2001]; Nishioka et al. [2003]; Tsuda et al. [2003]
H, vertical extent of dust plume, (m)	2-3 $x10^3$	2-3 $x10^3$	Uno et al., 2001
$[Fe]_{enrich}$ (nM)	0.07-0.4 (0.01-0.06)	8-50 $x10^{-11}$ ($1-7\ x10^{-11}$)	Equation 5.3

(1) Numbers in the parenthesis shows DIF and $[Fe]_{enrich}$ without considering the effect of photo-chemistry and wind-driven physical processes on hematite solubilization rates.

5.5 The Expected Change in Chlorophyll Concentration from the Fe Enrichment

As previously discussed, marine ecosystem productivity in the surface ocean waters of subarctic North Pacific is limited by the availability of micronutrient Fe. So it is quite realistic to assume that all mobilized Fe, deposited to the surface waters of this region by the dust storms, will be taken up by the planktonic community. Therefore, to calculate the expected increase in algal carbon content due to the episodic Fe enrichment, the cellular Fe to carbon $(Fe:C)_{cell}$ ratio for phytoplankton species needs to be considered. Published values for $(Fe:C)_{cell}$ ratios for different aquatic species vary 50-fold or more

[Wells et al., 1995; Sunda and Huntsman, 1995; Schmidt and Hutchins, 1999]. Therefore, to further evaluate the expected increase in algal carbon content of the North Pacific Ocean waters, we need to know which phytoplankton species are able to grow rapidly after the Fe enrichment and thereby using up the extra Fe and dominating the biomass in the Fe-enriched patch.

The SEEDS experiment demonstrated that a mesoscale Fe enrichment in the Subarctic Pacific waters of ~3 nM caused a rapid increase of algal carbon with chlorophyll *a* values inside the patch approaching 20 mg/m^3 [Tsuda et al., 2003]. The Fe infusion transformed a largely recycling pico-planktonic community into a community of large chain-forming centric diatoms with one dominant species, *Chaetoceros debilis* (10-30 μm wide) [Tsuda et al., 2003]. Estimated $(Fe:C)_{cell}$ molar ratios suggested in the literature for centric diatoms in subarctic North Pacific waters range between 30 to 90 μmol Fe:mol C [Martin et al., 1989; Wells et al., 1995; Boyd and Harrison, 1999; Schmidt and Hutchins, 1999]. Adopting this range, it follows that an Fe enrichment of 0.07 to 0.4 nM of Fe (that calculated for the *Mid-Troposphere with Descent* simulation) would have caused an algal biomass concentration increase of ~ 0.8 to 13 mmol C/m^3 (or 10 to 160 mg C/m^3).

In order to further compare these results with the satellite data, the above increase in biomass carbon (essentially a measure of the particulate organic carbon or POC content) of the ocean waters needs to be converted to the parameter seen by the satellite sensor; i.e., the chlorophyll *a* (Chl *a*) concentration. Estimated C:Chl *a* ratios for centric diatoms range from 20 to 50 mg C (mg Chl *a*)$^{-1}$ [Gallegos and Vant, 1996; Landry et al., 2000; Boyd and Harrison, 1999; Geider et al., 1997; Taylor et al., 1997]. By using this

ratio we predict that the plume simulated in *Mid-Troposphere with Descent* case would have increased chlorophyll *a* concentration in North Pacific Ocean waters by 0.2 to 8 mg/m^3. The large range in this result (more than an order of magnitude) is indicative of the need for more experimental measurements quantifying the relationship between dissolved Fe concentrations, Fe uptake rates and the resulting $(Fe:C)_{cell}$ ratios for the main diatomic species in Fe limited regions of the North Pacific Ocean.

Carrying out the same calculations for the *Mid-Troposphere* simulation, with significantly smaller values for DIF and $[Fe]_{enrich}$, it is found that chlorophyll *a* concentration would have increased by $<1 ng/m^3$. Such small increase in algal carbon content would not have been observable.

5.6 The Algal Response Time after Fe Enrichment

In the SEEDS experiment, phytoplankton chlorophyll *a* concentration in the Fe treated patch began to show rapid increases about six days after the initial dissolved Fe enrichment; maximum chlorophyll *a* concentrations reached maximum value on the 10^{th} day [Tsuda et al., 2003]. In the *Mid-Troposphere with Descent* simulation, the plume was calculated to have arrived at the Fe-stressed region of the North Pacific Ocean where it encountered a precipitation event on March 19, 2001 (see Figure 3.8). On the basis of this calculation and the SEEDS observation, we can conclude that the first signs of the increased chlorophyll *a* concentration from the effects of the Fe enrichment from the plume should have been observable after March 25, 2001 and the algal carbon content should have approached its maximum value around March 29, 2001.

5.7 Episodic Aeolian Dust Deposition and Marine Ecosystem Productivity

Figures 5.4a and b show MODIS surface chlorophyll *a* concentration images of North Pacific Ocean for the mid-March early April, 2001. Chlorophyll *a* retrievals near the patch at 36°N-39°N, 151°W-158°W (i.e., the region where we earlier estimated that the plume from the *Mid-Troposphere with Descent* simulation encountered strong precipitation event and likely deposited its dust) were sparse due to obscuration of the sea surface by clouds, therefore all MODIS chlorophyll *a* images shown here are for the 8 day averaged concentration. The black color on the images denotes the missing data due to the clouds and the thin white lines indicate the coastal boundary.

This figure clearly demonstrates that in the week of March 30 to April 6, 2001 the chlorophyll *a* content of the patch at 36°N-39°N, 151°W-158°W increased significantly, approaching a maximum concentration of about 3 mg/m^3. High amount of clouds did not allow daily retrievals of chlorophyll a contents inside the patch, but the elevated concentration of algal carbon was clearly seen through clouds on March 30, 2001 (not shown). Figures 5.5a, b, and c show that the bloom can be tracked over a period of about 20 days.

The maximum chlorophyll *a* concentration inside the patch of 3 mg/m^3 is consistent with the chlorophyll *a* enhancement estimated earlier for the area on the basis of the model calculations. It is also more than an order of magnitude higher than that of the waters in the surrounding region for a period of about 3 weeks (see discussion below), and thus can be considered as a clear visual indication of a phytoplankton bloom. The fate of phytoplankton bloom was most likely caused by the Fe limitation, although calculations using the Redfield value for C:N molar ratio and measured NO_3

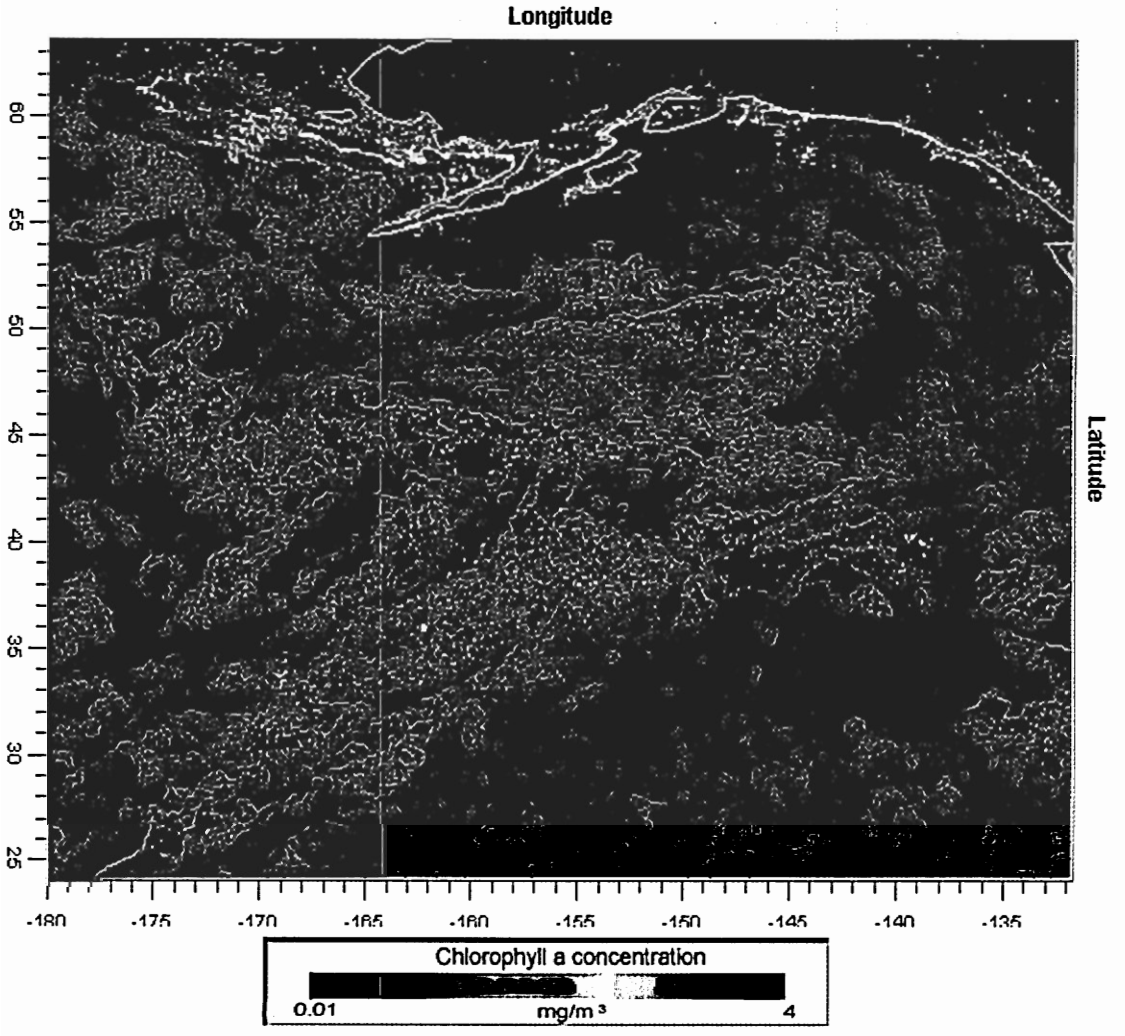
Longitude
Latitude
60
55
50
45
40
35
30
25
-180
-175
-170
-165
-160
-155
-150
-145
-140
-135
Chlorophyll a concentration
0.01
mg/m 3
4

a)

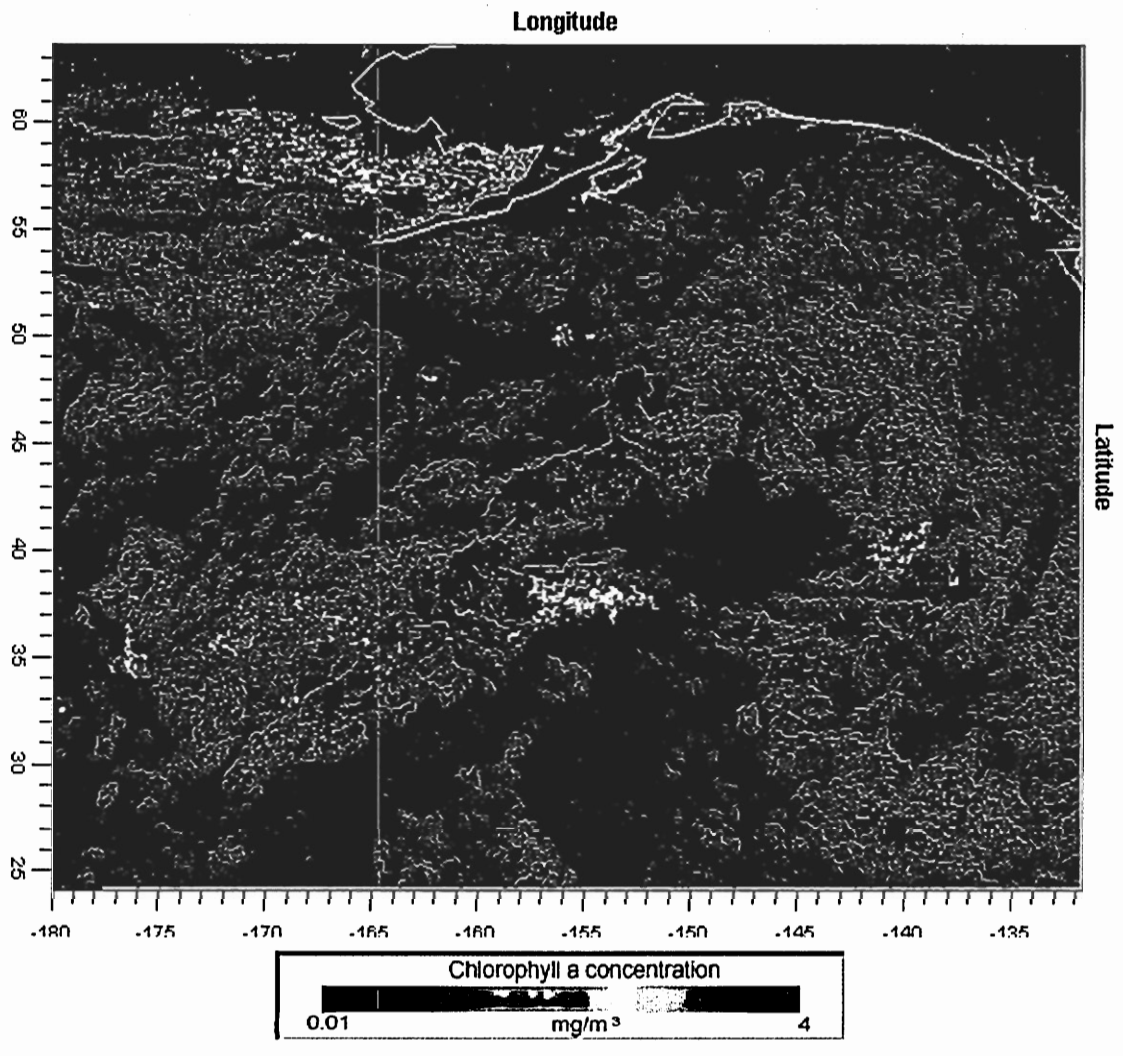

b)

Figure 5.4 The eight day average a) 14 to 21 March, 2001 and b) 30 March to 6 April, 2001 MODIS surface chlorophyll *a* image.

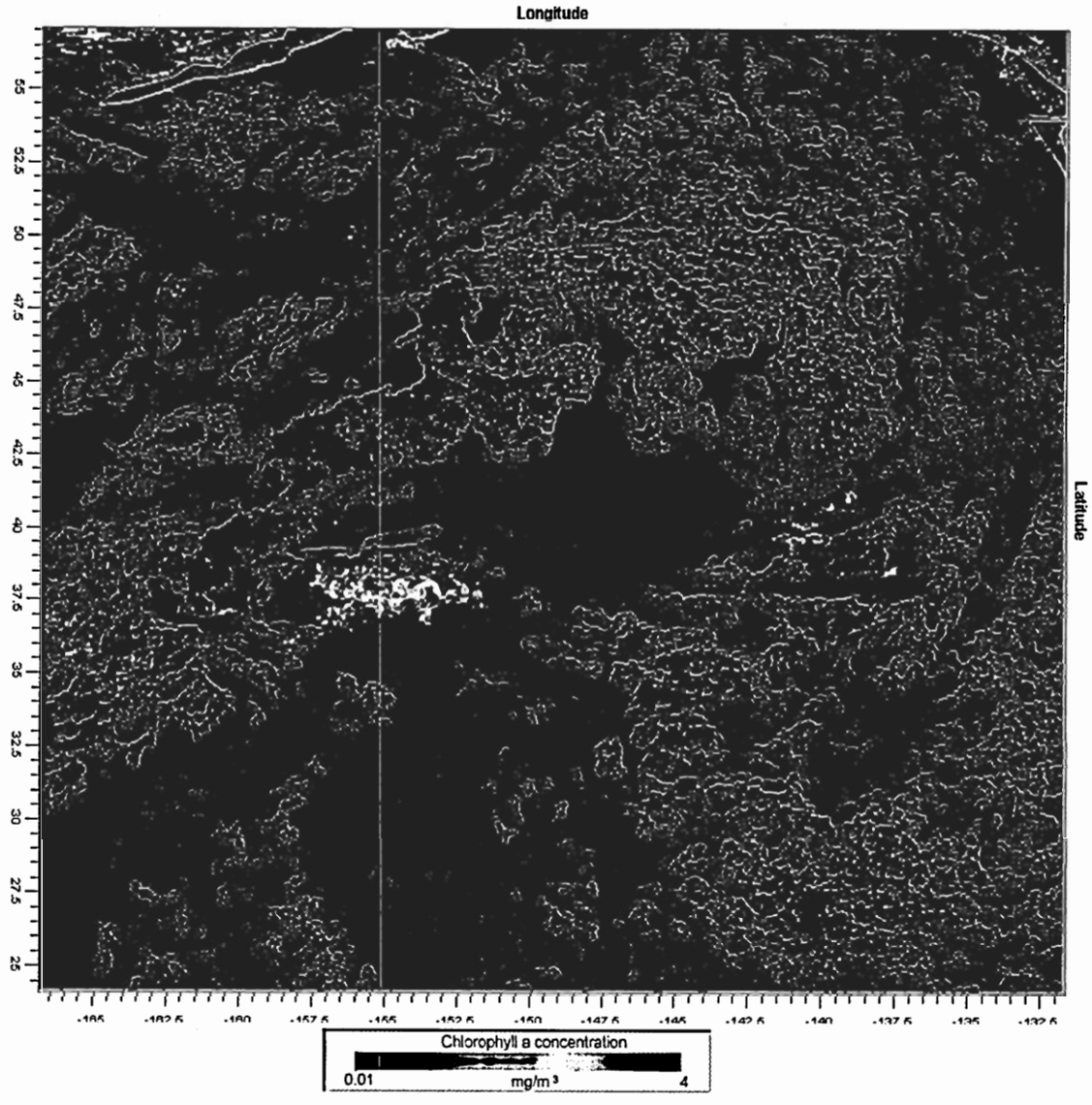
Longitude
Latitude
55
52.5
50
47.5
45
42.5
40
37.5
35
32.5
30
27.5
25
Chlorophyll a concentration
0.01
mg/m³
4

a)

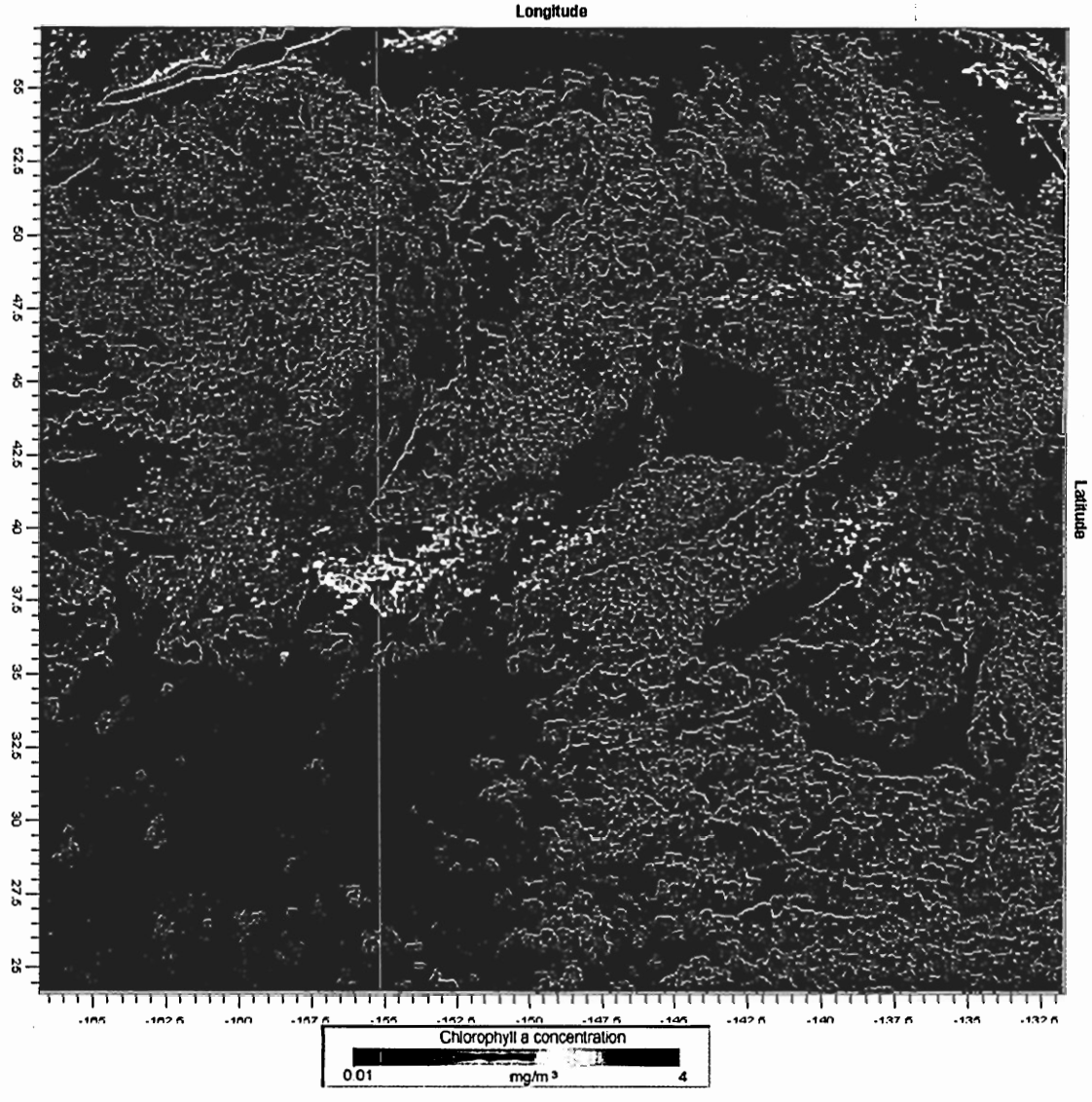
Longitude
Latitude
55
52.5
50
47.5
45
42.5
40
37.5
35
32.5
30
27.5
25
Chlorophyll a concentration
0.01
mg/m³
4

b)

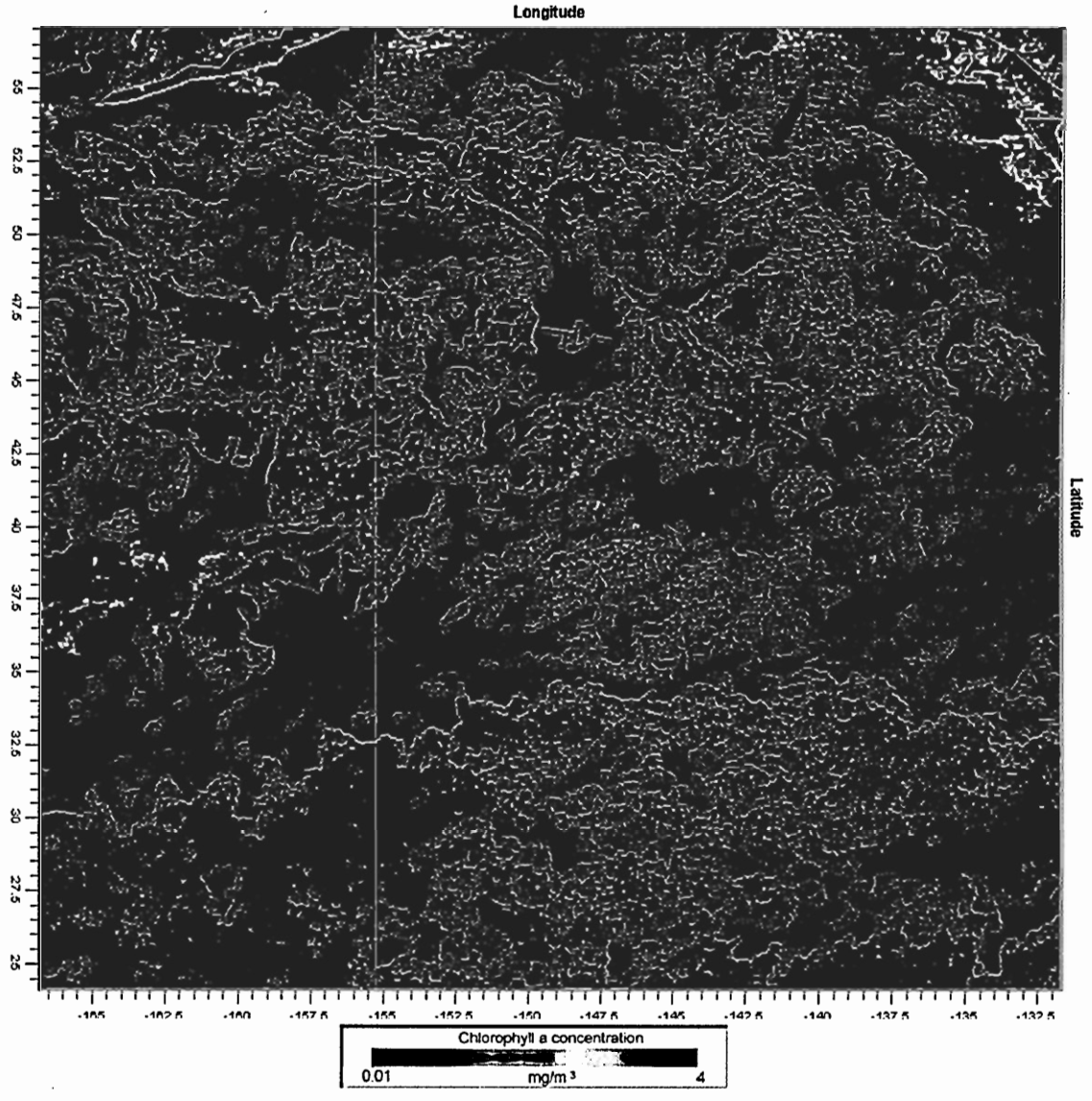

c)

Figure 5.5 The eight day average a) 30 March to 6 April, 2001, b) 7 to 14 April, 2001 and c) 15 to 22 April, 2001 MODIS surface chlorophyll *a* image. Figure a) was enlarged from 5.1b to show the change of the bloom location with the time.

concentrations for the station located close to the patch (39.60°N, 140.77°W) [Martin et al., 1989] suggest that algal growth could have become co-limited by the availability of nitrate.

As an extension of our discussion, Figures 5.6a, b, and c display MODIS surface chlorophyll *a* concentration images for the HNLC waters of subarctic North Pacific Ocean prior and after the dust passage simulated in the *Mid-Troposphere* case. Careful examination of these figures does not reveal any noticeable changes in Chlorophyll *a* content at the offshore regions of subarctic North Pacific. This result is also in accord with model predicted negligible DIF-values for this plume.

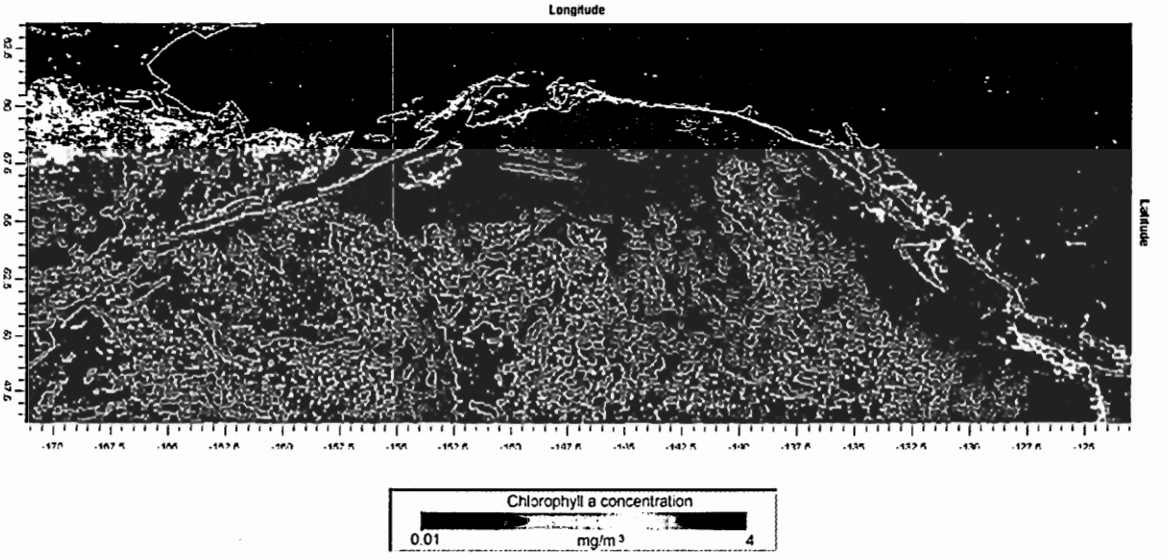

a)

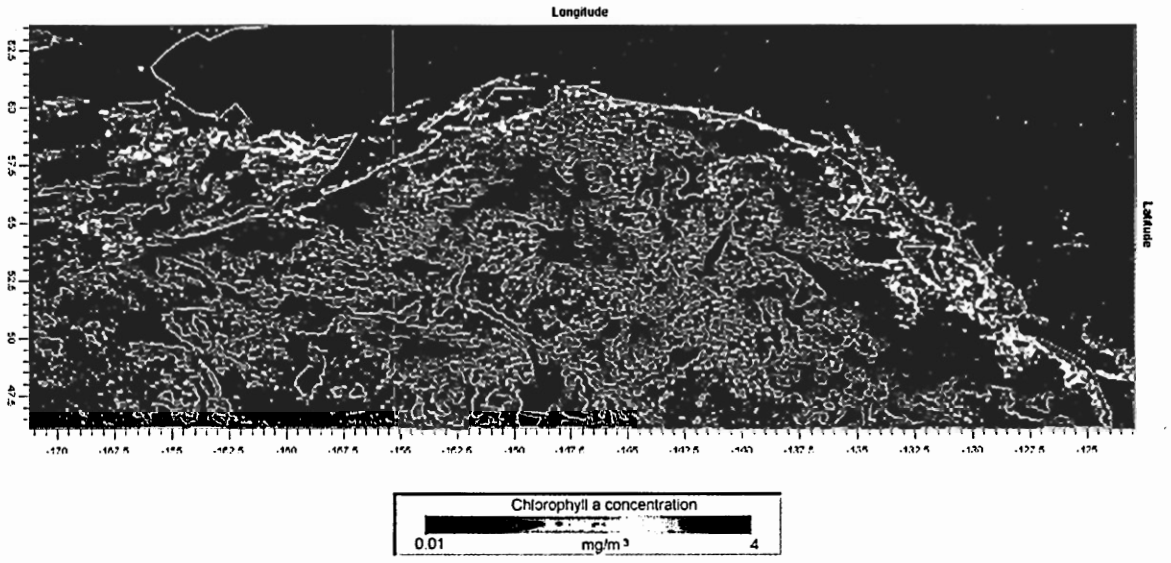

b)

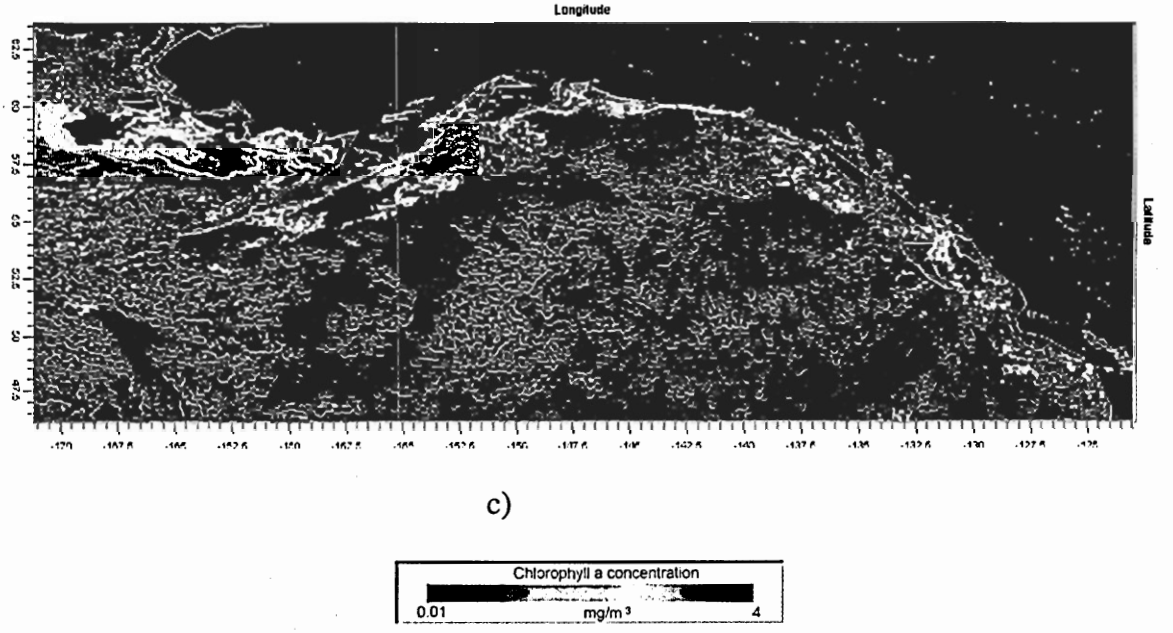

c)

Figure 5.6 The eight day average a) 7 to 14 April, 2001, b) 15 to 22 April, 2001 and c) 23 to 30 April, 2001 MODIS surface chlorophyll *a* image.

5.8 The Possible Role of Upwelling

In their recent article, Lin et al. [2003] showed that strong winds associated with cyclones can cause entrainment (vertical mixing) and upwelling of nutrient-rich waters (from 70-90 m depth) to euphotic zone, fueling photosynthesis, and even causing phytoplankton blooms. Such deep water entrainments are usually associated with a simultaneous depression in sea surface temperatures (SST) [Dickey et al., 1998], and in the bloom observed by Lin et al. [2003] a large pool of cold SST was found to be co-located with the bloom.

To evaluate the possible contribution of the deep-water upwelled Fe to the increased Chlorophyll *a* content of the patch, the 8 day average MODIS SST data over the patch is shown in Figure 5.7. This image does not reveal any significant difference between the SSTs of the patch where the bloom occurred and the surrounding area. This suggests that there was at most minor upwelling during the passage of the low pressure system over the patch (see discussion in Chapter 3). In addition, the vertical distribution of dissolved Fe concentration at a location close to the patch (39.60°N, 140.77°W) [Martin et al., 1989] indicates that the ocean waters at a 50 to 100 m are usually significantly depleted in dissolved Fe content compared to that of the surface ocean (~20m). Based on these arguments, it would appear that upwelling in the region could not have supplied the Fe needed to explain the bloom observed over the patch by MODIS.

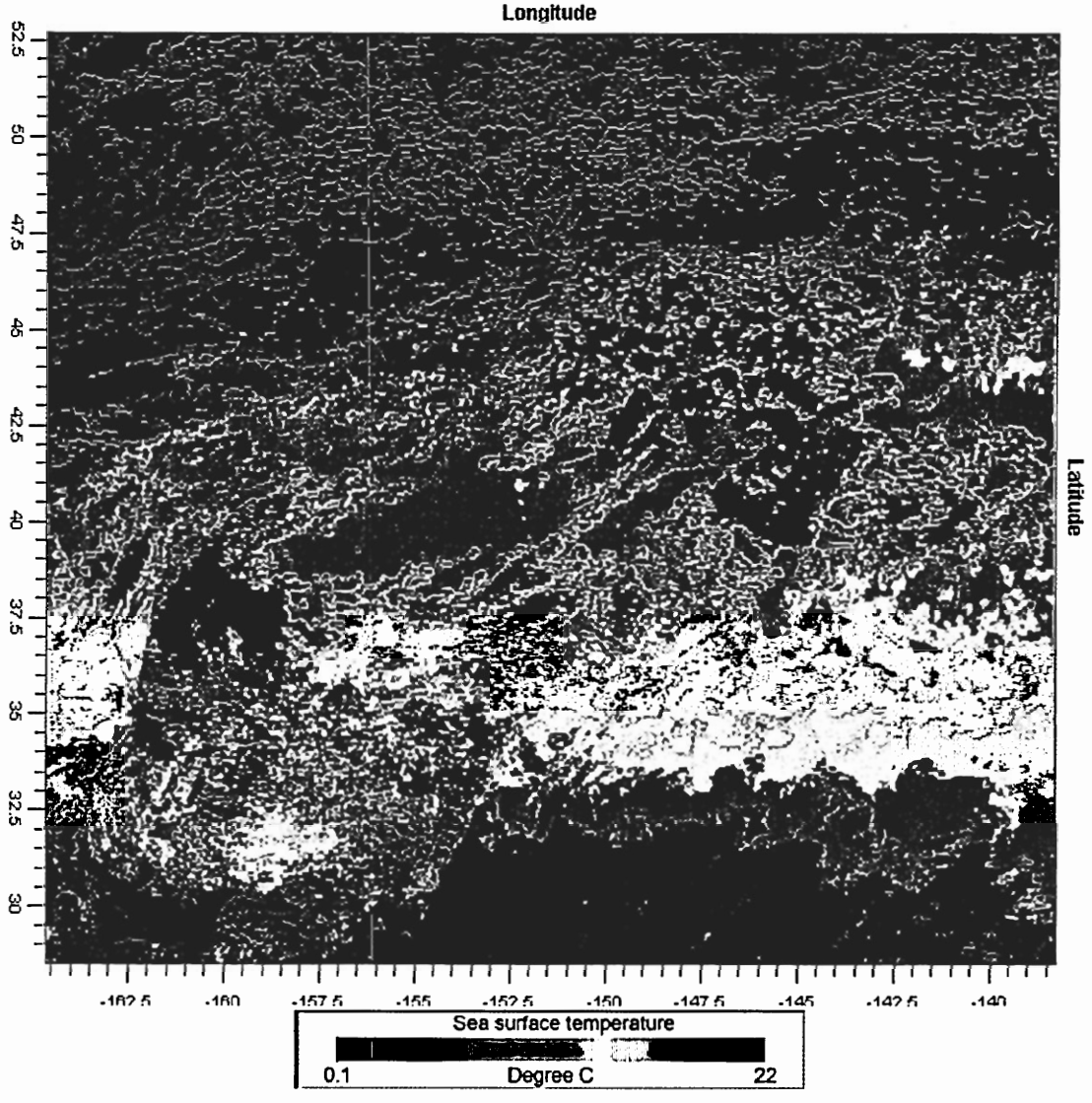

Figure 5.7 The eight day average (22 to 29 March, 2001) MODIS sea surface temperature image.

5.9 Discussions

It was discussed in Chapter 3 that in order for gobi-dust plumes to reach HNLC waters of subarctic North Pacific ocean they need to be lifted up by strong convective motion into the mid-troposphere and rapidly transported to the east [Yienger et al., 2000; Husar et al., 2001; Murayama et al., 2001; Uno et al., 2001]. Such strong convective motions usually entrain significant amounts of dust to the atmosphere and, according to the modeling results given in Chapter 4, in order to produce the targeted 0.5 - 2% DIF in such large mineral dust plumes by acid mobilization the amounts of SO_2 available to be mixed in dust plumes should be at least factor of 5 higher than typical springtime concentrations of Beijing. In addition, dust plumes that subside to the warmer marine boundary layer are most likely to have higher DIF. Such conditions are not commonly met (i.e., large dust storms in East Asia are usually associated with strong zonal winds [Husar et al., 2001; Uno et al., 2001; Liu et al., 2003] that reduce the amounts of pollutants at the source regions). For example, in the case of the large and intense dust storm of early April, 2001 (the storm treated in the *Mid-Troposphere* simulation) satellite photographs such as that of Figure 5.1 suggest that anthropogenic air pollutants were advected in front of the storm without significant mixing with dust-laden portion of the plume. Finally, analyses of the past three years of MODIS data revealed that chlorophyll *a* increase in the patch (at 36-39°N, 151-158°W) that occurred between March 30- April 22, 2001 was the only time when significant phytoplankton bloom was observed in the waters of North Pacific Ocean. Thus, algae blooms caused by the deposition of acid-mobilized Fe contained in Asian dust plumes are probably an unusual phenomena.

5.10 Conclusions

Satellite imagery of the gobi-dust transport episodes presented in this chapter suggest that the very large dust advection that occluded on April 11-14, 2001 over the HNLC waters of subarctic North Pacific Ocean did not cause any visible change to the marine ecosystem productivity. Model simulations of the same dust plume revealed that the amount of SO_2 mixed with the plume was not high enough to acidify mineral dust; therefore the amount of acid mobilized Fe supplied by the plume was insufficient to cause phytoplankton bloom.

On the other hand, satellite images showed a well distinguished phytoplankton bloom occurring in the Fe limited offshore waters of the North Pacific Ocean in a region known as subarctic boundary between the mid-ocean gyre and the HNLC region. The chlorophyll *a* concentration in the patch approached its maximum value around March 30, 2001 and the bloom lasted about 20 days. The geographical location, timing and the magnitude of chlorophyll *a* pulse is consistent with the model estimated transport of the average sized dust plume from East Asia and the enrichment of the ocean waters with the mobilized Fe. The dust plume contained exceptionally large amounts of SO_2 and the trajectory of the plume descended to the marine boundary layer. The model predicted DIF of this plume was about 3.5%.

If the limited analysis presented in this chapter is generally applicable to the dust plumes from East Asia, the model simulations using acid mobilization mechanism can be summarized as follows:

(1) Large dust storms mixed with the nominal springtime concentrations of SO_2 will most likely have insignificant DIF and not be able to deposit acid mobilized Fe in

quantities necessary for causing visible changes to marine ecosystem productivity in the Fe limited regions;

(2) The combination of considerable dust mixed with the unusually high concentrations of anthropogenic air pollutants (particularly SO_2) with subsequent descent of the plume trajectory to the marine boundary layer are likely to cause visible phytoplankton blooms in the North Pacific Ocean.

CHAPTER 6

CONCLUSIONS

6.1 Introduction

The modeling results shown in this work indicated that air pollution in China can have considerable effect on the DIF-values of mineral dust plumes emanating from the gobi deserts of northern China and Mongolia and advecting over the remote Pacific Ocean. In this chapter model simulations are used to explore the possible effects of future changes in anthropogenic S-emissions in China on the fluxes of mobilized Fe to the surface waters of North Pacific Ocean. A summary of accomplishments, conclusions, and recommendations for future model development and research goals are also given below.

6.2 The Possible Role of SO_2 Emissions in China to the Future Climate Change

Because of the importance of anthropogenic SO_2 emissions from China in our calculations, the future trends in the emissions are of interest. Given coal is one of the major energy sources used to fuel a fast-growing economy it is often assumed that SO_2 emissions from China will continue to grow in the coming decades. And in fact, many projections predicted that SO_2 emissions will continue to grow [Streets and Waldoff, 2000; Nakicenovic et al., 2001; Klimont et al., 2001]. However, since 1995 S-emissions in China have actually declined due to a combination of economic slowdown, environmental regulations and the fundamental reconstruction of the Chinese economy

[Streets et al., 2001; Carmichael et al., 2002; Streets et al., 2003]. The goal China set for 2005 anticipates further reductions in SO_2 emissions, lowering it to 70% of its 1995 level. Whether this trend of lower SO_2 emissions will continue is not certain at this time [Carmichael et al., 2002].

Figure 6.1 shows modeling results for DIF as a function of plume transport time. Model calculations were initialized with different amounts of SO_2 (keeping all other parameters constant) and run for the Low Dust/Standard Pollution case of the *Boundary Layer* simulations. If we assume that alterations in S-emissions in China would roughly cause the corresponding change in the amounts of SO_2 entrained in the advecting mineral dust plumes, then different initial concentrations of SO_2 used in the model simulations can be thought of as different anthropogenic sulfur emission scenarios. For example, suppose the Base case on Figure 6.1 represents DIF that can be mobilized in the advecting dust plumes for 1995 SO_2 emission levels in China, then from the Figure 6.1 we see that a 30% decrease in SO_2 emissions would translate into more than a factor of 10 decrease in DIF, and presumably also in the flux of dissolved Fe to the remote North Pacific. A 30% increase in SO_2 emissions, equivalent to the mildly increasing emission scenarios of A1 MESSAGE and A1 MiniCAM for Asia developed by Intergovernmental Panel on Climate Change (IPCC) [Nakicenovic et al., 2001] would result in approximate factor of 3 increase in DIF.

These modeling results suggest that anthropogenic activities in China, particularly the ones related to SO_2 emissions, can considerably affect fluxes of the dissolved iron to the North Pacific Ocean. It further suggests that to the extent that this mobilized Fe is then acting as a limiting micronutrient in oceanic ecosystems, air pollution from China is

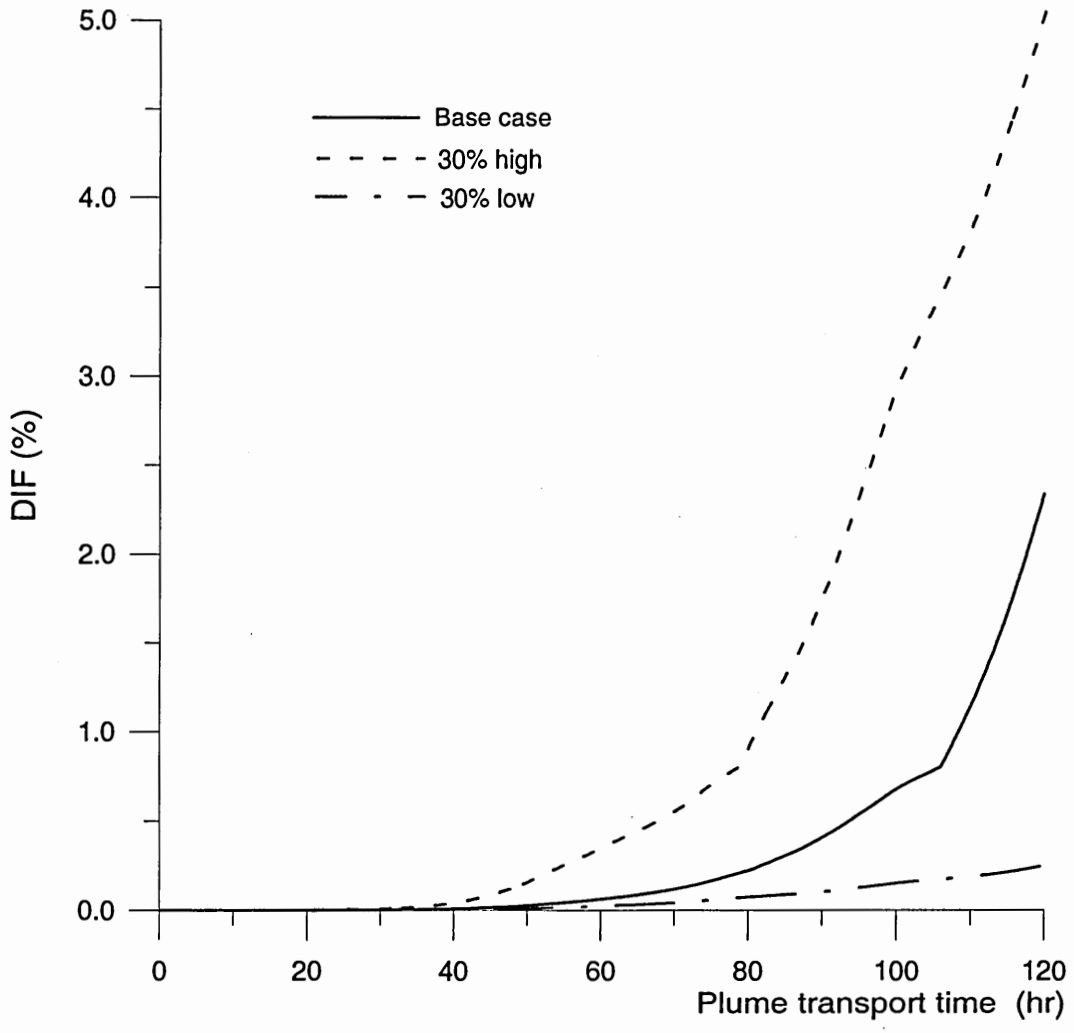

Figure 6.1 Dissolved Iron Fraction as a function of plume transport time. Initial parameters for the Base Case were set from Low Dust/Standard Pollution case of the *Boundary Layer* simulations (see Table 4.1) and 30% high and 30% low correspond to the model runs in which SO_2 concentration was changed respectively, keeping all other parameters constant.

actually responsible for enhancing the productivity of these waters. By extension, air pollution controls in China that lowered SO_2 emissions might actually depress C-uptake in these same waters. The possible impact of S-emissions from China on CO_2 and climate needs to be further investigated.

6.3 Main Results

The following is a summary of the major results presented in this dissertation encompassing Fe mobilization in advecting mineral dust plumes and the possible effect of SO_2 emissions in China on the C-uptake of the North Pacific Ocean.

- Fe in mineral dust from East Asia can be mobilized in significant quantities during its transport in the atmosphere in a two-step process consisting of: (1) acidification of the mineral dust by the incorporation of acids arising from air pollutants (and in particular SO_2) that are mixed into the plumes containing dust as these plumes advect over the urban and industrial centers; and (2) dissolution of the Fe in the resultant acidic solutions;
- A Lagrangian box model was developed and used to simulate the evolution of DIF in different cases of mineral dust advection from East Asia to the Pacific Ocean. The modeling results suggest that the incorporation of average springtime SO_2 values, frequently measured in the industrial/urban centers of China, into the advecting small dust plumes can increase the acidity of the plume to the levels required to mobilize 0.5 - 2% of Fe within an average atmospheric lifetime of dust particle. The model simulations also indicate that the SO_2 mixing ratios several times higher than the nominal values are required to attain 0.5 – 2% range of DIF

in large dust plumes. Based on the model results it is suggested that relative amounts of Dust and SO_2 mixed in the advecting plumes can be employed to determine the amounts of acid mobilized Fe;

- Simulations of the different altitude dust passages indicate that out of several physical parameters dust plumes encounter along their path, temperature appears to have significant impact on Fe mobilization rates. Low atmospheric temperatures, encountered by the dust plumes during their mid-troposphere transport, can effectively reduce Fe mobilization rates well below the values required for the production of 0.5 – 2% of DIF;
- The subsidence of the dust plume to the marine boundary layer, the photochemical reductive dissolution of hematite and the increase of dust particle reactive surface area due to the wind-driven physical processes are proposed as two mechanisms that can mobilize considerable amounts of Fe in mineral dust plumes pursuing high altitude trajectory to the HNLC waters of subarctic North Pacific Ocean;
- Based on the consistency of the satellite measurements and the model predictions for the expected increase of the ecosystem productivity after mobilized dust-Fe infusion to the ocean, it is suggested that the combination of significant dust mixed with unusually high concentrations of SO_2 and descent of the plume trajectory to the marine boundary layer can cause phytoplankton blooms in the North Pacific Ocean;
- The simulations using different initial SO_2 values, assumed to be representative of different anthropogenic S-emission scenarios in China, suggest that future

changes in SO_2 emissions in Asia can affect the rate at which atmospheric CO_2 is fixed by oceanic biota and may even exert a global-scale influence on climate.

6.4 Implications for Future Work

The most important result of this research is suggested possible link between anthropogenic air pollution from the East Asia and the C-uptake in the North Pacific Ocean. While the modeling results presented in the study indicate that ecosystem productivity of North Pacific Ocean can be affected by anthropogenic activities in China (particularly ones related to SO_2 emissions), long-term simulations by coupling the iron mobilization algorithm with the global three-dimensional (3D) atmospheric transport models might be necessary to determine the significance of this modeling result to the global fluxes of dissolved Fe deposited to the oceans.

Future improvements to the model should include more detailed parameterization of dust entrainment, mixing and deposition processes to allow better estimates for the Fe enrichment of the surface ocean waters by intermittent dust transport episodes. One of the advantages of using box models is that computational resources can be devoted to explicit calculations of physical state and chemical composition of multiphase atmospheric aerosols. However, the assumption of homogeneous mixture of dust and pollutants can reduce model application. Analysis of data collected during TRACE-P /ACE-Asia missions indicated that mineral dust and anthropogenic air pollutants in the Asian outflow were not always uniformly mixed [Jacob et al., 2003; Huebert et al., 2003]. Plumes with elevated mixing ratios of reactive species, characteristic to the industrial/urban pollution, were occasionally sampled inside large dust storms even at

significant distances from the source regions. Such segregation of mineral dust and pollution could substantially affect heterogeneous oxidations rates employed in the model.

An additional level of complexity should be introduced into the Fe mobilization mechanism to account for the effects of organic species (i.e., oxalate, acetate, formate) and sunlight as well as complex redox cycling between highly insoluble ferric (Fe-III) and relatively more soluble ferrous (Fe-II) ions. Laboratory studies have shown, that such processes can affect Fe solubility in mineral aerosols, particularly when dust samples were collected close to the industrial/urban centers [Simnad and Smoluchowski, 1955; Faust and Hoffman, 1986; Behra and Sigg, 1990; Zhuang et al., 1992a; Zhu et al., 1992; Spokes and Jickells, 1996; Jickells and Spokes, 2001]. Addition of new processes to the existing model will lead to more complete treatment of Fe solubilization in mineral aerosols and perhaps will allow us to explore other (in addition to acid mobilization) mechanisms for producing dissolved Fe in mineral dust plumes.

In addition to changes in Fe chemistry, projected model developments include extension of ISORROPIA by adding crustal species with appropriate oxides, oxy-hydroxides and inorganic forms. It was discussed previously, that current approach is appropriate when acid mobilization is used as the major mechanism for producing dissolved Fe in mineral dust plumes. However, improved thermodynamic module will allow exploring other possible mechanisms for Fe mobilization that might be associated with less acidic mineral dust.

Further investigations, involving more detailed observations, satellite data analysis and modeling studies of the interactions between airborne dust and air pollutants

are needed to test acid-mobilization hypothesis and determine the extent to which the data used in this study are typical of dust plumes emanating from East Asia.

APPENDIX A

The lifetime for the removal of the gas phase nitric acid by mineral dust, τ_{HNO_3} can be approximated as [Jacob, 2000]:

$$\tau_{HNO_3} = \left(\frac{D_p}{2D_g} + \frac{4}{\bar{c}\gamma} \right) \cdot A^{-1} \qquad \text{(A1)}$$

where D_p is mineral dust particle diameter (cm); D_g is the gas-phase molecular diffusion coefficient of HNO_3 in the air ($0.135 cm^2/s$ [Massman, 1998; Seinfeld and Pandis, 1998]); $\bar{c}$ is the mean molecular speed of HNO_3 in the gas phase (3.1×10^4 cm/s); γ is a reaction probability that $HNO_3(g)$ molecules impacting the mineral dust particle surface undergo reaction with the range of 0.1-0.17 [Dentener et al., 1996; Hanisch and Crowley, 2001a, 2001b]; and A is the mineral dust surface area per unit volume of air (cm^2/cm^3air). Adopting an average vales for A and D_p measured during the highlighted portion of Flight 13 of $\sim 1 \times 10^{-5}$ and 1×10^{-4} to 1×10^{-3}, respectively, [Jordan et al., 2003b] from Equation (A1) the lifetime of $HNO_3(g)$ with respect to processing by mineral dust is

$$1.5 \text{ min} < \tau_{HNO_3} < 6 \text{ min}.$$

This result suggests that equilibrium assumption between $HNO_3(g)$ and $[NO_3^-]$ for the highlighted portion of TRACE P Flight 13 is most likely correct. However, it is worth noticing that reaction probability for $HNO_3(g)$ uptake on mineral dust particles was derived in the laboratory using Knudsen cell reactor using technique that could suffer from the complications due to surface saturation and gas diffusion into the underlying layers of powdered samples [Li et al., 2002]. If, for some reason, the reaction probability in the atmosphere appears to be significantly smaller (about two orders of magnitude)

measured in the Knudsen cell reactor, assumption of thermodynamic equilibrium between gas phase nitric acid and mineral dust will be violated.

APPENDIX B

The gravitational settling velocity of particles considered in the transportable fraction of mineral dust (with $D_p \leq 20\,\mu m$) can be determined using Stocks law [Tegen and Fung, 1994; Ginoux et al., 2001; Zender et al., 2003] with

$$v_{stk} = \frac{D_p^2 \rho_p g C_c}{18\mu} \tag{B1}$$

where D_p is the particle diameter, ρ_p is particle density, g is the acceleration of gravity, μ is the dynamic viscosity of the air and C_c is the slip correction factor [Seinfeld and Pandis, 1998].

As particles of different sizes have different atmospheric lifetimes (See Table B1) the particle deposition parameter $\xi(t)$, is allowed to vary in the following way:

$$\xi(t) = \frac{\hat{v}(r) - \sum_{i=0}^{4} v_i}{\hat{v}(r)} \tag{B2}$$

where $\hat{v}(r) = v_1 + v_2 + v_3 + v_4$ with indices denoting particle classes having different diameters (see Table B1) and the summation is carried out according to lifetime of dust particles. For example, when model time t<26 hr, $\xi(t)=1$; if 26<t<103 hr, $\xi(t) = \frac{v_2 + v_3 + v_4}{\hat{v}(r)}$ and etc.

Table A1 summarizes $\xi(t)$ values at different t.

Table B1. Lifetime of mineral dust particles [1]

Index	D_p, (μm)	Lifetime, (hr)	$\xi(t)$
1	0.1-2	336	0.01
2	2-4	216	0.08
3	4-6	103	0.32
4	6-12	26	1.00

(1) From Ginoux et al. [2001].

REFERENCES

Alkattan, M., E.H. Oelkers, J.L. Dandurand, and J. Schott, An experimental study of calcite and limestone dissolution rates as a function of pH from -1 to 3 and temperature from 25 to 80°C, *Chem. Geol., 151*(1-4), 199-214, 1998.

Alpert, P. and E. Ganor, Sahara mineral dust measurements from TOMS: Comparison to surface observations over the Middle East for the extreme dust storm, March 14-17, 1998, *J. Geophys. Res., 106* (16), 18,275-18,286, 2001.

Andronache, C., W.L. Chameides, D.D. Davis, B.E. Anderson, R.F. Pueschel, A.R. Bandy, D.C. Thornton, R.W. Talbot, P. Kasibhatla, C.S. Kiang, Gas-to-particle conversion of tropospheric sulfur as estimated from observations in the western North Pacific during PEM-West B, J. Geophys. Res., 102 (D23), 28,511-28,538, 1997.

Archer, D.E. and K. Johnson, A Model of the iron cycle in the ocean, *Global Biogeochem. Cy., 14*(1), 269-279, 2000.

Arimoto, R., B.J. Ray, N.F. Lewis, N.F. U. Tomza, and R.A. Duce, Mass-particle size distributions of atmospheric dust and the dry deposition of dust to the remote ocean, *J. Geophys. Res., 102*, 15,867-15,874, 1997.

Arimoto, R., Eolian dust and climate: relationships to sources, tropospheric chemistry, transport and deposition, *Earth-Sci Rev, 54*(1-3), 29-42, 2001.

Azuma, K. and H. Kametani, Kinetics of dissolution of ferric oxide, *Trans. Met. Soc., AIME, 230*, 853-862, 1964.

Balmer, M.E. and B. Sulzberger, Atrazine degradation in irradiated iron oxalate systems: Effects of pH and oxalate, *Environ. Sci. Technol., 33*(14), 2418-2424, 1999.

Banwart, S., S. Davies, and W. Stumm, The role of oxalate in accelerating the reductive dissolution of hematite (α-Fe_2O_3) by ascorbate, *Colloid. Surface, 39* (4), 303-309, 1989.

Behra, P. and L. Sigg, Evidence for redox cycling of iron in atmospheric water droplets, *Nature, 344*, 419-421, 1990.

Bi, S.P., A simple-model for predicting the ph values of acidic natural-waters, *Anal. Chim. Acta., 314*(1-2), 111-119, 1995.

Bi, S.P., S.Q. An, and F. Liu, A practical application of Driscoll's equation for predicting the acid-neutralizing capacity in acidic natural waters equilibria with the mineral phase gibbsite, *Environ. Int., 26*(5-6), 327-333, 2001a.

Bi, S.P., X.D. Yang, F.P. Zhang, X.L. Wang, and G.W. Zou, Analytical methodologies for aluminium speciation in environmental and biological samples - a review, *Fresen. J. Anal. Chem., 370*(8), 984-996, 2001b.

Bishop, J.K.B., R.E. Davis, and J.T. Sherman, Robotic observations of dust storm enhancement of carbon biomass in the North Pacific, *Science, 298*, 817-821, 2002.

Blackadar, A.K., *Turbulence and diffusion: Lectures in environmental sciences*, p.185, Springer-Verlag, 1998.

Blesa, M.A., P.J. Morando, and A.E. Regazzoni, *Chemical dissolution of metal oxides*, CRC press, 401 p. 1994.

Blum, A.E. and L.L. Stilling, Feldspar dissolution kinetics, in *Chemical weathering rates of silicate minerals*, Reviews in mineralogy, 31, 174-233, 1995.

Böke, H., E.H. Göktürk, E.N. Caner-Saltik, and Ş. Demirci, Effect of airborne particle on SO_2-calcite reaction, *Appl. Surf. Sci., 140* (1-2), 70-82, 1999.

Boyd, P.W., C.S. Wong, J. Merrill, F. Whitney, J. Snow, P.J. Harrison, and J. Gower, Atmospheric iron supply and enhanced vertical carbon flux in the NE subarctic Pacific: Is there a connection?, *Global Biogeochem. Cy., 12*, 429-441, 1998.

Boyd, P. and P.J. Harrison, Phytoplankton dynamics in the NE subarctic Pacific, *Deep-Sea Res. Pt. II, 46*, 2405-2432, 1999.

Boyd, P.W., A.J. Watson, C.S. Law, E.R. Abraham, T. Trull, R. Murdoch, D.C.E. Bakker, A.R. Bowie, K.O. Buesseler, H. Chang, M. Charette, P. Croot, K. Downing, R. Frew, M. Gall, M. Hadfield, J. Hall, M. Harvey, G. Jameson, J. LaRoche, M. Liddicoat, R. Ling, M.T. Maldonado, R.M. McKay, S. Nodder, S. Pickmere, R. Pridmore, S. Rintoul, K. Safi, P. Sutton, R. Strzepek, K. Tanneberger, S. Turner, A. Waite, and J. Zeldis, A mesoscale phytoplankton bloom in the polar Southern Ocean stimulated by iron fertilization, *Nature, 407*, 695-702, 2000.

Brandt, C and R. van Eldik, Transition metal-catalyzed oxidation of sulfur(IV) oxides, atmospheric-relevant processes and mechanisms", *Chem. Rev. 95*, 119-190, 1995.

Bromley, L.A., Thermodynamic properties of strong electrolytes in aqueous solution, *AIChE J., 19*, 313-320, 1973.

Burch, T.E., K.L. Nagy, and A.C. Lasaga, Free energy dependence of albite dissolution kinetics at 80°C and pH 8.8, *Chem. Geol., 105* (1-3), 137-162, 1993.

Cama, J., C. Ayora, and A.C. Lasaga, The deviation-from-equilibrium effect on dissolution rate and on apparent variations in activation energy, *Geochim. Cosmochim. Acta, 63*, 2481-2486, 1999.

Carmichael G.R., D.G. Streets, G. Calori, M. Amann, M.Z. Jacobson, J. Hansen and H. Ueda, Changing trends in sulfur emissions in Asia: Implications for acid deposition, air pollution, and climate, *Environ. Sci. Technol., 36*, 4707, doi:10.1021/es011509c, 2002.

Carroll, S.A. and J.V. Walter, Kaolinite dissolution at 25°, 60°, and 80°C, *Am. J. Sci, 290*, 797-810, 1990.

Chang, H.C. and E. Matijevic, Interactions of metal hydrous oxides with chelating-agents. 4. Dissolution of hematite, *J. Colloid. Interf. Sci. 92* (2), 479-488, 1983.

Chang, Y.S., R.L. Arndt, and G.R. Carmichael, Mineral base-cation deposition in Asia, *Atmos. Environ., 30* (13), 2417-2427, 1996.

Chen, M., R.C.H. Dei, W.X. Wang, and L.D. Guo, Marine diatom uptake of iron bound with natural colloids of different origins, *Mar. Chem., 81*, 177, doi: 10.1016/S0304-4203(03)00032-X, 2003.

Chen, Y., H. Quan, X. Dong, N. Sugimoto, I. Matsui, and A. Shimizu, Continuous measurements of dust aerosols with a dual-polarization lidar in Beijing, Nagasaki Workshop, 2001.

Chin, M., P. Ginoux, R. Lucchesi, B. Huebert, R. Weber, T. Anderson, S. Masonis, B. Blomquist, A. Bandy, and D. Thornton, A global aerosol model forecast for the ACE-Asia field experiment, *J. Geophys. Res., 108*(23), doi: 10.1029/ 2003JD003642, 2003.

Chisholm, S.W., Stirring times in the Southern Ocean, *Nature, 407*, 685-687, 2000.

Chou, L., R.M. Garrels, and R. Wollast, Comparative-study of the dissolution kinetics and mechanisms of carbonates in aqueous-solutions, *Chem. Geol., 70*(1-2), 77-77, 1988.

Claquin, T., M. Schulz and Y.J. Balkanski, Modeling the mineralogy of atmospheric dust sources, *J. Geophys. Res., 104*, 22,243-22,256, 1999.

Clarke, A.D., Y. Shinozuka, V.N. Kapustin, S. Howell, B. Huebert, S. Masonis, T. Anderson, D. Covert, R. Weber, J. Anderson, H. Zin, K.G. Moore II, C. McNaughton, Size-distributions and mixtures of black carbon and dust aerosols in Asian outflow: Physico-chemistry, optical properties, and implications for CCN, submittet to *J. Geophys. Res.*, 2003.

Clegg, S.L., P. Brimblecombe, A.S. Wexler, Thermodynamic model of the system H^+-NH_4^+-SO_4^{2-}-NO_3^--H_2O at tropospheric temperatures, *J. Phys. Chem. A,102*, 2137-2154, 1998.

Coale, K.H., K.S. Johnson, S.E. Fitzwater, R.M. Gordon, S. Tanner, F.P. Chavez, L. Ferioli, C. Sakamoto, P. Rogers, F. Millero, P. Steinberg, P. Nightingale, D. Cooper, W.P. Cochlan, M.R. Landry, J. Constantinou, G. Rollwagen, A. Trasvina, R. Kudela, A massive phytoplankton bloom induced by an ecosystem-scale iron fertilization experiment in the equatorial Pacific Ocean, *Nature, 383*, 495-501, 1996.

Coale, K.H., K.S. Johnson, S.E. Fitzwater, S.P.G. Blain, T.P. Stanton, T.L. Coley, IronEx-I, an in situ iron-enrichment experiment: Experimental design, implementation and results, *Deep-Sea Res. Pt. II.*, 45(6), 919-945, 1998.

Coey, J.M.D., Magnetic Properties of iron in soil iron oxides and clay minerals, in *Iron in Soils and Clay Minerals*, edited by J.W. Stucki, B.A. Goodman, and U. Schwertmann, NATO ASI Series, 217, 1988.

Colin, J.L., J.L. Jaffrezo, and J.M. Gros, Solubility of major species in precipitation - factors of variation, *Atmos. Environ., 24* (3), 537-544, 1990.

Cooper, D.J., A.J. Watson and P.D. Nightingale, Large decrease in ocean-surface CO_2 fugacity in response to in situ iron fertilization, *Nature*, 383, 511-513, 1996.

Cornell, R.M. and U. Schwertmann, *The Iron Oxides, Structure, Properties, Reactions, Occurrence and Uses,* 573 pp., Weinheim, New York, 1996.

Crawford, J., D. Davis, G. Chen, J. Bradshaw, S. Sandholm, Y. Kondo, S. Liu, E. Browell, G. Gregory, B. Anderson, G. Sachse, J. Collins, J. Barrick, D. Blake, R. Talbot and H. Singh, An assessment of ozone photochemistry in the extratropical western North Pacific: Impact of continental outflow during the late winter early spring, *J. Geophys. Res., 102* (D23), 28,469-28,487, 1997.

Csanady, G.T., *Turbulent diffusion in the environment*, p. 248, D. Reidel Publishing Co., Dordrecht, Holland, 1973.

Dalton, R., Ocean tests raise doubts over use of algae as carbon sink, *Nature, 420*, 722, 2002.

Davis, D.D., G. Chen, J. H. Crawford, S. Liu, D. Tan, S. T. Sandholm, P. Jing, D. M. Cunnold, B. DiNunno, E. V. Browell, W. B. Grant, M. A. Fenn, B. E. Anderson, J. D. Barrick, G. W. Sachse, S. A. Vay, C. H. Hudgins, M. A. Avery, B. Lefer, R. E. Shetter, B. G. Heikes, D. R. Blake, N. Blake, Y. Kondo, and S. Oltmans, An assessment of western North Pacific ozone photochemistry based on springtime observations from NASA's

PEM-West B (1994) and TRACE-P (2001) field studies, *J. Geophys. Res.*, *108*(D21), 8829, doi:10.1029/2002JD003232, 2003.

de Baar, H.J.W., J.T.M. de Jong , D.C.E. Bakker, B.M. Loscher, C. Veth, U. Bathmann, and V. Smetacek, Importance of iron for plankton blooms and carbon-dioxide drawdown in the southern-ocean, *Nature, 373*, 412-415, 1995.

de Baar, H.J.W. and J.T.M. de Jong, Distributions, sources and sinks of iron in seawater, in *The biogeochemistry of iron in seawater*, edited by D.R. Turner, and K.A. Hunter, pp. 85-121, J. Wiley & Sons, New York, 2001.

Deer, W. A., R. A. Howie, and J. Zussman, *An introduction to the rock-forming minerals*, Longman, 1998.

Dentener, F.J. and P.J. Crutzen, A 3-dimensional model of the global ammonia cycle, *J. Atmos. Chem., 19* (4), 331-369, 1994.

Dentener, F.J., G.R. Carmichael, Y. Zhang, J. Lelieveld, and P.J. Crutzen, Role of mineral aerosol as a reactive surface in the global troposphere, *J. Geophys. Res.*, *101*, 22,869-22,889, 1996.

Desboeufs, K.V., R. Losno, and J.L. Colin, Factors influencing aerosol solubility during cloud processes, *Atmos. Environ.*, *35*, 3529-3537, 2001.

Dibb, J.E., R.W. Talbot, E.M. Scheuer, D.R. Blake, N.J. Blake, G.L. Gregory, G.W. Sachse, and D.C. Thornton, Aerosol chemical composition and distribution during the Pacific Exploratory Mission (PEM) Tropics, *J. Geophys. Res.*, *104*, 5785-5800, 1999.

Dickey, T., D. Frye, J. McNeil, D. Manov, N. Nelson, D. Sigurdson, H. Jannasch, D. Siegel, T. Michaels, and R. Johnson, Upper-ocean temperature response to Hurricane Felix as measured by the Bermuda testbed mooring, *Mon. Weather. Rev., 126* (5), 1195-1201, 1998.

Dousma, J., D. den Ottelander and P.L. de Rruyn, The influence of sulfate ions on the formation of iron(III) oxides, *J. Inorg. Nucl. Chem., 41*, 1565-1568, 1979.

Draxler, R.R. and Rolph, G.D., 2003. HYSPLIT (HYbrid Single-Particle Lagrangian Integrated Trajectory) Model access via NOAA ARL READY Website (http://www.arl.noaa.gov/ready/hysplit4.html). NOAA Air Resources Laboratory, Silver Spring, MD.

Duce, R.A. and N.W. Tindale, Atmospheric transport of iron and its deposition in the ocean, *Limnol. Oceanogr.*, *36*, 1715-1726, 1991.

Duce, R.A., P.S. Liss, J.T. Merrill, E.L. Atlas, P. Buat-Ménard, B.B. Hicks, J.M. Miller, J.M. Prospero, R. Arimoto, T.M. Church, W. Ellis, J.N. Galloway, L. Hansen, T.D. Jickells, A.H. Knap, K.H. Reinhardt, B. Schneider, A. Soudine, J.J. Tokos, S. Tsunogai, R. Wollast, and M. Zhou, The atmospheric input of trace species to the world ocean, *Global Biogeochemical Cy.*, 5, 193-259, 1991.

Duce, R.A., Sources, distributions, and fluxes of mineral aerosols and their relationship to climate, In Dalhem Workshop on Aerosol Forcing of Climate, Edited by R.J. Charlson, and J. Heintzenberg, John Willey, New York, 1995.

Dugdale, R.C. and F.P. Wilkerson, New production in the upwelling center at point conception, California - temporal and spatial patterns, *Deep-Sea Res., 36*, 985-1007, 1989.

Elliott, S., D.R. Blake, R.A. Duce, C.A. Lai, L. McCreary, L.A. McNair, F.S. Rowland, A.G. Russell, G.E. Streit, and R.P. Turco, Motorization of China implies changes in Pacific air chemistry and primary production, *Geophys. Res. Lett. 24*(21), 2671-2674, 1997.

Faust, B.C. and M.R., Hoffmann, Photoinduced reductive dissolution of $\alpha-Fe_2O_3$ by bisulfite, *Environ. Sci. Technol., 20*, 943-948, 1986.

Faust, B.C. and R.G. Zepp, Photochemistry of aqueous iron(III) polycarboxylate complexes - roles in the chemistry of atmospheric and surface waters, *Environ. Sci. Technol., 27* (12), 2517-2522, 1993.

Ferek, R.J., P.V. Hobbs, J.A. Herring, K.K. Laursen, R.E. Weiss, and R.A. Rasmussen, Chemical composition of emissions from the Kuwait oil fires, J. Geophys. Res., 97 (D13), 14483-14489, 1992.

Firme, G.F., E.L. Rue, D.A. Weeks, K.W. Bruland, and D.A. Hutchins, Spatial and temporal variability in phytoplankton iron limitation along the California coast and consequences for Si, N, and C biogeochemistry, *Global Biogeochem. Cy., 17,* doi:10.1029/2001GB001824, 2003.

Fuelberg, H. E., C. M. Kiley, J. R. Hannan, D. J. Westberg, M. A. Avery, and R. E. Newell, Meteorological conditions and transport pathways during the Transport and Chemical Evolution over the Pacific (TRACE-P) experiment, *J. Geophys. Res.*, *108*(D20), 8782, doi:10.1029/2002JD003092, 2003.

Fung, I.Y., S.K. Meyn, I. Tegen, S.C. Doney, J.G. John, and J.K.B. Bishop, Iron supply and demand in the upper ocean, *Global Biogeochem. Cy.*, *14*, 281-295, 2000.

Gallegos, C.L. and W.N. Vant, An incubation procedure for estimating carbon-to-chlorophyll ratios and growth-irradiance relationships of estuarine phytoplankton, *Mar. Ecol-Prog Ser., 138*, 275-291, 1996.

Gao, Y., Y.J. Kaufman, D. Tanre, D. Kolber, and P.G. Falkowski, Seasonal distributions of aeolian iron fluxes to the global ocean, *Geophys. Res. Lett., 28,* 29-32 2001.

Gao, Y., S.-M. Fan and J.L. Sarmiento, Aeolian iron input to the ocean through precipitation scavenging: A modeling perspective and its implication for natural iron fertilization in the ocean, *J. Geophys. Res., 108*, 4221, doi:10.1029/ 2002JD002420, 2003.

Garrett, T.J., L.M. Russell, V. Ramaswamy, S.F. Maria, and B.J. Huebert, Microphysical and radiative evolution of aerosol plumes over the tropical North Atlantic Ocean, *J. Geophys. Res.108* (D1), 4022, 2003.

Geider, R.J., H.L. MacIntyre and T.M. Kana, Dynamic model of phytoplankton growth and acclimation: Responses of the balanced growth rate and the chlorophyll a:carbon ratio to light, nutrient-limitation and temperature, *Mar. Ecol-Prog. Ser., 148*, 187-200, 1997.

Ginoux, P., M. Chin, I. Tegen, J.M. Prospero, B. Holben, O. Dubovik, and S-J. Lin, Sources and distributions of dust aerosols simulated with the GOCART model, *J. Geophys. Res., 106*, 20,255-20,273, 2001.

Gledhill, M. and C.M.G. van den Berg, Determination of complexation of iron (III) with natural organic complexing ligands in seawater using cathodic stripping voltammetry, *Mar. Chem., 47*, 41-54, 1994.

Gomes, L., G. Bergametti, G. Coudegaussen, and P. Rognon, Submicron desert dusts - A sandblasting process, *J. Geophys. Res., 95*(D9), 13927-13935, 1990.

Gong, S.L., X.Y. Zhang, T.L. Zhao, I.G. McKendry, D.A. Jaffe, and N.M. Lu, Characterization of soil dust aerosol in China and its transport and distribution during 2001 ACE-Asia: 2. Model simulation and validation, *J. Geophys. Res., 108* (D9), doi:10.1029/2002JD002633, 2003.

Goodman, A.L., G.M. Underwood, and V.H. Grassian, A laboratory study of the heterogeneous reaction of nitric acid on calcium carbonate particles, J. *Geophys. Res., 105*, 29,053-29,064, 2000.

Goodman, A.L., E.T. Bernard, and V.H. Grassian, Spectroscopic study of nitric acid and water adsorption on oxide particles: Enhanced nitric acid uptake kinetics in the presence of adsorbed water, *J. Phys. Chem. A, 105*, 6443-6457, 2001.

Gorichev, I.G., S.G. Ashkharua, S.K. Vainman, and N.G. Klyuchnikov, The applicability of the topochemical model to the dissolution of certain oxides in acids, *Russ. J. Phys Chem., 50*, 975-976, 1976.

Gran, H.H., On the conditions for the production of plankton in the sea, *Rapp. Proc. Verb. Réun. Cons. Int. Expl. Mer, 75*, 37-46, 1931.

Greene, R.M., Z.S. Kolber, D.G. Swift, N.W. Tindale, and P.G. Falkowski, Physiological limitation of phytoplankton photosynthesis in the eastern equatorial pacific determined from variability in the quantum yield of fluorescence, *Limnol. Oceanogr., 39*(5), 1061-1074, 1994.

Guieu, C. and A.J. Thomas, Saharan aerosols: From the soil to the ocean, In *The Impact of Desert Dust across the Mediterranean*, pp.207-216, edited by S. Guerzoni and R. Chester, Kluwer, Dordrecht, 1996.

Hanisch, F. and J.N. Crowley, The heterogeneous reactivity of gaseous nitric acid on authentic mineral dust samples, and on individual mineral and clay mineral components, *Phys. Chem. Chem. Phys., 3*, 2474, doi:10.1039/b101700o, 2001a.

Hanisch, F. and J.N. Crowley, Heterogeneous Reactivity of Gaseous Nitric Acid on Al_2O_3, $CaCO_3$, and Atmospheric Dust Samples: A Knudsen Cell Study, *J. Phys. Chem. A, 105,* 3096, doi: 10.1021/jp001254, 2001b.

Harrison, P.J., P.W. Boyd, D.E. Varela, and S. Takeda, Comparison of factors controlling phytoplankton productivity in the NE and NW subarctic Pacific gyres, *Prog. Oceanogr., 43,* 205-234, 1999.

Havers, N., P. Burba, J. Lambert, and D. Klockow, Spectroscopic characterization of humic-like substances in airborne particulate matter, *J. Atmos. Chem., 29* (1), 45-54, 1998.

Herman, J.R., P.K. Bhartia, O. Torres, C. Hsu, C. Seftor, and E. Celarier, Global distribution of UV-absorbing aerosols from Nimbus 7/TOMS data, *J. Geophys. Res., 102*(14), 16,911-16,922, 1997.

Herring, J.A., R.J. Ferek and P.V. Hobbs, Heterogeneous chemistry in the smoke plume from the 1991 Kuwait oil fires, *J. Geophys. Res., 101*, 14,451-14,463, 1996.

Hislop, K.A. and J.R. Bolton, The photochemical generation of hydroxyl radicals in the UV-vis/ferrioxalate/H_2O_2 system, *Environ. Sci. Technol., 33* (18), 3119-3126, 1999.

Hodson, M.E., Micropore surface area variation with grain size in unweathered alkali feldspars: Implications for surface roughness and dissolution studies, *Geochim. Cosmochim. Acta., 62*, 3429-3435, 1999.

Hoell, J.M., D.D. Davis, S.C. Liu, R. Newell, M. Shipham, H. Akimoto, R.J. McNeal, R.J. Bendura, and J.W. Drewry, Pacific exploratory Mission-West A (PEM-West A): September October 1991, *J. Geophys. Res., 101*(D1), 1641-1653, 1996.

Hoell, J.M., D.D. Davis, S.C. Liu, R.E. Newell, H. Akimoto, R.J. McNeal, and R.J. Bendura, The Pacific Exploratory Mission West phase B: February-March, 1994, *J. Geophys. Res., 102*(D23), 28,223-28,239, 1997.

Hseung, Y. and M. L. Jackson, Mineral composition of the clay fraction: III Of some main soil groups of China, *Soil Sci. Soc. Am. P., 16*, 294-297, 1952.

Huebert, B.J., T. Bates, P.B. Russell, G. Shi, Y.J. Kim, K. Kawamura, G. Carmichael and T. Nakajima, An overview of ACE-Asia: strategies for quantifying the relationships between Asian aerosols and their climatic impacts, submitted to: *J. Geophys. Res,* 2003.

Husar, R.B., D.M. Tratt, B.A. Schichtel, S.R. Falke, F. Li, D. Jaffe, S. Gasso, T. Gill, N.S. Laulainen, F. Lu, M.C. Reheis, Y. Chun, D. Westphal, B.N. Holben, C. Gueymard, I. McKendry, N. Kuring, G.C. Feldman, C. McClain, R.J. Frouin, J. Merrill, D. DuBois, F. Vignola, T. Murayama, S. Nickovic, W.E. Wilson, K. Sassen, N. Sugimoto, and W.C. Malm, Asian dust events of April 1998, *J. Geophys. Res., 106,* 18,317-18,330, 2001.

Hutchins, D.A., A.E. Witter, A. Butler and G.W. Luther, Competition among marine phytoplankton for different chelated iron species, *Nature, 400*, 858-861, 1999.

Jacob, D.J., Heterogeneous chemistry and tropospheric ozone, *Atmos. Environ., 34* , 2131-2159, 2000.

Jacob, D. J., J. H. Crawford, M. M. Kleb, V. S. Connors, R. J. Bendura, J. L. Raper, G. W. Sachse, J. C. Gille, L. Emmons, and C. L. Heald, Transport and Chemical Evolution over the Pacific (TRACE-P) aircraft mission: Design, execution, and first results, *J. Geophys. Res.,108*(D20),9000, 10.1029/2002JD003276.

Jickells, T.D. and L.J. Spokes, Atmospheric iron inputs to the oceans, in *The biogeochemistry of iron in seawater*, edited by D.R. Turner, and K.A. Hunter, pp. 85-121, J. Wiley & Sons, New York, 2001.

Johnson, K.S., R.M. Gordon, and K.H. Coale, What controls dissolved iron concentrations in the world ocean?, *Mar. Chem., 57*, 137-161, 1997.

Jordan, C. E., J. E. Dibb, B. E. Anderson, and H. E. Fuelberg, Uptake of nitrate and sulfate on dust aerosols during TRACE-P, *J. Geophys. Res., 108*(D21), 8817, doi:10.1029/2002JD003101, 2003a.

Jordan, C. E., B. E. Anderson, R. W. Talbot, J. E. Dibb, H. E. Fuelberg, C. H. Hudgins, C. M. Kiley, R. Russo, E. Scheuer, G. Seid, K. L. Thornhill, and E. Winstead, Chemical and physical properties of bulk aerosols within four sectors observed during TRACE-P, *J. Geophys. Res., 108*(D21), 8813, doi:10.1029/2002JD003337, 2003b.

Judeikis H.S., T.B. Stewart, and A.G. Wren, Laboratory studies of heterogeneous reactions of SO_2, *Atmos. Environ., 12*, 1633-1641, 1978.

Kaufman, Y.J., D. Tanre, and O. Boucher, A satellite view of aerosols in the climate system, *Nature, 419*, 215-223, 2002.

Kim, B.G. and S.U. Park, Transport and evolution of a winter-time Yellow sand observed in Korea, *Atmos. Environ., 35* (18), 3191-3201, 2001.

Klimont, Z., J. Cofala, W. Schöpp, M. Amann, D.G. Streets, Y. Ichikawa, and S. Fujita, Projections of SO_2, NO_x, NH_3 and VOC emissions in East Asia up to 2030, *Water air and soil pollution, 130*, 193-198, 2001.

Kolber, Z.S., R.T. Barber, K.H. Coale, S.E. Fitzwater, R.M. Greene, K.S. Johnson, S. Lindley, and PG Falkowski, Iron limitation of phytoplankton photosynthesis in the equatorial pacific-ocean, *Nature, 371*, 145-149, 1994.

Kondo, Y., M. Koike, S. Kawakami, H.B. Singh, H. Nakajima, G.L. Gregory, D.R. Blake, G.W. Sachse, J.T. Merrill, and R.E. Newell, Profiles and partitioning of reactive nitrogen over the Pacific Ocean in winter and early spring, *J. Geophys. Res., 102*, 28,405-28,424, 1997.

Kuma, K., J. Nishioka and K. Matsunaga, Controls on iron(III) hydroxide solubility in seawater: The influence of pH and natural organic chelators, *Limnol. Oceanogr., 41*, 396-407, 1996.

Kurosaki, Y. And M. Mikami, Recent frequent dust events and their relation to surface wind in East Asia, *Geophys. Res. Lett., 30*(14)1736, doi:10.1029/2003GL017261, 2003.

Kusik, C.L. and H.P. Meissner, Electrolyte activity coefficients in inorganic processing, *AIChE Symp.Series, 173*, 14-20, 1978.

Lasaga, A.C., J.M. Soler, J. Ganor , T.E. Burch, and K.L. Nagy, Chemical-weathering rate laws and global geochemical cycles, *Geochim. Cosmochim. Acta, 58*, 2361-2386, 1994.

Lee, Y.-N., R. Weber, Y. Ma, D. Orsini, K. Maxwell-Meier, D. Blake, S. Meinardi, G. Sachse, C. Harward, T.-Y. Chen, D. Thornton, F.-H. Tu, A. Bandy, Airborne measurement of inorganic ionic components of fine aerosol particles using the particle-into-liquid sampler coupled to ion chromatography technique during ACE-Asia and TRACE-P, *J. Geophys. Res.,108* (23),8646, doi:10.1029/ 2002JD003265, 2003.

Leinen, M., J.M. Prospero, E. Arnold, and M. Blank, Mineralogy of aeolian dust reaching the north Pacific-Ocean .1. Sampling and analysis, *J. Geophys. Res.,* 99 (D10), 21,017-21,023, 1994.

Li, P., H.A. Al-Abadleh, and V.H. Grassian, Measuring heterogeneous uptake coefficients of gases on solid particle surfaces with a Knudsen cell reactor: Complications due to surface saturation and gas diffusion into underlying layers, *J Phys. Chem. A., 106*(7), 1210-1219, 2002.

Lin, I., W.T. Liu, C.C. Wu, G.T.F. Wong, C.M. Hu, Z.Q. Chen, W.D. Liang, Y. Yang and K.K. Liu, New evidence for enhanced ocean primary production triggered by tropical cyclone, *Geophys. Res. Lett., 30*, 1718, doi:10.1029/2003GL017141, 2003.

Lindsay, W.L., Chemical equilibria in soils, 449 pp., New York, J. Wiley, 1979.

Liu, M., D.L. Westphal, S. Wang, A. Shimizu, N. Sugimoto, J. Zhou, and Y. Chen, A high-resolution numerical study of the Asian dust storms of April 2001, *J. Geophys. Res., 108*(D23), 8653, doi:10.1029/2002JD003178, 2003.

Liu, X., D.A. Hegg, and M.T. Stoelinga, Numerical simulation of new particle formation over the northwest Atlantic using the MM5 mesoscale model coupled with sulfur chemistry, *J. Geophys. Res., 106* (D9), 9697-9715, 2001.

Liu, X. and F.J. Millero, The solubility of iron in seawater, *Marine Chemistry, 77*, 43-54, 2002.

Luo, C. N. Mahowald, M., and J del Corral, Sensitivity study of meteorological parameters on mineral aerosol mobilization, transport, and distribution, *J. Geophys. Res.Vol., 108*(D15),4447, doi: 10.1029/2003JD003483, 2003.

Maldonado, M.T. and N.M. Price, Utilization of iron bound to strong organic ligands by plankton communities in the subarctic Pacific Ocean, *Deep-Sea Res. Pt. II, 46,* 2447-2473, 1999.

Martin J.H. and S.E. Fitzwater, Iron deficiency limits phytoplankton growth in the north-east Pacific subarctic, *Nature, 331*, 341-343, 1988.

Martin, J.H. and R.M. Gordon, Northeast Pacific iron distributions in relation to phytoplankton productivity, *Deep-Sea Res., 35*, 177-196, 1988.

Martin, J.H., R.M. Gordon, S. Fitzwater, and W.W. Broenkow, VERTEX: Phytoplankton/iron studies in the Gulf of Alaska, *Deep-Sea Res., 36*, 649-671, 1989.

Martin, J.H., R.M. Gordon, and S.E. Fitzwater, Iron in Antarctic waters, *Nature, 345*, 156-158, 1990.

Martin, J.H., R. M. Gordon, and S.E. Fitzwater, The case for iron, *Limnol. Oceanogr., 36,* 1793-1802, 1991a.

Martin, J.H., S.E. Fitzwater, and R.M. Gordon, We still say iron-deficiency limits phytoplankton growth in the sub-arctic pacific, *J. Geophys. Res., 96*, 20,699-20,700, 1991b.

Martin, J.H. and K.H. Coale, Testing the iron hypothesis in ecosystems of the equatorial Pacific Ocean, *Nature, 371*, 123, 1994.

Massman, W. J., A review of the molecular diffusivities of H_2O, CO_2, CH_4 ,CO, O_3, SO_2, NH_3, N_2O, NO, and NO_2 in air, O_2 and N_2 near STP, *Atmos. Environ., 32* (6), 1111-1127, 1998.

McDonald, D., T.F. Pedersen, and J. Crusius, Multiple late Quaternary episodes of exceptional diatom production in the Gulf of Alaska, *Deep-Sea Res. Pt. II, 46*, 2993-3017, 1999.

Meng, Z., J.H. Seinfeld, P. Saxena, and Y.P Kim, Atmospheric Gas aerosol equilibrium: IV. Thermodynamics of Carbonates, *Aerosol Sci. Technol. 23*, 131-154, 1995.

Metzger, S., F. Dentener, M. Krol, A. Jeuken, and J. Lelieveld, Gas/aerosol partitioning 2. Global modeling results, *J. Geophys. Res.,107*, doi:10.1029/2001JD001103, 2002.

Millero, F.J., Y. Wensheng and J. Aicher, The speciation of Fe(II) and Fe(III) in natural waters, *Mar. Chem.*, 50, 21-39, 1995.

Millero, F.J., Solubility of Fe(III) in seawater, *Earth. Planet. Sc. Lett., 154*(1-4), 323-329, 1998.

Minas, H.J., M. Minas, and T.T. Packard, Productivity in upwelling areas deduced from hydrographic and chemical fields, *Limnol. Oceanogr., 31*, 1182-1206, 1986.

Moore, J.K., S.C. Doney, D.M. Glover, and I.Y. Fung, Iron cycling and nutrient-limitation patterns in surface waters of the World Ocean, *Deep-Sea Res. Pt. II,* 463-507, 2002.

Mori, I., M. Nishikawa and Y. Iwasaka, Chemical reaction during the coagulation of ammonium sulphate and mineral particles in the atmosphere, *Sci. Total. Environ., 224* (1-3), 87-91, 1998.

Morse, J.W. and R.S. Arvidson, The dissolution kinetics of major sedimentary carbonate minerals, *Earth-Sci. Rev., 58*(1-2), 51-84, 2002.

Moya, M., A.S. Ansari, and S.N. Pandis, Partitioning of nitrate and ammonium between the gas and particulate phases during the 1997 IMADA-AVER study in Mexico City, *Atmos. Environ. 35* (10), 1791-1804, 2001.

Munger, J.W., S.M. Fan, P.S. Bakwin, M.L. Goulden, A.H. Goldstein, A.S. Colman, and S.C. Wofsy, Regional budgets for nitrogen oxides from continental sources: Variations of rates for oxidation and deposition with season and distance from source regions, *J. Geophys. Res., 103*(D7), 8355-8368, 1998.

Murad, E. and W.R. Fischer, The Biogeochemical cycle of iron, in *Iron in Soils and Clay Minerals*, edited by J.W. Stucki, B.A. Goodman, and U. Schwertmann, NATO ASI Series, 217, 1988.

Murayama, T., N. Sugimoto, I. Uno, K. Kinoshita, K. Aoki, N. Hagiwara, Z.Y. Liu, I. Matsui, T. Sakai, T. Shibata, K. Arao, B.J. Sohn, J.G. Won, S.C. Yoon, T. Li, J. Zhou, H.L. Hu, M. Abo, K. Iokibe, R. Koga, Y. Iwasaka, Ground-based network observation of Asian dust events of April 1998 in east Asia, *J. Geophys. Res., 106* (16), 18,345-18,359, 2001.

Nagy, K.L., Dissolution and precipitation kinetics of sheet silicates, in *Chemical weathering rates of silicate minerals*, Reviews in mineralogy, 31, 174-233, 1995.

Nakicenovic, N., J. Alcamo, G. Davis, B. de Vries, J. Fenhann, S. Gaffin, K. Gregory, A. Grübler, T. Y. Jung, T. Kram, E. L. La Rovere, L. Michaelis, S. Mori, T. Morita, W. Pepper, H. Pitcher, L. Price, K. Riahi, A. Roehrl, H.-H. Rogner, A. Sankovski, M. Schlesinger, P. Shukla, S. Smith, R. Swart, S. van Rooijen, N. Victor, Z. Dadi, *Emissions Scenarios, Special report of the Intergovernmental Panel on Climate Change (IPCC),* edited by N. Nakicenovic and R. Swart, pp. 570, Cambridge Univ. Press, Cambridge, UK, 2001.

Nenes, A., S.N. Pandis and C. Pilinis, ISORROPIA: A new thermodynamic equilibrium model for multiphase multicomponent inorganic aerosols, *Aquat. Geochem., 4*, 123-152, 1998.

Nishikawa, M., S. Kanamori, N. Kanamori and T. Mizoguchi, Kosa aerosol as eolian carrier of anthropogenic material, *Sci. Tot. Environ., 107*, 13-27, 1991.

Nishioka J, S. Takeda, C.S. Wong, and W.K. Johnson, Size-fractionated iron concentrations in the northeast Pacific Ocean: distribution of soluble and small colloidal iron, *Mar. Chem., 74*, 157-179, 2001.

Nishioka, J., S. Takeda, I. Kudo, D. Tsumune, T. Yoshimura, K. Kuma, and A. Tsuda, Size-fractionated iron distributions and iron-limitation processes in the subarctic

NW Pacific, *Geophys. Res. Lett., 30*(14),1730, doi: 10.1029/2002GL016853, 2003.

Parungo, F., Z. Li, X. Li and D. Yang, Gobi dust storms and The Great Green Wall, *Geophys. Res. Letters., 21*, 999-1002, 1994.

Pehkonen, S.O., R. Siefert, Y. Erel, S. Webb, and M.R. Hoffmann, Photoreduction of iron oxyhydroxides in the presence of important atmospheric organic-compounds, *Environ. Sci. Technol., 27* (10), 2056-2062, 1993.

Phadnis, M.J. and G.R. Carmichael, Numerical investigation of the influence of mineral dust on the tropospheric chemistry of East Asia, *J. Atmos. Chem., 36*, 285-323, 2000.

Prospero, J.M. and E. Bonatti, Continental dust in the atmosphere of the eastern equatorial Pacific, *J. Geophys. Res., 74*, 3362-3371, 1969.

Prospero, J.M., The atmospheric transport of particles to the ocean, in *Particle flux in the ocean*, edited by V. Ittekkot, P. Schäffer, S. Honjo and P.J. Depetris (Eds.), John Willey, New York, 1996.

Rolph, G.D., Real-time Environmental Applications and Display sYstem (READY) Website (http://www.arl.noaa.gov/ready/hysplit4.html), NOAA Air Resources Laboratory, Silver Spring, MD, 2003.

Rue, E.L. and K.W. Bruland, Complexation of iron(iii) by natural organic-ligands in the central north pacific as determined by a new competitive ligand equilibration adsorptive cathodic stripping voltammetric method, *Mar. Chem., 50*, 117-138, 1995.

Sander, S. P., Friedl, R.R., D. M. Golden, M. J. Kurylo, R.E. Huie, V.L. Orkin, G.K. Moortgat, A. R. Ravishankara, C.E. Kolb, M. J. Molina, and B.J. Finlayson-Pitts, Chemical kinetics and photochemical data for use in atmospheric studies, Evaluating number 14, *JPL Publ., 02-25*, 2003.

Schmidt, M.A. and D.A. Hutchins, Size-fractionated biological iron and carbon uptake along a coastal to offshore transect in the NE Pacific, *Deep-Sea Res. Pt. II, 46*, 2487-2503, 1999.

Sedlak, D.L. and J. Hoigné, The role of copper and oxalate in redox cycling of iron in atmospheric waters, *Atmos. Environ., 27A*, 2173-2185, 1993.

Seinfeld, J.H. and S.N. Pandis, Atmospheric chemistry and physics: From air pollution to climate change, John Wiley & Sons, Inc., p.1326, 1998.

Siefert R.L., S.O. Pehkonen, Y. Erel, and M.R. Hoffmann, Iron photochemistry of aqueous suspensions of ambient aerosol with added organic-acids, *Geochim. Cosmochim. Ac. 58,* 3271-3279, 1994.

Siefert, R.L., S.M. Webb, and M.R. Hoffmann, Determination of photochemically available iron in ambient aerosols, *J. Geophys. Res., 101*(D9), 14,441-14,449, 1996.

Siffert, C. and B. Sulzberger, Light-induced dissolution of hematite in the presence of oxalate: A case-study, *Langmuir, 7*(8), 1627-1634, 1991.

Simnad, M. and R. Smoluchowski, Effect of proton irradiation upon the rate of solution of Fe_2O_3 in hydrochloric acid, *J. Chem. Phys., 23*, 1961, 1955.

Sjöberg, E.L., A fundamental equation for calcite dissolution kinetics, *Geochim. Cosmochim. Ac., 40*(4), 441-447, 1976.

Skopp, J.M., Physical properties of primary particles, in *Handbook of Soil Science*, edited by M.E. Sumner, pp. 3-17, CRC Press, Boca Raton, 2000.

Soil Survey Staff, *Keys to soil taxonomy*, Eighth edition, p.328, United States Department of Agriculture, National Resource Conservation Service, 1998.

Song, C.H. and G.R. Carmichael, The aging process of naturally emitted aerosol (sea-salt and mineral aerosol) during long range transport, *Atmos. Environ.*, 33, 2203-2218, 1999.

Song, C.H. and G.R. Carmichael, A three-dimensional modeling investigation of the evolution processes of dust and sea-salt particles in east Asia, *J. Geophys. Res., 106*, 18,131-18,154, 2001.

Spokes, L.J., T.D. Jickells, and B. Lim, Solubilization of aerosol trace metals by cloud processing: A laboratory study, *Geochim. Cosmochim. Acta, 58*, 3281-3287, 1994.

Spokes, L. and T.D. Jickells, Factors controlling the solubility of aerosol trace metals in the atmosphere and on mixing into seawater, *Aquatic Chemistry, 1*, 355-374, 1996.

Sreets, D.G. and S.T. Waldhoff, Present and future emissions of air pollutants in China: SO_2, NO_x and CO, *Atmos. Environ., 34*, 363-374, 2000.

Streets, D.G., K.J. Jiang, X.L. Hu, J.E. Sinton, X.Q. Zhang, D.Y. Xu, M.Z. Jacobson, J.E. Hansen, Climate change - Recent reductions in China's greenhouse gas emissions, *Science, 294*,1835-1837, 2001.

Streets, D.G., T.C. Bond, G.R. Carmichael, S.D. Fernandes, Q. Fu, D. He, Z. Klimont, S.M. Nelson, N.Y. Tsai, M.Q. Wang, J.-H. Woo, and K.F. Yarber, An inventory of gaseous and primary aerosol emissions in Asia in the year 2000, *J. Geophys. Res., 108*(D21), 8809, doi:10.1029/2002JD003093, 2003.

Stumm, W. and J.J. Morgan (Eds.), *Aquatic chemistry: An Introduction Emphasizing Chemical Equilibria in Natural Waters*, 780 pp., J. Wiley & Sons, New York, 1981.

Sullivan, T.J., C.T. Driscoll, S.A. Gherini, R.K. Munson, R.B. Cook, D.F. Charles, and C.P. Yatsko, Influence of aqueous aluminum and organic-acids on measurement of acid neutralizing capacity in surface waters, *Nature, 338*(6214), 408-410, 1989.

Sulzberger, B. and H. Laubscher, Reactivity of various types of iron(III) (hydr)oxides towards light-induced dissolution, *Mar. Chem., 50,* 103-115, 1995.

Sun, J., M. Zhang and T. Liu, Spatial and temporal characteristics of dust storms in China and surrounding regions, 1960-1999: Relations to source area and climate, *J. Geophys. Res.*, 106, 10,325-10,333, 2001.

Sunda, W.G. and S.A. Huntsman, Iron uptake and growth limitation in oceanic and coastal phytoplankton, *Mar. Chem, 50,* 189-206, 1995.

Talbot, R.W., J.E. Dibb, B.L. Lefer, J.D. Bradshaw, S.T. Sandholm, D.R. Blake, N.J. Blake, G.W. Sachse, J.E. Collins, B.G. Heikes, J.T. Merrill, G.L. Gregory, B.E. Anderson, H.B. Singh, D.C. Thornton, A.R. Bandy, and R.F. Pueschel, Chemical characteristics of continental outflow from Asia to the troposphere over the western Pacific Ocean during February-March 1994: Results from PEM-West B, J. *Geophys. Res., 102,* 28,255-28,274, 1997.

Talbot, R., J. Dibb, E. Scheuer, G. Seid, R. Russo, S. Sandholm, D. Tan, H. Singh, D. Blake, N. Blake, E. Atlas, G. Sachse, and M. Avery, Reactive nitrogen in Asian continental outflow over the western Pacific: Results from the NASA Transport and Chemical Evolution over the Pacific (TRACE-P) airborne mission, *J. Geophys. Res., 108*(D20), 8803, doi:10.1029/2002JD003129, 2003.

Tan, Q., Y. Huang and W.L. Chameides, Budget and export of anthropogenic SOx from East Asia during continental outflow conditions, *J. Geophys. Res., 107*, DOI: 10.1029/2001JD000769, 2002.

Taylor, S.R. and S.M. McLennan, *The continental crust: Its composition and evolution*, 312 pp., Blackwell, Malden, Mss., 1985.

Taylor, A.H., R.J. Geider, and F.J.H. Gilbert, Seasonal and latitudinal dependencies of phytoplankton carbon-to-chlorophyll a ratios: Results of a modelling study, Mar. Ecol-Prog. Ser .,152(1-3), 51-66, 1997.

Tegen, I., and I. Fung, Modeling of mineral dust in the atmosphere : Sources, transport, and optical-thickness, *J. Geophys. Res., 99* (D11), 22,897-22,914, 1994.

Tennekes, H. and J. L. Lumley, *A first course in turbulence,* MIT Press, 300 p., 1972.

Tessier, D., Behavior and microstructure of clay minerals, in: Soil Colloids and Their Associations in Aggregates, edited by M.F. De Boodt, M. Hayes and A. Herbillon, pp. 347-415, Plenum Press, New York, 1990.

Thornton, D.C., A.R. Bandy, B.W. Blomquist, R.W. Talbot, and J.E. Dibb, Transport of sulfur dioxide from the Asian Pacific Rim to the North Pacific troposphere, *J. Geophys. Res., 102*, 28,489-28,499, 1997.

Tratt, D.M., R.J. Frouin, and D.L. Westphal, April 1998 Asian dust event: A southern California perspective, *J. Geophys. Res., 106,* 18,317-18,330, 2001.

Tsuda, A., S. Takeda, H. Saito, J. Nishioka, Y. Nojiri, I. Kudo, H. Kiyosawa, A. Shiomoto, K. Imai, T. Ono, A. Shimamoto, D. Tsumune, T. Yoshimura, T. Aono, A. Hinuma, M. Kinugasa, K. Suzuki, Y. Sohrin, Y. Noiri, H. Tani, Y. Deguchi, N. Tsurushima, H. Ogawa, K. Fukami, K. Kuma, and T. Saino, A mesoscale iron enrichment in the western Subarctic Pacific induces a large centric diatom bloom, *Science, 300*, 958-961, 2003.

Tsunogai, S., T. Suzuki, T. Kurata, and M. Uematsu, Seasonal and areal variation of continental aerosol in the surface air over the Western North Pacific Region, J. *Oceanogr. Soc. Jpn., 41*, 427-434, 1985.

Turner, S.M., P.D. Nightingale, L.J. Spokes, M.I. Liddicoat and P.S. Liss, Increased dimethyl sulphide concentrations in sea water from in situ iron enrichment, *Nature, 383*, 513-517, 1996.

Turner, D.R., K.A. Hunter, and H.J.W. de Baar, Introduction, in *The biogeochemistry of iron in seawater*, edited by D.R. Turner, and K.A. Hunter, pp. 1-7, J. Wiley & Sons, New York, 2001.

Ullerstam, M., R. Vogt, S. Langer, and E. Ljungstrom, The kinetics and mechanism of SO_2 oxidation by O_3 on mineral dust, *Phys. Chem. Chem. Phys., 4*(19), 4694, doi:10.1039/b203529b, 2002.

Underwood, G.M., T.M. Miller and V.H. Grassian, Transmission FT-IR and Knudsen cell study of the heterogeneous reactivity of gaseous nitrogen dioxide on mineral oxide particles, *J. Phys. Chem. A, 103*, 6184-6190, 1999.

Uno, I., H. Amano, S. Emori, K. Kinoshita, I. Matsui, and N. Sugimoto, Trans-Pacific yellow sand transport observed in April 1998: A numerical simulation, *J. Geophys. Res., 106,* 18,331-18,344, 2001.

Voelker, B.M., F.M.M. Morel, and B. Sulzberger, Iron redox cycling in surface waters: Effects of humic substances and light, *Environ. Sci. Technol., 31* (4), 1004-1011, 1997.

Wang, T., V.T.F. Cheung, M. Anson, and Y.S. Li, Ozone and related gaseous pollutants in the boundary layer of eastern China: Overview of the resent measurements at a rural site, *Geophys. Res. Letters*, 28, 2373-2376, 2001.

Warneck, P., *Chemistry of the natural Atmosphere*, International Geophysics Series 41, p. 757, Academic Press, San Diego, California, 1988.

Watson, A.J., Iron limitation in the oceans, in *The biogeochemistry of iron in seawater*, edited by D.R. Turner, and K.A. Hunter, pp. 85-121, J. Wiley & Sons, New York, 2001.

Webb, R.W., C.E. Rosenzweig, and E.R. Levine, Global Soil Texture and Derived Water-Holding Capacities, Available on-line [http://www.daac.ornl.gov /] from Oak Ridge National Laboratory Distributed Active Archive Center, Oak Ridge, Tennessee, U.S.A., 2000.

Wells, M.L., N.M. Price, and K.W. Bruland, Iron chemistry in seawater and its relationship to phytoplankton: a workshop report, Mar. Chem., 48, 157-182, 1995.

Wells, M.L., The level of iron enrichment required to initiate diatom blooms in HNLC waters, *Mar. Chem., 82*, 101, doi: 10.1016/S0304-4203(03)00055-0, 2003.

Wexler, A.S., F.W. Lurmann, J.H. Seinfeld, Modeling urban and regional aerosols .1. Model development, *Atmos. Environ., 28*(3), 531-546, 1994.

Wild, O., J. K. Sundet, M. J. Prather, I. S. A. Isaksen, H. Akimoto, E. V. Browell, and S. J. Oltmans, Chemical transportmodel ozone simulations for spring 2001 over the western Pacific: Comparisons with TRACE-P lidar, ozonesondes, and Total Ozone Mapping Spectrometer columns, J. Geophys. Res., 108(D21), 8826, doi:10.1029/2002JD003283, 2003.

Wong, C. S., N. A. D. Waser, Y. Nojiri, F. A. Whitney, J. S. Page and J. Zeng, Seasonal cycles of nutrients and dissolved inorganic carbon at high and mid latitudes in the North Pacific Ocean during the *Skaugran* cruises: determination of new production and nutrient uptake ratios, *Deep-Sea Res. II, 49*, 5317-5338, 2002.

Wonik, T., Gamma-ray measurements in the Kirchrode I and II boreholes, *Palaeogeogr. Palaeocl.*, 174 (1-3), 97-105, 2001.

Xiao, H., G.R. Carmichael, J. Durchenwald, D. Thornton, and A. Bandy, Long-range transport of SO_x and dust in East Asia during the PEM B Experiment, *J. Geophys. Res.*, *102*, 28,589-28,612, 1997.

Yienger, J.J., M. Galanter, T.A. Holloway, M.J. Phadnis, S.K. Guttikunda, G.R. Carmichael, W.J. Moxim, and H. Levy, The episodic nature of air pollution transport from Asia to North America, *J. Geophys. Res.*, 105 (22), 26,931-26,945, 2000.

Zender, C.S., H.S. Bian, and D Newman, Mineral Dust Entrainment and Deposition (DEAD) model: Description and 1990s dust climatology, *J. Geophys. Res., 108* (D14), 4416, 2003.

Zhang, X.Y., S.L. Gong, Z.X. Shen, F.M. Mei, X.X. Xi, L.C. Liu, Z.J. Zhou, D. Wang, Y.Q. Wang and Y. Cheng, Characterization of soil dust aerosol in China and its transport and distribution during 2001 ACE-Asia: 1. Network observations, *J. Geophys. Res.*, 108(D9), doi:10.1029/2002JD002632, 2003.

Zhou, G. and K. Tazaki, Seasonal variation of gypsum in aerosol and its effect on the acidity of wet precipitation on the Japan Sea side of Japan, *Atmos. Environ., 30* (19), 3301-3308,1996.

Zhu, X., J.M. Prospero, F.J. Millero, D.L. Savoie, and G.W. Brass, The solubility of ferric ion in marine mineral aerosol solutions at ambient relative humidities, *Mar. Chem.*, *38*, 91-107,1992.

Zhu, X., J.M. Prospero, D.L. Savoie, F.J. Millero, R.G. Zika, and E.S. Saltzman, Photoreduction of iron (III) in marine mineral aerosol solutions, *J. Geophys. Res.*, *98*(D5), 9039-9046, 1993.

Zhuang, G., Z. Yi, R.A. Duce, and P.R. Brown, Link between iron and sulphur cycles suggested by detection of Fe(II) in remote marine aerosols, *Nature*, 355, 537-539, 1992a.

Zhuang, G., Z. Yi, R.A. Duce, and P.R. Brown, Chemistry of iron in marine aerosols, *Global Biogeochem. Cycles*, *6*, 161-173, 1992b.
(Correction, *Global Biogeochem. Cycles*, *7*, 711, 1993).

Zinder, B., G. Furrer and W. Stumm, The coordination chemistry of weathering: II Dissolution of Fe(III) oxides, *Geochim. Cosmochim. Acta*, *50*, 1861-1869, 1986.

Zuo,Y. and J. Holgne, Formation of hydrogen-peroxide and depletion of oxalic-acid in atmospheric water by photolysis of iron(III)-oxalato complexes, *Environ. Sci. Technol., 26*, 1014-1022, 1992.

Vita

Nicholas Meskhidze was born on 18 April 1971 in Tbilisi, Georgia. He received a B.S. in Physics from Tbilisi State University, Tbilisi, Georgia in 1993. After graduation, he worked as an assistant to professor in the laboratory of semiconductor physics. From the year 1992 till 1995 he pursued his Master's Degree in Environmental Management and Planning in the Accredited Branch of the University of Georgia, USA. Nicholas began his Ph.D. in Atmospheric Chemistry at Georgia Institute of Technology in the fall of 1999. After four years as a research and teaching assistant, he received his Ph.D. in Atmospheric Chemistry from the School of Earth and Atmospheric Sciences.